Redesign and Performance Evaluation of a Cardiac Pulse Duplicator

by
Reynaldo Adrián Rodriguez

Thesis presented in partial fulfilment of the requirements for the degree of Master of Engineering (Mechatronic) in the Faculty of Engineering at Stellenbosch University

Supervisor: Dr. Jacobus Hendrik Müller
Co-supervisor: Dr. Kiran Hamilton Dellimore

December 2017

Declaration

By submitting this thesis electronically, I declare that the entirety of the work contained therein is my own, original work, that I am the sole author thereof (save to the extent explicitly otherwise stated), that reproduction and publication thereof by Stellenbosch University will not infringe any third party rights and that I have not previously in its entirety or in part submitted it for obtaining any qualification.

Date: December 2017

Abstract

The worldwide demand for prosthetic heart valve (PHV) replacements is increasing rapidly. Although developing countries have the largest demand due to the high incidence of rheumatic heart disease, the mismatch between the available resources and the cost of PHVs often renders them inaccessible in these locations. This raises the need for lower cost PHVs which calls for reduced development costs. A cardiac pulse duplicator (CPD) plays a crucial role in the PHV design process and CPDs built in-house can represent large savings over commercial alternatives. However, they are complex devices and without the appropriate level of expertise their development can result in a time consuming, expensive process which offsets any benefits derived from building it in-house. This thesis documents the redevelopment of a PHV testing device and the methods used to evaluate its performance, providing guidelines to assist those interested in developing a CPD. This was also done to enable the Biomedical Engineering Research Group at Stellenbosch University to test, in accordance to the ISO5840 standard, the PHV it developed.

A literature survey confirmed the increasing importance of CPDs in PHV development and in a variety of other cardiovascular research topics but also indicated that there are no established guidelines to quantify or directly assess a CPD's performance. Due to the difficulty of distinguishing between the hydrodynamic performance of the PHV and that of the device used to test it, the standardisation of methods to assess the performance of CPDs is proposed. The concept of fidelity is presented as a first step towards a means of quantifying CPD performance which can improve the quality of PHV test data.

A high performance system was designed and implemented to control the motion of the pump used to generate pulsatile flow. Various other aspects of the CPD were designed and implemented or manufactured. This included control, acquisition and analysis software as well as a number of connected hydraulic elements making up a flexible platform for testing PHVs. Rigorous tests were devised to assess the performance of the CPD's control system. Commercially available PHVs were tested to evaluate the electrical and hydrodynamic performance of the CPD. To compare the overall performance of the CPD to that of a widely cited counterpart, further tests were carried out so that the results obtained could be compared directly against those found in the literature.

Analysis of the results showed the control system to be highly dynamic, accurate (0.019 ±0.006 mm deviation from setpoint at 70 bpm) and repeatable (2.426 ±1.335 mmHg RMSE cycle-to-cycle). The hydrodynamic performance achieved with the hydraulic components that were designed was satisfactory. The measured pressure data showed good agreement with published data for the available reference PHV, although some deviations were noted. These deviations were used to investigate some phenomena that ought to be taken into consideration during the design phase of CPDs.

Some shortcomings present in the final implementation of the CPD were identified and recommendations made to address them. Despite its limitations and a cost of R 160 951, the CPD offers similar performance to a commercial system eight times this cost.

Opsomming

Die wêreldwye aanvraag na prostetiese hartklep (PHK) plaasvervangers neem vinnig toe. Alhoewel ontwikkelende nasies die grootste aanvraag het as gevolg van die hoë voorkoms van rumatiese hartsiekte, veroorsaak die wanverhouding tussen die beskikbare hulpbronne en die koste van PHKs dat hulle dikwels ontoeganklik in hierdie lande is. Dit gee aanleiding tot die behoefte aan 'n goedkoper PHK wat verminderde ontwikkelingskostes vereis. ‘n Hartpolsnabootser (HPN) speel 'n belangrike rol in die PHK ontwerpsproses en HPNe wat plaaslik gebou word kan grooter besparings inhou as kommersiële alternatiewe. Hulle is egter ingewikkelde toestelle en sonder die toepaslike kundigheid kan hul ontwikkeling tot 'n tydrowende, duur proses lei wat enige voordele wat uit die plaaslike proses voortspruit neutraliseer. Dié tesis dokumenteer die herontwikkeling van 'n PHK toetsapparaat en die metodes wat gebruik is om die werkverrigting te evalueer, om sodoende riglyne te verskaf aan diegene wat belangstel in die ontwikkeling van 'n HPN. Bowendien, is die Biomediese Ingenieurswese Navorsings Groep aan die Universiteit van Stellenbosh in staat gestel om die HPN wat daar ontwikkel is in ooreenstemming met die ISO5840 standaard te toets.

'n Literatuur studie bevestig die toenemende belangrikheid van HPNe in PHK ontwikkeling, sowel as in 'n verskeidenheid van ander kardiovaskulêre-navorsingsonderwerpe, maar het ook aangedui dat daar geen gevestigde riglyne om die werkvirrigting van ‘n HPN te kwantifiseer of direk te evalueer bestaan nie. As gevolg van die probleme om te onderskei tussen die hidrodinamiese prestasie van die PHK en dié van die toestel gebruik om dit te toets, is die standaardisering van metodes om die prestasie van HPNe te evalueer voorgestel. Die konsep van getrouheid word aangebied as 'n eerste stap na 'n wyse om die prestasie van ‘n HPN te kwantifiseer, wat die gehalte van PHK toetsdata kan verbeter.

'n Hoë-prestasie stelsel is ontwerp en geïmplementeer om die beweging van die pomp wat gebruik word om polsmatige vloei te genereer te beheer. Verskeie ander aspekte van die HPN is ontwerp en geïmplementeer of vervaardig. Dit sluit in beheer-, verkryging- en analisesagteware, sowel as 'n aantal gekoppelde hidrouliese elemente wat 'n buigsame omgewing vir die toets van HPNe skep. Streng toetse is ontwerp om die werkverrigting van die HPN se beheerstelsel te evalueer. Komersiële PHKs is getoets om die elektriese en hidrodinamiese werkverrigting van die HPN te evalueer. Om die algehele werkverrigting van die HPN met dié van 'n wyd aangehale ewebeeld te vergelyk, is verdere toetse uitgevoer sodat die resultate wat verkry is direk teen dié wat in die literatuur voorkom vergelyk kon word.

Ontleding van die resultate het getoon dat die beheerstelsel hoogs dinamies en akkuraat is (0.019 ±0.006 mm afwyking om ‘n stelpunt teen 70 spm) met herhaalbare uitkomste (2.426 ±1.335 mmHg WGKF siklus-tot-siklus). Die hidrodinamiesеprestasie behaal met die hidrouliese komponente wat ontwerp is was bevredigend. Die data vir die gemete druk het goeie ooreenkoms getoon met gepubliseerde data vir die beskikbare verwysings PHK, hoewel sommige afwykings opgemerk is. Hierdie afwykings is gebruik om 'n paar verskynsels wat tydens die ontwerpsfase van HPNe in ag geneem behoort te word te ondersoek.

Sommige tekortkominge teenwoordig in die finale implementering van die HPN is geïdentifiseer en aanbevelings is gemaak om hulle aan te spreek. Ten spyte van sy beperkinge en koste van R160 951, is die werkverigting van die HPN soortgelyk aan kommersiële stelsels wat agt keer duurder is.

To Cris,
for keeping my heart beating.

To my parents,
for the gift of education.

Acknowledgements

This project could not have been completed without the help and support of numerous people. A few of them deserve to be acknowledged in a special way and therefore I would like to express my sincere gratitude to:

- The late Prof Cornie Scheffer, my initial supervisor, for providing me with this unique opportunity and accepting me as his student, and Prof Anton Basson, who also played a crucial role in facilitating this opportunity. Their support and understanding as employers enabled me to pursue this project.

- Dr Kiran Dellimore, my co-supervisor, for encouraging me to embark on this academic undertaking. His enthusiasm for this project, passion for research and mentoring were essential to my academic development.

- Dr Cobus Müller, my supervisor, for willingly taking over this project after Prof Scheffer's tragic passing and having the ability to calm me down during times of panic. He provided the necessary guidance to find direction again and facilitated equipment that proved critical to the successful completion of this project.

- All the staff in the workshop, for welcoming me into their domain as one of their own. Mr Anton van den Berg deserves special mention not only for his excellent workmanship but also for taking the time to mentor me in his art. Being able to manufacture my own designs brought me great satisfaction and ultimately played a key role in this highly practical project.

- My close friends, Kevin Neaves and Kobus Hoffman, who took up this challenge with me, and Melody van Rooyen, for all the encouragement and interest in my work. This endeavour would have been far more difficult without their friendship.

- My parents, for the financial and emotional support, the interest in my project and always believing in me.

- Cris, the shoulder I leaned on all these years, for the incredible patience and constant encouragement; for sharing the experience, celebrating the highs and getting me through the lows; for always being positive and giving me hope.

- God, for this undertaking would neither have started nor finished had He not moved so many people along the way to help me and opened so many doors.

Table of contents

List of figures

List of tables

List of abbreviations

AC	Alternating current
BERG	Biomedical Engineering Research Group
bpm	beats per minute
CNC	Computer numerically controlled
CO	Cardiac output
CPD	Cardiac pulse duplicator
DAQ	Data acquisition
EOA	Effective orifice area
FDA	Food and Drug Administration
FPGA	Field programmable gate array
HR	Heart rate
ISO	International Organization for Standardization
LVDT	Linear variable differential transformer
LVOT	Left ventricular outflow tract
MAP	Mean arterial pressure
PC	Personal computer
PHV	Prosthetic heart valve
PID	Proportional-Integral-Derivative
PIV	Particle image velocimetry
PWV	Pulse wave velocity
RF	Rheumatic fever
RHD	Rheumatic heart disease
RMS	Root mean square
RMSE	RMS error
RT	Real time
RTD	Resistance temperature detector
SD	Standard deviation
SJM	St Jude Medical
SUN	Stellenbosch University
SV	Stroke volume
SVE	Shared Variable Engine
SWL	Stroke work loss
VI	Virtual instrument

List of symbols

C	Compliance
e	Measured positioning error
P_{dias}	Diastolic pressure
P_{sys}	Systolic pressure
$P_{sys\_mean\_art}$	Mean systolic arterial pressure
$P_{sys\_mean\_vent}$	Mean systolic ventricular pressure
ΔP	Differential pressure across the open test valve
ΔP_{mean}	Mean systolic pressure difference
ΔP_{peak}	Peak systolic pressure difference
$-\Delta P_{mean}$	Mean back pressure
Q_{mean}	Mean flow rate
$q_{v_{RMS}}$	Root mean square forward flow
$q_v(t)$	Instantaneous flow rate
R	Resistance
ρ	Test fluid density
T_d	Derivative action time constant of the position controller
T_i	Integral action time constant of the position controller
K_p	Proportional gain of the position controller
T_{sys}	Duration of systole
u	Position controller output
$V_{closing}$	Closing regurgitant volume of the test valve
$V_{leakage}$	Leakage volume of the test valve
V_{reg_total}	Total regurgitant volume of the test valve
$\mathcal{F}$	Fidelity metric

1 Introduction

1.1 Background and motivation

Rheumatic heart disease (RHD)[1] is the most serious complication of childhood rheumatic fever (RF) and it is a major health problem in developing countries such as South Africa. Together, RF and RHD represent a major source of cardiovascular diseases across the globe, although their effect is most evident in developing countries [1]. It has been shown that previous diagnostic techniques may have underestimated the incidence of RHD by almost 10 times [2] and while thought to be primarily a childhood disease, a South African study reported newly diagnosed RHD in an adult population with an incidence of 23.5 cases per 100 000 per annum for patients above 14 years of age [3]. The resultant chronic RHD leads to the development of aortic and/or mitral valve stenosis (see Figure 1.1) and varying degrees of regurgitation (backward flow of blood through the closed valve), often presenting the need for heart valve replacement as was the case for 22% of the South African study's cohort. But while RHD is the main reason for valvular replacements, there are various other pathologies that may lead to severe heart valve dysfunction and the subsequent need for replacement. These include but are not limited to endocarditis[2], congenital defects, calcific stenosis[3], heart attack and valvular damage or degeneration arising from chronic high blood pressure, radiation and atherosclerosis[4], among others [4, 5].

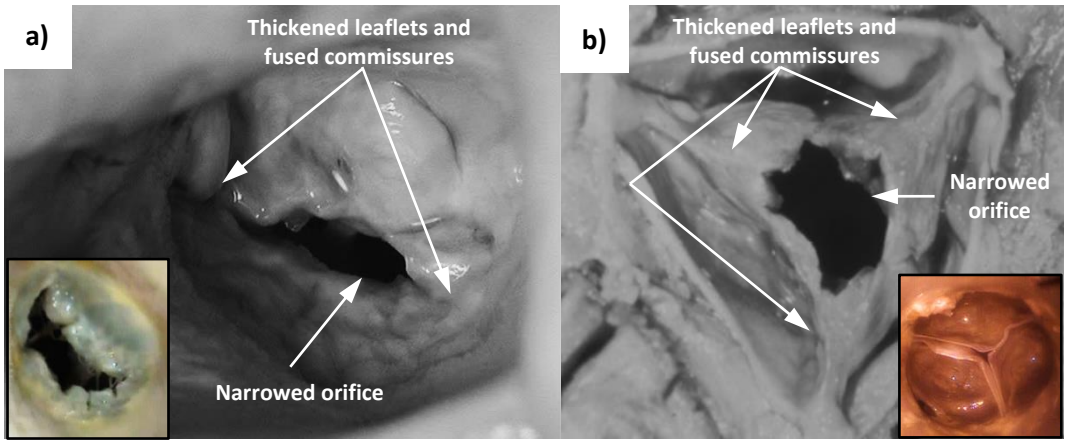

Figure 1.1: Stenosis of heart valves caused by RHD. Mitral valve (a) (adapted from [6 pp329]) and aortic valve (b) (adapted from [7 pp15]) showing characteristic RHD pathology. Insets: healthy valves, respectively. (Adopted from [8] and [9]).

It is widely documented that RHD is most prevalent in developing regions of the world and particularly Africa [1, 2, 3, 10, 11, 12, 13, 14], as shown in Figure 1.2. This not only makes it difficult to control and treat RF in order to prevent RHD but it also means that

[1] An inflammation of the heart leading to fibrotic repair of tissue and subsequent valvular dysfunction.
[2] The inflammation of the endocardium (the heart chambers' inner walls).
[3] The progressive narrowing of a valve's orifice due to calcium deposits on its leaflets.
[4] The thickening of an arterial wall as a result of a lesion.

regions with the highest demand for valvular replacements have very limited resources available to use in alleviating the burden of the disease and reducing RHD mortality rate. This is compounded by the fact that the prosthetic heart valve (PHV) replacement market is expensive when compared to limited health budgets and per capita income: the cost of a single prosthetic device can range from 2 000 USD to 10 000 USD for surgical valves and up to 25 000 USD (2010) for transcatheter[5] valves [15]. These costs are dependent on location, as is the procedure and related hospitalisation costs. In South Africa, the average cost of a transcatheter aortic valve implantation procedure in 2011 was estimated to be ZAR 335 500 (46 255 USD) [16]. This situation, together with an increasing as well as older world population, advances in diagnostic techniques and new prosthetics technologies all contribute to a large demand for heart valve replacement systems that are more accessible to the resource constrained areas of the world where they are most needed. Indeed, it is estimated that by 2050, over 850 000 patients will need a heart valve replacement per annum. This is nearly 3 times more than in 2003 [17].

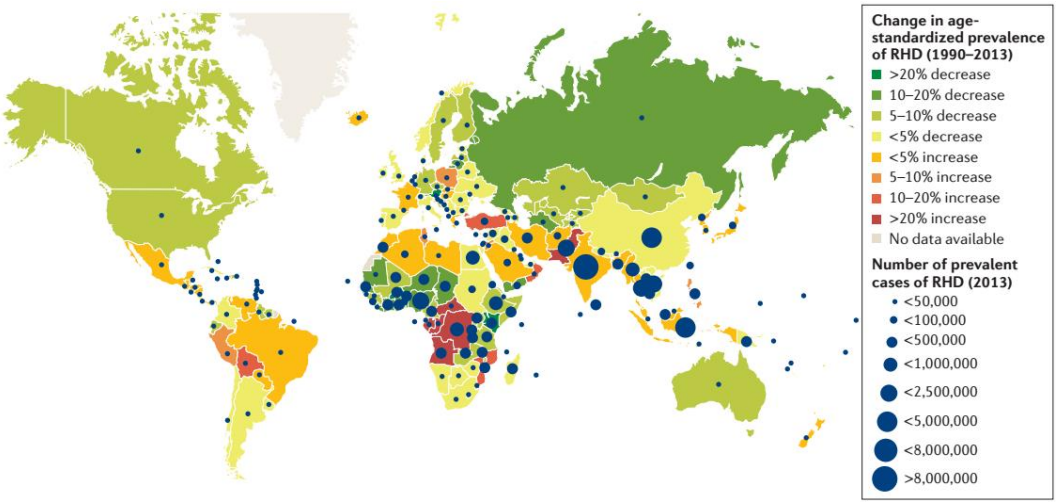

Figure 1.2: Prevalence of worldwide RHD. (Adopted from [14]).

The field of PHV replacements has grown dramatically over the last 60 years after the first successful valve implant attempts in the late 1950s and early 1960s [18]. Since then, thanks to advancements in technology and high demand, heart valve replacements have been the focus of great interest with much research and development resulting in more than 70 different mechanical and tissue PHV designs [19]. Currently, over 10 well known manufacturers produce a range of PHVs, including surgically implantable mechanical and tissue valves as well as transcatheter designs.

An important aspect of prostheses development is the equipment used to test the prostheses' functionality and durability. Such equipment is crucial to the iterative design process, providing real world test data that are used to further develop, optimize and verify the performance of the prosthetic device. This includes, among others, cardiac

[5] Transcatheter PHVs differ from their surgical counterparts in that their implantation procedure is minimally invasive, requiring only a few small incisions. Implantation of surgical PHVs requires open heart surgery.

pulse duplicators, echocardiographic machines, high speed cameras, flow visualisation systems (such as particle image velocimetry (PIV) and laser Doppler anemometry) and accelerated valve fatigue testers. Acquisition of these devices can prove prohibitively expensive for many academic institutions with the expertise and interest in the development and testing of PHVs as well as phenomena surrounding their operation. In line with this, the Biomedical Engineering Research Group (BERG) at Stellenbosch University (SUN) built a cardiac pulse duplicator (CPD) to study the performance of the transcatheter PHV replacement that it developed (Figure 1.3) [20, 21, 22, 23, 24, 25, 26, 27]. This CPD was based on Krynauw's design [28] and suffered from several drawbacks which will be described in detail Section 3.1.2. Further, Krynauw's design was conceived as a dual purpose rig with fatigue testing as the primary mode of operation which posed several challenges for hemodynamic tests. Since then the BERG developed a stronger interest in hemodynamic testing and in order to use this CPD for the desired purposes, several modifications and upgrades were required for the system as described in the following section.

Figure 1.3: BERG valve.

1.2 Aim

The aim of this project was to upgrade an existing CPD that was developed in house so that it could be used to test PHVs according to the International Organization for Standardization in the International Standard ISO5840:2005 (Cardiovascular implants – Cardiac valve prostheses)[6] [29]. As a means of evaluating the performance of the upgraded CPD and ensuring it is capable of producing the required quality of data, it was established that a reference PHV needed to be tested. Lastly, an important goal was to document the challenges and solutions related to the development of CPDs so as to enable easier, faster and more cost effective in-house development at other institutions. In order to achieve the above aims, the following objectives were identified:

- Redesign the CPD's left ventricular outflow tract (LVOT) and compliance chamber to encourage good laminar flow and allow reliable pressure and flow measurements while providing good optical access to the test valve.

[6] ISO5840-1:2015 (Cardiovascular implants – Cardiac valve prostheses) became available during the later stages of this project. Given the status of the project at that point in time it was decided to keep to the testing conventions stipulated in ISO5840:2005.

- Design and manufacture a mechanism to reliably control the peripheral resistance of the CPD with good repeatability.
- Replace the ventricle drive system to provide flexibility in terms of stroke volume (SV) and ventricular flow rate during testing.
- Create a new control and acquisition program with a user friendly interface.
- Establish and verify adequate operating and performance parameters for the CPD.

1.3 Thesis overview

This chapter has framed the context of the project, explaining the needs that motivate this undertaking. The key aims and the related objectives that guided the project were outlined in no particular order of importance.

Chapter 2 (Literature review), presents the knowledge required to understand the project. It includes basic cardiac anatomy and function (in the context of this project) as well as an introduction to CPDs, their increasing importance, development and evaluation. Importantly, it also states the typical working envelope for CPDs.

Chapter 3 (Materials and methods) begins by describing the state of the existing apparatus prior to the start of the project and identifies the most prominent problems related to it. Details of the hardware and software that were developed to fulfil the aims stated in Section 1.2 are then discussed. The last part of the chapter presents a series of tests and techniques that were devised to evaluate the performance of the new CPD. Chapter 4 (Results) closely follows the structure of the testing section from Chapter 3, presenting results for all the tests either in graphical or tabular form. Statistical information is given where applicable.

Chapter 5 (Discussion) reports the limitations of the design, explaining how they affect the functioning of the CPD. The second part of the chapter focuses on analysing and comparing the data acquired to data found in the literature, produced by a well cited CPD. A few important aspects of CPD design which directly affect PHV performance were investigated and are discussed in this chapter which also presents the need for a standardised approach to evaluating a CPD's performance.

Chapter 6 (Conclusion and Recommendations) ends this document summarising the work done, stating the outcomes of the project and highlighting the contributions that were made to the field. The recommendations section outlines the most important aspects of the machine that could be improved, offering solutions where necessary.

2 Literature Review

2.1 The human heart and overview of CPDs

The human heart consists of four chambers: the right and left atria, and the right and left ventricles (Figure 2.1). Functionally, the heart can be divided into two separate pumps: the right heart and the left heart. The right side pumps blood through the pulmonary circulation while the left circulates blood through the systemic circulation. The right atrium accepts blood from the systemic circulatory system and delivers it to the right ventricle which pumps it to the lungs. Once oxygenated, blood from the lungs returns to the heart at the left atrium. As the left ventricle starts to relax, the diastolic phase of the cardiac cycle begins and the mitral valve opens allowing blood in the left atrium to fill the expanding left ventricular cavity. Shortly after the left ventricle is fully relaxed it begins to contract, signalling the start of the systolic phase, and the mitral valve closes. This creates pressure inside the ventricle, causing the aortic valve to open and blood to be ejected through the aorta which distributes it to the rest of the body using the systemic circulatory system. As soon as the ventricle starts to relax, the pressure in the aorta becomes larger than inside the ventricle causing the aortic valve to close preventing any blood flow from the aorta into the ventricle and as the ventricle continues to relax the mitral valve opens, starting a new cycle. This entire process occurs for every heartbeat. In a normal, healthy heart the valves open quickly, allowing blood to flow through them with minimal resistance. They also close very quickly, staying tightly shut until the next heartbeat.

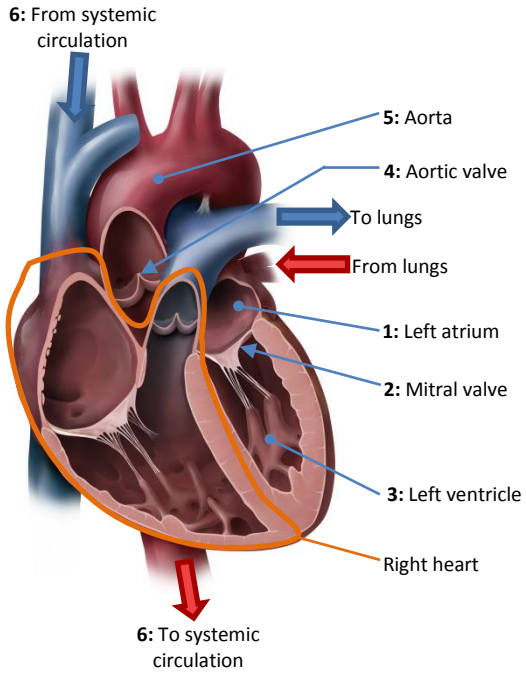

Figure 2.1: Anatomic model of the heart in coronal section view. (Adapted from [30]).

Modern CPDs are electromechanical devices that replicate the above process so they must be capable of reproducing the range of pressure and flow patterns observed in and around a healthy heart. This involves creating pulsatile flow, as can be seen in Figure 2.2

which graphically summarises this process with normal cardiac values. Since the right and left hearts have the same function of independent pumps, in practice only one of them needs to be implemented. The left heart has to pump blood through the entire body (as opposed to just the lungs) so it is stronger and operates at higher pressures. As a result, normally only the left heart is implemented because it can also replicate the function of the right heart. Figure 2.3 shows a CPD's hydraulic loop and functional diagram. The numbered items and labels relate the mechanical components to their anatomical counterparts, accordingly numbered in Figure 2.1.

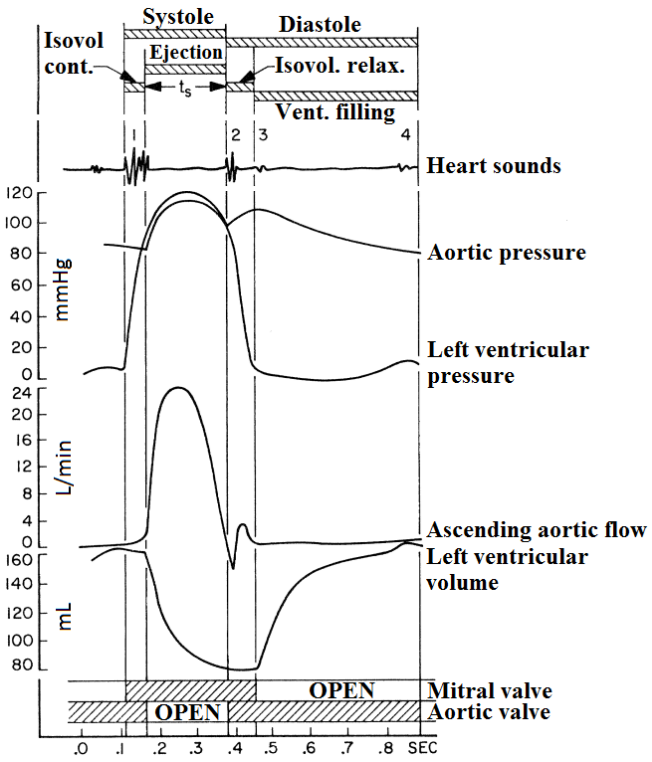

Figure 2.2: Events and physiological values of the cardiac cycle. (Adapted from [31]).

Cardiac preload and afterload determine the amount of work the heart does and thus the pressures at which it operates. Preload is related to the ventricle's ability to relax. The more the ventricle relaxes (or stretches), the more blood volume it can accept and the higher the preload so preload refers to the end diastolic volume of a ventricle. Afterload is the pressure that the ventricle must generate to eject blood while contracting. Afterload is determined by a number of parameters dependent on the conditions of the arterial tree [32] which are discussed in detail in Section 2.2.2. The effects of preload and afterload on the muscular (compliant) nature of the ventricles and their ability to relax and contract determine the characteristic pressure curves shown in Figure 2.2. Therefore, besides generating the pulsatile flow, CPDs must also mimic these properties. This is achieved by simulating the circulation system. The following section explains the different circulatory system simulation models, diagrammatically represented in Figure 2.3 as a separate system.

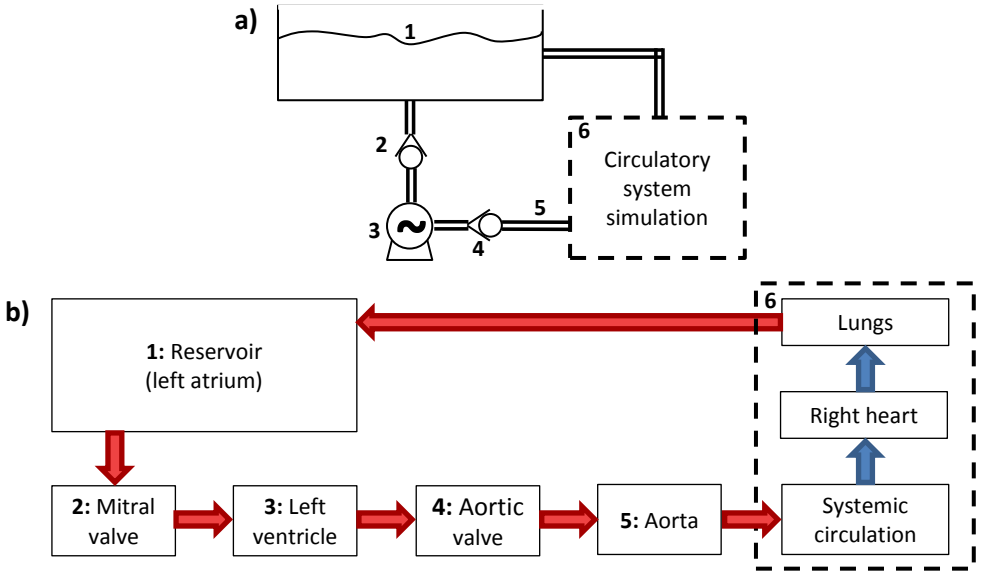

Figure 2.3: Hydraulic loop (a) and functional diagram (b) for a generic CPD. See Figure 2.1 for anatomical reference.

2.2 Types of CPDs and circulatory system simulation

CPDs are broadly classified in accordance to the method used to simulate cardiac load which to an extent also determines the roles they are intended to play in cardiovascular research. Cardiac load is generated primarily by the arterial system (afterload) with large and small arteries affecting two basic variables of hemodynamics, respectively: compliance and resistance [33]. The elastic nature of vessels is most prominent in large arteries causing these to store a fraction of the blood ejected during systole and release it during diastole, acting as a filter. This has the effect of smoothing flow, which is pulsatile close the heart but becomes steady as it approaches the venous system [34], allowing capillaries to receive continuous flow even during diastole. The small arteries offer resistance to flow, which combined with the action of the large arteries helps maintain systemic pressure [35]. Taking this into consideration, two basic types of arterial system simulations exist: the wave propagation model and the lump parameter model.

2.2.1 Wave propagation model

The wave propagation model simulates afterload by physically replicating the circulatory system. This is achieved by arranging compliant pipes (usually made of latex rubber or silicone) of different diameters in an anatomically correct manner [36]. The wave propagation model is useful for investigating pressure and flow as they develop through the main arteries and propagate down the circulation system [36, 37]. Figure 2.4 depicts a wave propagation setup (left) and the arterial tree used showing the descending aorta and main arterial branches (right).

Since this type of CPD physically replicates the circulatory system it can be quite large, complex and difficult to manufacture. However, it allows pressure to be measured at nearly any point in the system and provides a realistic environment to test the

deployment of valves designed for transcatheter delivery. Since almost any point of the circulation system can be studied, this type of CPD can be used to test not only valve prostheses but also vascular grafts (prosthetic arteries or veins). However, their main purpose remains to develop and validate mathematical models of the arterial system [38]. Since such a complete representation of the circulatory system is not necessary to study heart valve behaviour, it will not be considered further.

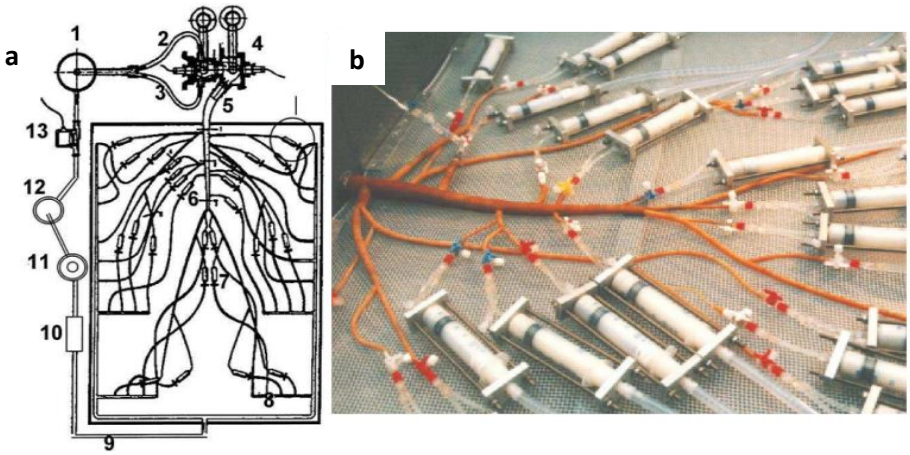

Figure 2.4: Wave propagation model CPD. (a): diagrammatic representation; (b) physical arterial tree used in this setup. (Adopted from [37]).

2.2.2 Lump parameter model

The lump parameter model (also known as the Windkessel model), based on the Windkessel effect and first described mathematically by Frank [39] in 1899 for the purposes of modelling hemodynamics, simulates afterload by applying the sum of the circulatory system effects on the ventricle and aortic valve. For example, the elasticity of all vessels and its effect on blood pressure at the aortic valve is simulated by a volume of air enclosed in a chamber after the aortic valve. This volume of air is compressed during the systolic phase of each heart beat while the fluid pressure is higher than the pressure of the entrapped air. When the ventricle goes into diastole and the aortic valves closes, the arterial pressure falls below the pressure of the air allowing the air to expand and gradually force the fluid through the next section of the system. Similarly, the resistance to blood flow created by the narrowing and length of all arteries can be achieved by a single flow restrictor located after the chamber that simulates compliance [40]. The gradual pressure applied by the expanding air causes the fluid to slowly flow through the restrictor giving the arterial pressure waveform its characteristic shape. This combination results in a compact, simplified system that has the same effect on the heart and aortic valve as a full wave propagation model. Therefore the lump parameter model is ideally suited to studying pressure and flow waveforms around PHVs [41].

Flow and pressure perceived by the left ventricle is determined by afterload which in turn is characterised by a number of parameters related to the state of the arterial tree. The body can regulate some of these parameters to affect flow and modify pressure at different areas of the body. Lump parameter model CPDs have discrete components that

simulate the effect of such parameters enabling them to create a realistic pressure and flow environment corresponding to the specific area of the body to be studied. These parameters are characteristic resistance (R_c), peripheral resistance (R_p), inertance (L) and compliance (C). The lumped parameter model is an approximation of the vascular system effects, mathematically representing each of these parameters with a passive electrical element (R_c = resistor, R_p = resistor, L = inductor, C = capacitor) which makes it possible to create an electrical circuit representative of the vascular system. By using electrical laws and the corresponding formulas for each element, the system's current and voltage can be calculated at any point in time, predicting values for flow and pressure respectively [40]. This approach has helped greatly to understand and simulate the effects of each parameter on pressure and flow as well as to establish appropriate physical values for the simulating components [38].

Frank's original model, however, only used one resistance and compliance making it a two element Windkessel model. Since then, several types of Windkessel models have been proposed [38, 42, 43, 44, 45] according to the number of elements that they include. The number of elements determines the accuracy of the model, although the improvements offered by the three and four element models are only perceivable during the systolic phase [41]. Figure 2.5 shows the analogy between a selection of 2, 3 and 4 element electrical Windkessel models and their equivalent hydraulic system.

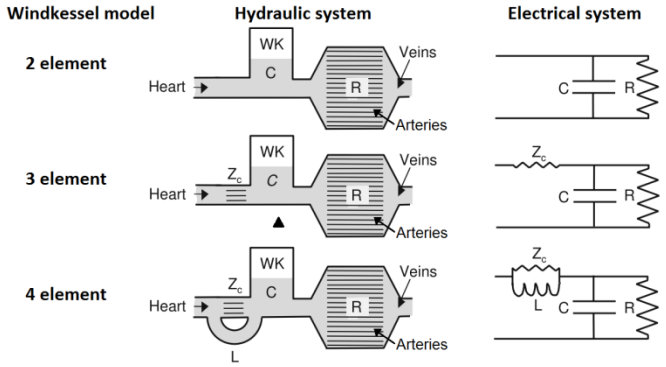

Figure 2.5: 2, 3 and 4 element Windkessel models (adapted from [41]).

The lump parameter model is not without limitations: any study related to the distributed nature of the circulation system cannot be undertaken. While the lump parameter model can be used to represent any part of the arterial system, it still cannot account for localised changes or effects within a larger system model, wave travel and transmission or the distribution of blood flow throughout the arterial tree [41]. However, because the physical implementation of the lump parameter model is compact and can simulate physiological conditions in the vicinity of the heart with sufficient accuracy, it is widely implemented by CPDs as a load to the heart and valve prostheses [41]. It offers the advantage that it can yield figures for compliance or resistance if the value of the other parameter is known [41, 45]; this is useful, for example, to determine the resistance or compliance of a specific vessel. Figure 2.6 shows the commercially available ViVitro Pulse Duplicator System (Vivitro Labs Inc., Victoria, BC, Canada), implementing the lump parameter model and the components used to regulate cardiac load.

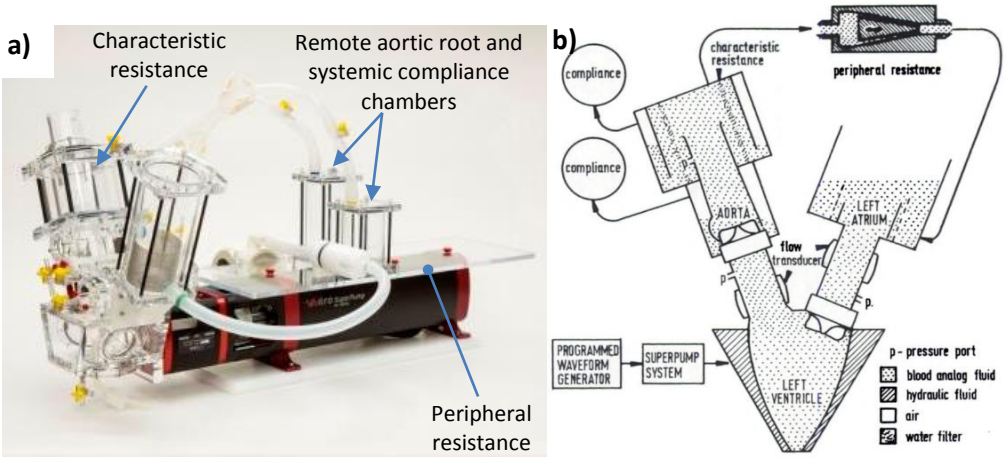

Figure 2.6: The ViVitro pulse duplicator system. a) Physical location (adapted from [46]) and b) diagrammatic representation (adopted from [47]) of lump parameter components.

2.3 Evolution of CPDs and the state of the art

The first documented CPDs appeared in the mid-1950s and were intended to gain insights into physiological cardiac and valvular function as well as studying the effects of heart valve pathologies [48, 49, 50, 51]. Most of these studies centred on acquiring pressure and visualising valve movement seeking to understand the fluid dynamics within the heart and around valves. Shortly thereafter, with the developments in surgical valve replacements in the early 1960s, a growing interest in CPDs was sparked to test valve replacements [52, 53]. Owing to a deeper understanding of the factors and phenomena affecting cardiac valve performance and emerging regulations for PHV testing, the following years saw the use of CPDs focus on studying more complex issues related to pressure and fluid dynamics around heart valves [54, 55, 56].

The pumps in these CPDs were driven pneumatically or by simple motors actuating either a lever arm or cam system. While some of these had the capability of adjusting the systolic fraction to some extent, this approach did not provide much flexibility in terms of ventricular control. The first commercially available CPD, developed by ViVitro Systems Inc., appeared in 1984 and used a reciprocal piston pump to implement the function of the left ventricle [57]. This year also saw the publication of the first edition of the ISO5840 standard, which provided the requirements for commercialisation of cardiac valve prostheses. From this point onwards commercial CPDs evolved alongside the design requirements of PHV replacements. The intense activity in this field meant significant research and effort was undertaken to improve the performance of CPDs and a greater focus was applied on user friendliness. With respect to performance, the efforts of Westerhhof's and Noordergraaf's groups [58, 59, 60, 61], related to the development of mathematical models, facilitated major advancements in the design and implementation of physical circulatory system simulators for CPDs.

The current embodiment of commercial CPDs has changed dramatically since the time they were first conceived and most modern implementations rely on a piston pump driven by a servomotor via a ball screw to simulate the ventricular action. This approach requires

advanced control techniques but provides the user with great flexibility. Pump control is achieved by sophisticated software that allows the discretisation of ventricular volume into as many as 2000 points [46, 62]. This would not be possible with the simple drive systems utilised by the early CPDs and is useful for simulating pathologies of the heart and studying their effects on circulation.

Since both pump control and acquisition of the data generated by the CPD has become computerised, users have come to expect all variables such as pressures, flow rate, fluid temperature and pump parameters to be monitored in real time and easily logged. Due to the complexity of the requirements dictated by PHV testing standards, it has further become necessary to process this data using computers. As a result, many manufacturers integrate software to perform automated analysis of the data and produce the necessary statistical reports into the control software. Typically, the analysis software performs the necessary calculations and displays valve performance indicators on a cycle to cycle basis. These include mean and root mean square (RMS) flow rates, mean arterial pressure (MAP), mean pressure difference across the valve, effective orifice area (EOA) and regurgitant volume, among others [46, 62]. Thus, a large part of the functionality of modern CPDs lies in the monitoring, analysis and reporting software that has come to form a standard part of CPD systems.

Table 2.1 shows commercially available CPD systems and their general capabilities. All the models shown provide the user with the ability to program and execute custom waveforms. While all of the systems are modular to some extent, some manufacturers (not included in Table 2.1) such as Shelley (Shelley CardioFlow 5000 MR) and Harvard Apparatus (Harvard Apparatus 1400 Series) only provide the pump and the user must supply the mock circulatory system. Some manufacturers listed in Table 2.1 produce several models of CPDs which are more focused on the development of certain devices. BDC Laboratories, for example, provides three different models of CPDs and pumps, each tailored to the development of a specific range of technologies: the PD-1100 (employed in the flagship HDT-500 CPD) is used for driving cardiovascular networks for the purpose of device testing and validation (pressure or flow measuring catheters, for example), the PD-0750 is intended for cardiac valve development and the PD-0500 for endovascular and vascular devices (balloons and stents, for instance) [63]. Besides the commercial CPD systems shown in Table 2.1, there are a few prominent academic projects which are often cited in published studies: the Sheffield University CPD, the RWTH Aachen Cardiovascular Engineering Pulse Duplicator and the Yoganathan-FDA pulse duplicator. Chew *et al* provide a description of each of these systems [47].

Table 2.1: Commercially available CPDs.

	**ViVitro Pulse Duplicator System**	
	Circulatory simulation	Lump parameter
	Heart rate (bpm)	3-200
	Flow rate (L/min)	0-15
	Stroke volume (mL)	0-180
	Drive technology	Servomotor driven piston pump
	Special features	• Preinstalled physiological waveforms
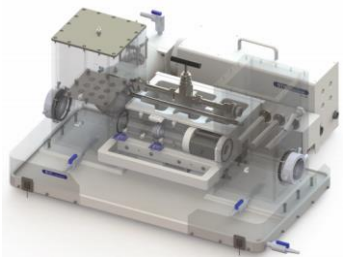	**BDC HDT-500**	
	Circulatory simulation	Lump parameter
	Heart rate (bpm)	2-240
	Flow rate (L/min)	0-10
	Stroke volume (mL)	0-300
	Drive technology	Not reported
	Special features	• No need to empty system to change test valves
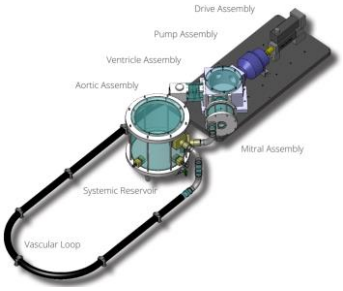	**Dynatek Labs MP3**	
	Circulatory simulation	Lump parameter, Wave propagation
	Heart rate (bpm)	Not reported
	Flow rate (L/min)	1-10
	Stroke volume (mL)	Not reported
	Drive technology	Servomotor or stepper-motor driven piston pump
	Special features	• No need to empty system to change test valves
	**MITL Modular Pulse Duplicator**	
	Circulatory simulation	Lump parameter Wave propagation
	Heart rate (bpm)	30-240
	Flow rate (L/min)	Not reported
	Stroke volume (mL)	100mL
	Drive technology	Linear voice coil actuator
	Special features	• Complete modularity and customisability

2.4 Significance and applications of CPDs

From their crude beginnings CPDs have played a crucial role in cardiovascular research. Over six decades ago they opened the window to the heart by allowing researchers to observe its internal components in action. Since then, they have been a vital tool that has deepened the understanding of the circulatory system and facilitates the development of most cardiovascular devices. Despite the extensive knowledge they facilitated in this subject since their use began, CPDs are still in widespread use for studying physiological phenomena [64] and the effects of pathologies [65] in the cardiovascular system. The effort to better predict and analyse the response of the cardiovascular system is on-going and CPDs are extensively used in order to develop, improve and validate mathematical models [66, 67, 68].

The main application of CPDs is in PHV development and testing. Areas of use in this field include validation and optimisation of the design as well as approval and certification of the final PHV design [22, 26, 69, 70], studies of leaflet kinematics [27, 71, 72] and generation of data for numerical simulations [23]. Further aspects of valve development in which CPDs play a role include valve leaflet tissue engineering and assessment. There is a growing interest in tissue engineered valves because they combine the best features of mechanical and bioprosthetic heart valves. Using this approach entails producing a valve leaflet scaffold which is seeded with stem cells and then placed in a bioreactor that stimulates the cells' development by exposing them to the target physiological environment (a CPD) for a period of time before being implanted [73, 74, 75, 76]. Besides leaflets, vascular grafts (prosthetic arteries or veins) are also grown in a similar fashion [77].

Furthermore, CPDs play a critical role in the field of implantable device development other than valves. An example is the development of ventricular assist devices and artificial vasculature devices. The former works by helping the ventricle to pump blood into the aorta while the latter is inserted in the aorta and actively modifies the afterload perceived by the ventricle. CPDs are used to help develop and test both the algorithms that control these devices and the operation of the device [78, 79].

Less frequently reported uses for CPDs include the development of non-invasive cardiovascular monitoring devices [80] and exploring new endovascular procedures [81]. Segers *et al* [36] sum up the potential uses of a CPD as testing valve prostheses, cardiovascular grafts, stents, cardiac assist devices, as well as performing valve studies and the validation and calibration of medical technology and measurement methods. The key point is that, through their various applications, CPDs have made enormous contributions to the field of cardiovascular research and medical technology which ultimately have led to a great improvement in the life expectancy and quality of life of millions of people around the world.

2.5 The development of CPDs and challenges

CPD design will always be a compromise between a simulation of the ideal physiological environment and the practicality of testing. However, there are three basic requirements for a CPD to recreate a realistic environment in which to test valves [47]. A CPD must:

1. generate physiological flow waveforms through the valves.
2. have an appropriately shaped representation of the left heart and aortic root.
3. use a test fluid (blood analogue) which has the same viscosity as blood.

The first requirement above is fulfilled by accurately replicating the action of the ventricle (by means of, for example, a servo motor driven piston pump as mentioned in Section 2.3) and the simulation of the effects of the arterial tree (using a lump parameter model, for example, as explained in Section 2.2) respectively. The second requirement must be built into the geometric design of the system. The third requirement dictates that the elements in the second requirement (left ventricle, left atrium and aortic root) must be to a scale of approximately 1:1. Since blood is non-Newtonian, its behaviour differs when flowing in small diameter vessels compared to when it flows within the heart. However, due to their size, it behaves as a Newtonian fluid in the heart and aorta. It is therefore important to maintain this scale so that its non-Newtonian effects can be ignored [47].

Noting the above conditions should pave the way for a good CPD design. However, despite doing so problems can still arise due to the large number of secondary design variables. The most common challenges in creating a realistic physiological environment are related to the generation of the correct flow waveform through the valves and obtaining the appropriate afterload conditions [82]. Krynauw [28] reported that building a system to serve the purposes of both a hydrodynamic and a high speed fatigue tester is not practically achievable. The parameters of the physical implementation that leads to good pressure and flow waveforms at physiological heart rates diverge from those that would work for testing at high speeds. Part of the reason for this is that to minimise uncontrollable resistance for hemodynamic testing, the use of large diameter pipes is an attractive alternative. However, this has the effect of increasing inertance which plays an increasing role as heart rate increases. The extra inertance created by the large volume of fluid in the pipes is not controllable and is undesirable for accelerated fatigue testing. As can be seen in Table 2.1, most commercial CPD systems intended for hydrodynamic testing limit the heart rate to a maximum of 240 beats per minute (bpm). Krynauw also noted that pressure measurements are highly sensitive to changes in peripheral resistance. This means that the peripheral resistance must be controlled in a very fine, accurate and repeatable manner, which may require the design and manufacture of a specialised device for this purpose.

Another important design consideration with a significant effect on the pressure and flow waveforms is ventricular compliance. Ventricular compliance refers to the elastic nature of the ventricles which not only helps absorb pressure spikes but also slows down the rate of change of pressure [28, 83]. Pressure spikes are caused by pressure wave reflection, water hammer and resonance but can be controlled by compliance [44]. Besides pressure spikes, the rigidity of the components in modern CPDs causes pressures to oscillate after rapid movement of the ventricle. These effects are most noticeable during valve opening and closing, particularly if the ventricle and its outflow tract are stiff [83]; the stiffer the system the higher the frequency of the pressure oscillations. Figure 2.7 clearly shows the

effects of ventricular compliance: reduced high frequency pressure oscillations and a less steep pressure gradient without changing the basic morphology of the waveform.

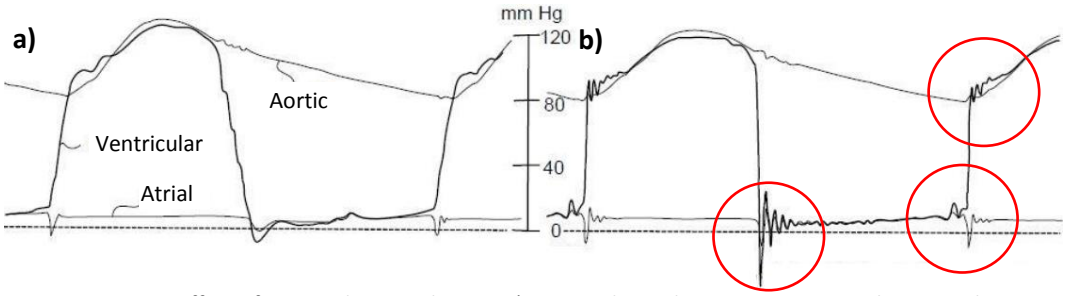

Figure 2.7: Effect of ventricular compliance. a) Ventricular and aortic pressures with ventricular compliance; b) ventricular and aortic pressures without ventricular compliance. The circled regions highlight the damping effect of ventricular compliance. (Adapted from [84]).

Most successful CPD systems implement some form of ventricular compliance. This is normally achieved by using an enclosed volume of air, similar to the way that aortic root compliance is implemented. Ventricular compliance is closely related to fluid isolation and they are often implemented together. Fluid isolation refers to the separation of the fluid to which the test sample is exposed and the fluid with which the pump components are in contact. There are various advantages to fluid isolation which usually takes the form of a flexible diaphragm:

- The working fluid does not need to be a saline solution. This reduces the possibilities of corrosion of the pump components which in turn leads to more relaxed requirements for material selection of these components.
- The amount of test fluid, which must be monitored more closely and replaced more often, is reduced.
- Seeding of the test fluid for PIV measurements poses no risks to pump seals and components subjected to friction.
- Using a flexible diaphragm to achieve isolation provides the perfect opportunity to create an anatomically correct shape for more natural flow within the ventricle.

Since CPDs are complex systems with so many design variables, their successful development requires experience and expertise. Fraser, of Vivitro Labs Inc., cites ten reasons to obtain a commercially available CPD instead of developing one in-house [85]: i) ease of use, ii) reliability, iii) availability of spares, iv) reputation, v) qualification, vi) training, vii) cost, viii) flexibility, ix) consistency and x) aesthetics. Each of these reasons can be taken as a point of advice to help shape the final product. Of these, reliability, flexibility, consistency and ease of use should be of primary importance as they will facilitate qualification (trustworthiness of calibration and device accreditation) and reputation (extensive use of the device and positive reports from the research community). Since they are critical to the success of a CPD design, they are further explained below:

- Reliability: CPDs are often operated with saline solution, which is corrosive. All the materials employed should take this into consideration to limit unexpected failures. Software should be built robustly and operated within a stable

environment as there may be a need to record repeatability many hours apart. Data acquisition and control systems should have good noise immunity.

- Flexibility: Ideally, a CPD should be built in a modular fashion so that more capabilities can be added in future if needed. This may include accessories for simulating valve delivery for transcatheter designs. The design of the test valve section should allow for a variety of valve types to be tested.
- Consistency: This refers to the ability of a system to produce repeatable results. This also applies to different systems of the same design. In other words, two different CPDs using the same theory of operation or circulatory system simulation should be able to produce the same pressure and flow waveforms for a given valve even if their implementation differs.
- Ease of use: This does not only refer to the hardware but also to the software. It should be easy to set up tests and swap test valves. The software should clearly display the relevant monitoring and control parameters as well as provide safety measures throughout the test.

A design that overlooks the above will likely result in a product with reduced service life, frequent modifications, unexpected costs or lack of credibility.

2.6 Guidelines for the assessment of CPDs

Given that the primary role of CPDs is PHV testing, their design requirements have been broadly described by the ISO5840:2005, Annex L.4 (Pulsatile-flow testing) [29]. While the Food and Drug Administration (FDA) had its own recommendations concerning *in vitro*, animal and clinical testing requirements for heart valve replacements, it now invokes the relevant ISO5840 standard with regards to all *in vitro* testing, which includes the guidelines for test apparatuses [86]. Annex L.4 indicates that the performance of a CPD should be evaluated by testing a reference PHV. As a result, while it is possible to evaluate certain components of the CPD individually from a technical point of view (discussed in Chapter 3), the overall performance of the device must be assessed by testing a reference valve and comparing the results obtained to those available in literature. A valve's hydrodynamic performance is assessed at three phases of the cycle: forward flow, closing phase and closed phase. The main parameters of interest are the pressure difference across the open valve for the duration of the forward flow phase and regurgitation volume for the closing and closed phases [47]. The following valve performance parameters help describe the operation of the valve and are normally reported: peak systolic pressure difference, mean systolic pressure difference, total regurgitant volume, valve leakage volume and effective orifice area [87, 88]. They can be used to compare a CPD's ability to recreate physiological conditions to an ISO5840 certified CPD.

Annex L.4 of the ISO5840:2005 standard also explains the functional requirements for the CPD, provides accuracy limits for the measuring equipment and suggests test conditions and parameters. A summary of the contents that should be included in the test report for cardiac valve prostheses offers information on features that should form part of the CPD's control and analysis software. The most important requirements are summarised below, in Table 2.2. Table 2.3 details the pressures and other cardiac parameters that the CPD should be capable of achieving while fulfilling the requirements described in Table 2.2.

Table 2.2: ISO5840:2005 requirements for cardiac pulse duplicators.

Accuracy	Pressure	±2 mmHg
	Flow	±2 mL
	Other	±5 % of full-scale
Functionality	Produce pressure and flow waveforms that approximate physiological conditions over the required physiological range.	
	Permit measurement of time-dependent pressures, volumetric flow rates, velocity fields and turbulent shear stress fields.	
	Allow the repeatability of the test system to be evaluated and documented.	
	Simulate the relevant dimensions of the cardiac chambers and vessels.	
	Allow the observer to view and photograph the PHV at all stages of the cycle.	
	Simulate relevant cardiac chamber compliances.	

Table 2.3: Operational environment parameters for aortic PHVs. (Adapted from [29]).

Parameter	**Values**		
Temperature	34-42 ^{o}C		
Heart rate	30 – 200 bpm		
Cardiac output	3 – 15 L/min		
Stroke volume	25 – 100 mL		
Blood pressure according to condition	Arterial peak systolic pressure (mmHg)	Arterial minimum diastolic pressure (mmHg)	Differential pressure across closed aortic valve (mmHg)
Hypotensive	60	40	50
Normotensive	100 – 130	65 - 85	95
Hypertensive			
Stage 1 (mild)	140 - 159	90 – 99	123
Stage 2 (moderate)	160 - 179	100 – 109	138
Stage 3 (severe)	180 – 209	110 - 119	155
Stage 4 (very severe)	> 210	> 120	185
Extreme (expected maximum for single cycle)	300	160	230

3 Materials and Methods

3.1 Existing apparatus

3.1.1 Apparatus description

The BERG CPD was based on a modified version of Krynauw's design which was extended, by replicating the test lines, to test up to four valves simultaneously. In-depth details related to the design of this CPD can be found in Knynauw's thesis [28] but a brief description of the basic physical layout and function follows.

The CPD used a lump parameter model for simulating afterload with pulsatile flow generated by a piston pump driven by a cam. The piston rod interacted with the cam via a roller follower which was kept in contact with the cam by means of a strong spring. The shaft carried four cams (one for each test line) and was connected to a standard 4-pole alternating current (AC) induction motor by a belt with a 2:1 reduction ratio. A variable speed drive was used to adjust the speed of the motor which controlled heart rate. Each test line consisted of a cam, the piston pump assembly, a mitral valve in the inlet side of the pump (coming from the fluid reservoir) and a test section (at the outlet of the pump) comprising the aortic valve test chamber, compliance chamber, the fluid return line and peripheral resistance control in the form of a ball valve. Figure 3.1 and the following labels supplement this description. *a:* motor; *b:* pulley and belt; *c:* cam, follower and spring of piston pump; *d:* piston pump; *e:* pump inlet with mitral valve; *f:* aortic valve chamber (providing optical access and pressure measurement points); *g:* peripheral resistance control; *h:* compliance chamber; *i:* fluid reservoir.

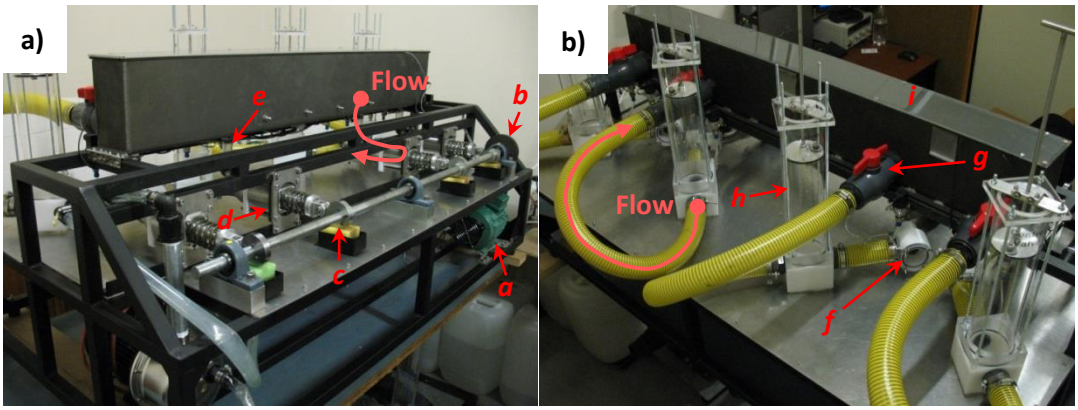

Figure 3.1: BERG CPD at the start of this project. a) Test section; b) pump section.

The test fluid used is a blood analogue consisting of 48% glycerol and 52% water by mass with sodium chloride added to form a 0.9% final saline solution. This mixture is kept at a constant temperature of 37 °C (+-0.2 °C) using a Delta DTA (Delta Electronics, Taiwan) proportional-integral-derivative (PID) temperature controller, a resistance temperature detector (RTD) PT100 sensor and two 300W RS Components (RS Components, Corby, United Kingdom) submersible heaters mounted among five HT HJ-541 submersible pumps to maintain even temperature distribution in the reservoir. When the system is at a steady state temperature of 37 °C this blood analogue results in a viscosity of 3.57×10^{-3} N·s/m^2 and specific gravity of 1 050 kg/m^3.

The software received at the commencement of this project provided a unified interface for machine control, acquisition and display of data. Controls let users set heart rate (motor speed), a time or number of cycles limit for a test, logging settings and safety pressures. Acquisition of pressures, cycle count (via an optical switch counting shaft revolutions) and fluid level (by use of a float switch mounted inside the reservoir) took place whenever the motor run. The interface also provided visual feedback for the ventricular and aortic pressures of all testing lines as well as maximum and minimum pressures of each line.

3.1.2 Problems identified

The system described had several limitations. The most relevant of those are summarised in Table 3.1 and discussed in the following paragraphs.

Table 3.1: Summary of problems and solutions to improve the original CPD.

Limitation	Consequence	Resolution
Rudimentary drive system.	Lack of adjustability, unreliable ventricular discharge.	Design a new drive system that would allow full ventricular motion control. (Sections 3.2.4.2 and 3.2.2.4)
Unknown cam design.	Difficulty in diagnosing measurement artefacts, inability to report parameters such as systolic duration, unknown ventricular discharge profile.	Obtain numerical cam profile by means of an experiment, design a new drive system that would allow full ventricular motion control. (Sections 3.3 and 3.2.4.2)
Inadequate data acquisition parameters.	Masking of real process conditions.	Acquire data at 1 kHz without any filtering. (Section 3.2.4.3)
Awkward lump parameter controls.	Difficulty in achieving the required test conditions, lack of repeatability.	Design a new resistive element, install a hand pump for aortic root compliance control. (Section 3.2.2.3)
Flawed test section geometry.	Non physiological flow and pressure phenomena	Design a new test section and LVOT. (Section 3.2.2.2)
Poor pressure tap design.	Unreliable pressure readings, Masking of real process conditions.	Design a new test section and LVOT, install pressure taps further from the test sample. (Section 3.2.2.2)

Drive system

The most evident limitation was the cam drive system. Because the piston was driven by a cam, not only was the stroke volume fixed but it was also impossible to control the ventricle outflow curve. This prevented any fine tuning to eliminate pressure spikes or

adjustments to the systolic fraction. However, the biggest drawback of having a predetermined stroke volume is the limitation imposed on the size of valves that can be tested. A stroke volume that is too large (for a healthy valve at a normal heart rate) produces uncontrollable pressure spikes and a strong stenotic effect manifested as a misleading high transvalvular pressure gradient. A further problem of the drive system was uneven rotational speed due to the sharp cam profile. Even though the cams were phased at 90^{o} from each other, there was a large variation in the torque requirements through one revolution of the shaft resulting in uneven rotational speed as the motor speed control was not a closed loop system and there was no flywheel. This was exacerbated by the motor operating at its torque limit while testing at physiological heart rates. Since the cam profile represents a time dependent process, the uneven speed defeated the purpose of the profile design causing a slower systole (larger systolic fraction) and a very abrupt diastolic phase. It was also found that at heart rates above 160 bpm the cam follower would lose contact with the cam at the beginning of the diastolic phase, knocking against it when it eventually caught up. To address all of these drawbacks it was decided that a new system, allowing customisable ventricular motion, should be employed. The design and implementation of the final system are detailed in Section 3.2.2.1.

Cam

The cams used to actuate the ventricle pumps were replicated from Krynauw's design but there was no detailed information (a mathematical model or numerical data) available to accurately establish their displacement profile. One of the hypotheses for the sharp pressure spike at the beginning of systole was that the slope of the cam profile was too steep (especially for a system without ventricular compliance) but there was no way of knowing the instantaneous velocity or acceleration of the piston. To establish these parameters, the experiment in Section 3.3 was set up to measure the cam's displacement. The experiment produced a numerical profile that could be used to analyse the operation of the cam and as a starting point to the user generated ventricular volume waveform used by the system above.

Sampling rate

The pressure sampling rate was too slow. The original data acquisition software used the following equation to determine the sampling rate:

$$\boldsymbol{n_{S/s} = \frac{Speed_{bpm}}{60} \times 300} \quad \text{if} \quad \boldsymbol{Speed_{bpm} < 200bpm} \qquad (1)$$

For testing at the ISO5840:2005 recommended heart rate of 70 bpm, this equation yields a sampling rate of 350 Hz. Also, a low pass filter with a cut-off frequency of 15 Hz was applied to the acquired data before being displayed and logged. Though the acquisition rate was similar to the rate of 400 Hz reported by Liu *et al* [89], the low pass filter cut-off frequency is very low when compared to the value of 60 Hz used by Liu. Further, it was found that among the modifications made to the software after the CPD was expanded to three testing lines the calculation for the sampling rate was bypassed and a fixed rate of 250 Hz used for all heart rates. The combination of slow sampling speed and strong filter masked several features of the physical process. Sampling at a 1000 Hz without any filters revealed many non-physiological characteristics present in the data as well as high frequency oscillations superimposed on the pressure waveforms. Through this process the real amplitude of the ventricular pressure spike was found to be much higher than

reported. It was thus decided that a sampling rate of 1000 Hz would be used to acquire data, and a low pass filter with a minimum cut of frequency of 60 Hz to display and perform any numerical analysis on the data, where necessary. Some results pertinent to the original configuration are included in Section 4.6.

Lump parameter controls

As can be seen in Figure 3.1, the return line which connects the compliance chamber and the peripheral resistance control is a 1m long, two inch diameter hydraulic pipe. Because this pipe precedes the peripheral resistance in the hydraulic loop, it introduces a large inertance component at higher speeds when peripheral resistance is decreased. Since there is no way of varying the amount of fluid inside the pipe, there is no way of adjusting the inertance. Another problem in this configuration was the choice of peripheral resistance control. The large ball valve proved to be difficult to operate in that it was impossible to finely adjust its opening. These two problems were overcome by designing a precision resistance valve which was mounted directly onto the new compliance chamber (discussed in Section 3.2.2). Moving the resistance control to the compliance chamber means that the fluid return to the tank is on the venous part of the circulatory system so it does not have a significant influence on the pressures measured in the arterial section.

The compliance chamber did not provide a means to reintroduce air once it was released. This made it extremely difficult to tune the compliance because if too much air was released the system had to be stopped and air reintroduced into the chamber by means of pressure equalisation after moving the plunger all the way to the top of the chamber. This was solved by the simple addition of a hand pump tapped into the plunger.

Test section geometry

The design of the aortic valve chamber was the source of a number of flow and pressure problems. Figure 3.2 shows the configuration of the valve chamber with blue arrows indicating the direction of flow and the red arrow showing the path the pressure wave must follow to reach the aortic pressure transducer. With a normal cardiac output of 5 L/min, this setup will cause the test fluid to crash into the viewing window at a right angle at approximately 1.5 m/s during systole. This will lead to highly turbulent flow into the outlet to the compliance chamber. However, the pressure wave that arrives at the window will be reflected into the test valve tube and interfere with the pressure readings and valve leaflet operation. This is primarily due to the short distance between the valve tube and the viewing window.

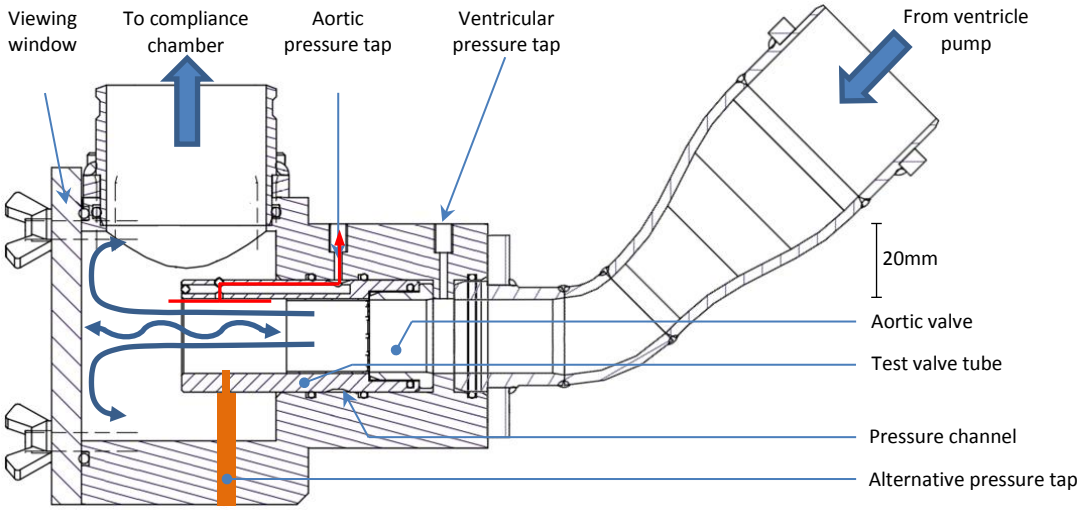

Figure 3.2: Original aortic valve chamber and inlet.

Pressure taps

Besides the problems associated with the flow characteristics of the chamber, the choice of location for the pressure taps was poor for several reasons:

- Given the inlet geometry (diameter reduction and 45° bend), the flow velocity profile at the ventricular pressure tap will not be symmetrical and turbulent flow will be experienced.
- The ventricular tap was too close to the valve. If a valve slightly smaller than the valve tube diameter is used then the tap is in the turbulent region of a sudden contraction, producing unreliable pressure measurements.
- The aortic tap was too close to the end of the test valve tube. The end of the tube represents a sudden expansion and with the flow behaviour previously described this tap is in a highly turbulent location. Also, it is likely that this section will experience bidirectional flow due to valve regurgitation (especially with a valve that is being developed) and under these circumstances the interfering effects of the sudden contraction and nearby turbulence outside the tube will be more prominent than with forward flow.
- The path from the aortic pressure tap to the transducer is too convoluted and contains sharp bends. Since the valve tube can be rotated within its bore in the valve chamber, should it not be perfectly aligned the pressure may have to be transferred to the port via the channel (refer to Figure 3.2), potentially along half the circumference of the valve tube. Therefore, pressure waves generated by the highly dynamic process of pulsatile flow and valve operation are attenuated along this tortuosity, masking the high pressure spikes and oscillations to which the test valve is really being subjected. This was proven by tapping directly on the opposite side of the valve tube through the wall of the valve chamber (shown as alternative pressure tap in Figure 3.2).

It should be noted that this valve chamber and inlet design is not Krynauw's. The CPD is known to have gone through two major revisions between the time that Krynauw's project was concluded and the start of this project. The valve chamber described above was implemented during the first revision in which two test lines were added to the CPD.

This arrangement is not representative of normal anatomy, as required by the ISO5840 [29], and given the various problems it presented it was decided to change it. A new ventricle outflow tract, valve test section and compliance chamber were designed and manufactured. The particulars of this new setup can be found in Section 3.2.2.

3.2 System development

3.2.1 Requirements and constraints

Apart from the requirements set out by the ISO5840:2005 (discussed in Chapter 2.6) and in line with the aims stated in Section 1.2, a number of other features were desired. Of primary importance were independent control of heart rate and cardiac output, as well as immediate presentation of raw data and valve performance indicators. Addressing the existing issues identified in the previous section such as the precision of the peripheral resistance, inertance control and sampling rate was also deemed essential.

Before any conceptualisation work was done, a number of design decisions were taken:

- Only one test line would be implemented, in line with commercial CPDs.
- The piston pump assembly would be reused but without the cam follower section.
- The control, monitoring and logging software would be completely rewritten.
- All the instrumentation from the existing setup (sensors, heaters and temperature controller) would be reused.

3.2.2 Mechanical design

3.2.2.1 Pump drive system

One of the most important aspects of this project was to redesign the ventricle pump system; as a result, a number of concepts were devised and explored. Three of them were chosen for final consideration. To objectively select the best concept, six criteria were identified to assess each concept and a weight was associated to each criterion. Each concept received a rating from 1 to 3 for each criterion (1 = low, 2 = medium, 3 = high) and the weight associated to each criterion was also assigned a value between 1 and 3 (1 = light, 2 = medium, 3 = heavy). The actual score for a criterion was the product of the rating and the weight. The final score for a concept was the sum of the weighted score of each criterion. The criteria (and weights) were:

1. Flexibility (3): Flexibility was a measure of how easily the system could reproduce different ventricular conditions. This was the main objective of the new drive system so it carries a heavy weight.
2. Efficiency (1): Efficiency considered the entire drive system: the source of power and power conversion. The rationale for assigning a low weight to efficiency was that CPDs, unlike durability testers, do not run for long periods of time.
3. Accuracy (3): Accuracy contemplated not only the smallest change the system was capable of achieving but also the ability to validate its effect. These are two important aspects of a device used for laboratory tests so it received a heavy weight value.
4. Ease of implementation (2): This is an indication of the difficulty and total amount of time required to design, build and control the system.

5. Ease of manufacture (2): This refers to the overall manufacturing effort, not only how easy it is to machine a part. Therefore, a concept with a large number of parts, even if they were easy to make, would have scored a low value.
6. Overall cost (3): This includes the cost of manufacture and raw materials. As the project had very limited financial resources cost carried a heavy weight.

Only solutions with rotary motors as their source of power were included in this analysis. Obtaining the resolution, accuracy and speed required for this application using pneumatics could have proven unachievable as shown by a similar application [90] and compressed air is often not readily available at many locations limiting the availability of the CPD itself. This decision was reinforced by the fact that no commercially available CPD system could be found that uses pneumatics. The preferred choice would have been a linear voice coil actuator, as utilised by the commercial MITL Modular Pulse Duplicator [91], but such a system was not within the financial reach of the project, especially after accounting for power source requirements and a feedback device.

Swash plate

This concept was the cheapest because it is run with a standard motor controlled by a simple and inexpensive variable speed drive, both of which were part of the existing system. However, the manufacturing effort was great and it had a high component count. This meant that although it only required a motor to rotate in one direction (resulting in high efficiency and a low cost source of power) overall cost was medium due to manufacturing expenses. The flexibility of the system was low because it would only have been possible to generate sinusoidal waves and although the SV could be adjusted it would have required stopping the motor and making manual adjustments with screws and counter nuts. Accuracy was compromised due to the difficulty of making precise changes to the SV and implementing a feedback system to measure pump position. While only very basic programming would have been necessary, the detailed mechanical design and construction required significant effort so ease of implementation was average. A model of this concept can be seen in Figure 3.3.

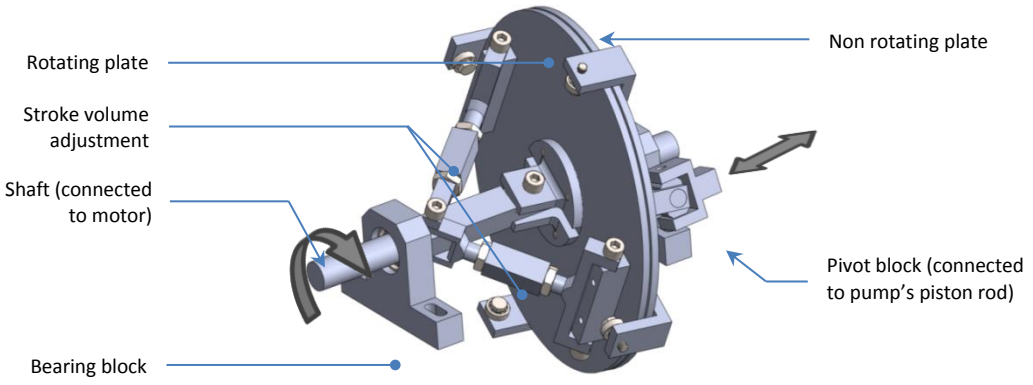

Figure 3.3: Swash plate pump drive system concept.

Ball screw

This concept provided full flexibility through the use of a servomotor. Using the servomotor's shaft encoder as position feedback in combination with a ball screw and

anti-backlash nut ensured excellent accuracy. Since the ball screw drive (shown in Figure 3.4) is made up of basic components, manufacturing and assembly was simple and quick. On the other hand, implementing a highly dynamic motion controller to accurately control the servomotor required careful software design and complex, efficient programming. This offset the advantages of an easy build so the ease of implementation was medium. While the efficiency of this setup can be improved by careful selection of the ball screw pitch, it will never be high because the servomotor is constantly changing direction with high accelerations. This also meant a highly dynamic servomotor and controller was required which represented a much greater cost than a simple variable speed drive as required by the swash plate concept. However, the ability to make small adjustments to the system's operating parameters on the fly made this the concept of choice.

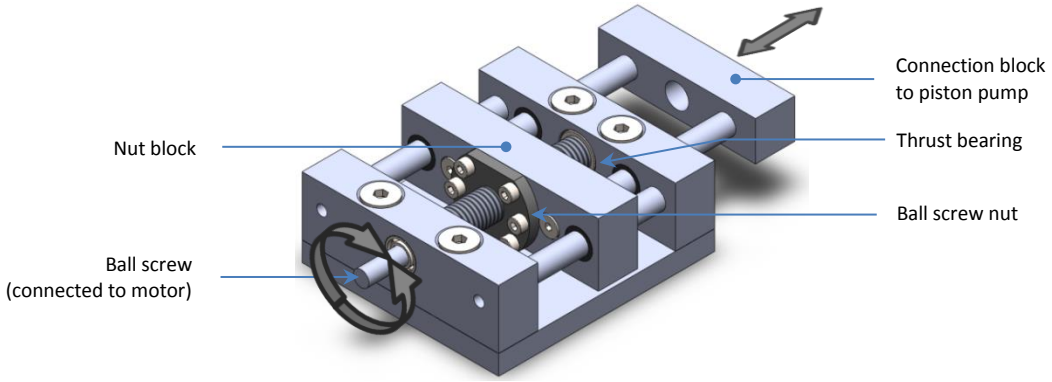

Figure 3.4: Lead screw pump drive system concept.

Electric cylinder

Very similar to the ball screw concept, an electric cylinder (e-cylinder), shown in Figure 3.5, is a high end servomotor and ball screw packaged as a compact and robust linear actuator. It presents the same characteristics of the ball screw concept but with only minimal manufacturing required for mounting. The cost, however, is the highest of all concepts.

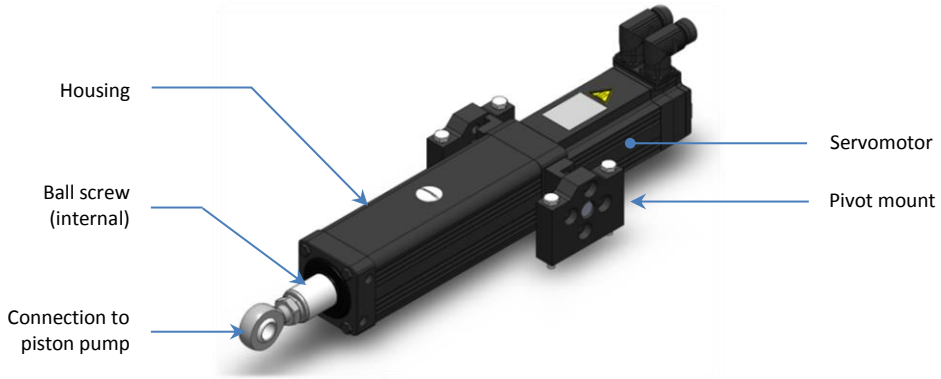

Figure 3.5: SEW CMS50M (150mm stroke) electric cylinder.

Summary

Table 3.2 summarises the evaluation of the different concepts considered for the pump drive system. Based on this assessment the ball screw was the better choice. However, when an electric cylinder together with a suitable motor controller became available to

the project it was chosen instead because implementing it required very little manufacturing and it represented no direct expenses. The electric cylinder used was a SEW CMS50M with 150mm stroke (CMS50M/KY/RH1M/SM1, SEW Eurodrive GmbH & Co KG, Bruchsal, Germany) controlled by a SEW MoviDrive MDX61B.

Table 3.2: Summary of concept comparison.

	Flexibility	Efficiency	Accuracy	Ease of implemen-tation	Ease of manufac-ture	Cost	Weighted total
Weight	3	1	3	2	2	3	42
Swash plate	Low	High	Low	Med	Low	Med	21
Weighted	3	3	3	4	2	6	
Ball screw	High	Med	High	Med	Med	Med	34
Weighted	9	2	9	4	4	6	
E-cylinder	High	Med	High	Med	High	High	33
Weighted	9	2	9	4	6	3	

3.2.2.2 Aortic root compliance chamber and optical access

A new aortic root compliance chamber was designed in order to facilitate better flow and avert the pressure wave reflections created between the piston and the viewing window. The new design eliminated the aortic valve chamber and modified the flow pattern inside the compliance chamber with the aim of solving some of the problems highlighted in Section 3.1.2. The internal diameter of the chamber was kept the same as the original compliance chambers so that the tube and plunger could be reused. To control the volume of air within the compliance chamber a hand pump from a blood pressure arm cuff was installed on the plunger, making it easy to introduce or release air. Pressure taps were positioned on the ventricular and aortic sides of the valve and connected to Wika A-10 1 bar pressure transducers (WIKA Alexander Wiegand SE & Co. KG, Klingenberg, Germany). The pressure taps were positioned at a distance of 50 mm from the valve to avoid taking measurements in potentially turbulent flow regions existing near the valve. See Figure 3.6 for a sectioned view of the compliance chamber and LVOT. The surgical aortic valve holder was designed in collaboration with Mr Kyle Davis of the BERG.

Since at the time of redesigning this part of the CPD ventricular compliance was not being considered, the geometry of this section was specifically designed to reduce pressure wave reflections in the original layout of the CPD. This geometry resulted in difficult optical access to the valve being tested and in order to see the valve in operation a correction lens had to be designed and manufactured.

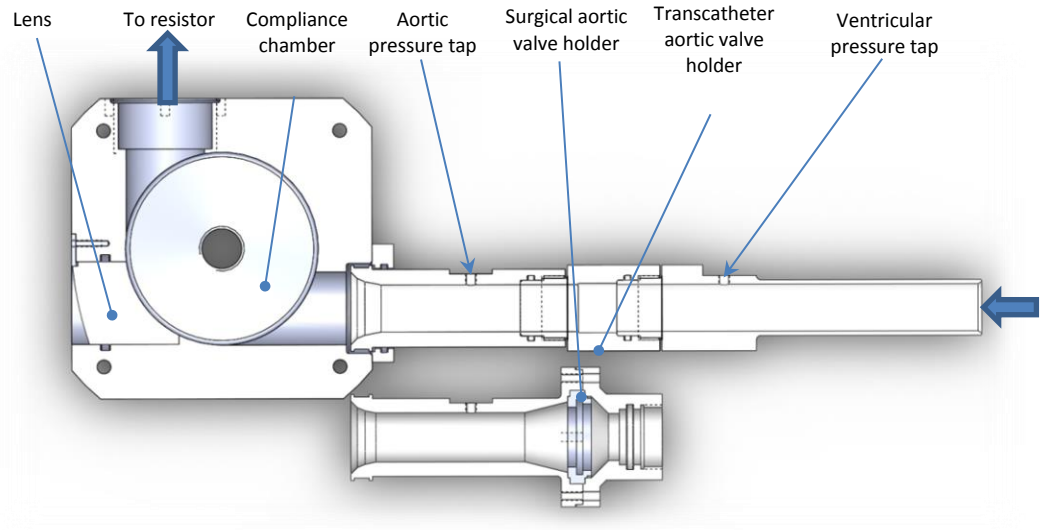

Figure 3.6: Section view of the new left ventricular outflow tract and aortic root compliance chamber.

The constraints for the lens design, which included a fixed radius for one of the faces, dissimilar indexes of refraction and space limitations, posed some unique challenges which led to certain compromises in the design. Each of the faces of the lens, which was made from polycarbonate, was cut on a computer numerically controlled (CNC) milling machine as a separate process and then polished by hand. Figure 3.7 shows the finished lens and the corrective optical effect. Note that in panels b) and c) the camera is very close to the face of the lens and the edge of the lens is not visible at all.

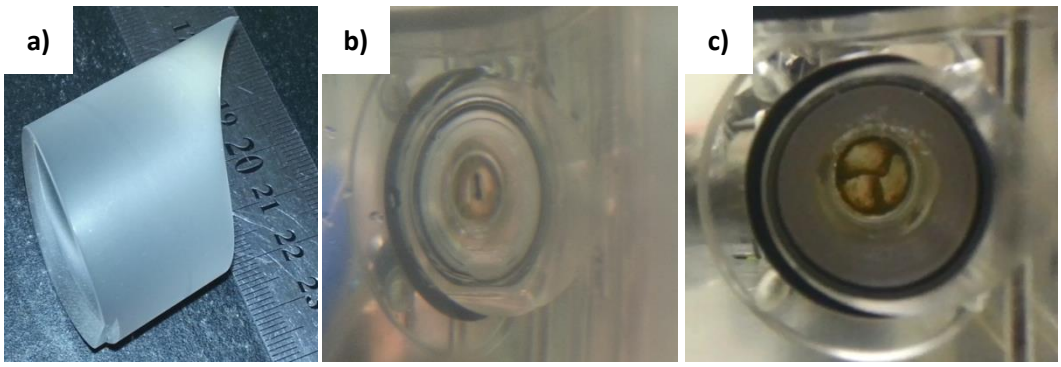

Figure 3.7: Optical effect of the corrective lens. a) the manufactured lens; b) view through the lens, the compliance chamber is empty; c) view through the lens, the compliance chamber is filled with blood analogue fluid.

3.2.2.3 Resistor

Since the original ball valve could not be operated accurately or with good repeatability, the device shown in Figure 3.8 was designed and manufactured to regulate flow. The design of the new resistor device is based on a needle valve and is such that when fully open the flow area is larger than the diameter of the tube on which the test valve is mounted (3.8 cm^2). The area open to the flow can be controlled by turning the needle until the flow is completely obstructed. This makes it possible to easily set the resistance

in a repeatable manner. Since the compliance chamber was designed not to reflect pressure waves, care was taken to ensure that the area of the resistor exposed to the compliance chamber did not present any surfaces against which waves could reflect directly. The design also considered the potential for future automation of the resistance setting so it provides an easy way to attach a motor to the needle.

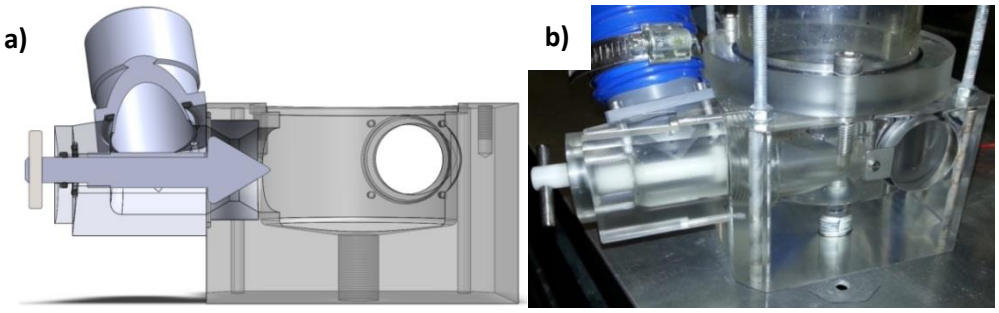

Figure 3.8: Resistor assembly. a) sectioned 3D model showing the internals of the resistor; b) the manufactured resistor mounted in position.

Krynauw recommended that the inertance be lowered and this was achieved by mounting the resistance control directly on the compliance chamber, eliminating the fluid volume of the pipes connecting the compliance chamber to the resistor. This has the greatest effect at low resistance values. Since the reservoir follows the resistor in this hydraulic loop, any flow after the resistor is considered venous so it does not have a significant influence on arterial pressure.

3.2.2.4 Fluid isolation and ventricular compliance

Fluid isolation was achieved by creating a flexible diaphragm from silicone. The shape of the diaphragm was modelled after the anatomy of the human ventricle, following guidelines from literature [92, 93] but scaled to fit to the piston pumps' end plates (refer to Figure 3.9 for dimensions). The dimensions were chosen to accommodate the piston pump's maximum safe stroke of 133 mL and care was taken to ensure that the end systolic volume, based on physiological values reported by Lang *et al* [93], also scaled appropriately.

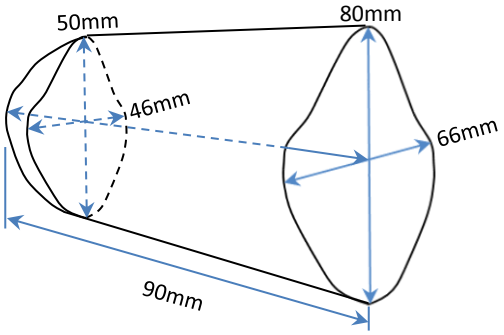

Figure 3.9: Ventricle dimensions.

The silicone ventricle was housed in a length of acrylic tube from an old compliance chamber contained between two end plates from old piston pump assemblies. One of the

old aortic valve chambers was repurposed as the ventricular compliance chamber and connected to the piston pump. The second outlet from the piston pump was connected to the ventricle through a ball valve to add resistance. Figure 3.10 depicts the physical installation.

The piston pump applies pressure to the outside of the ventricle causing it to collapse and eject the test fluid through the LVOT once the mitral valve is closed. The ventricular compliance is controlled by adjusting the volume of air in the chamber using two syringes connected to the chamber via three way valves. The working fluid is a solution of 20% glycerol and 80% distilled water, by volume. Glycerol is used as a lubricant for the pump seals.

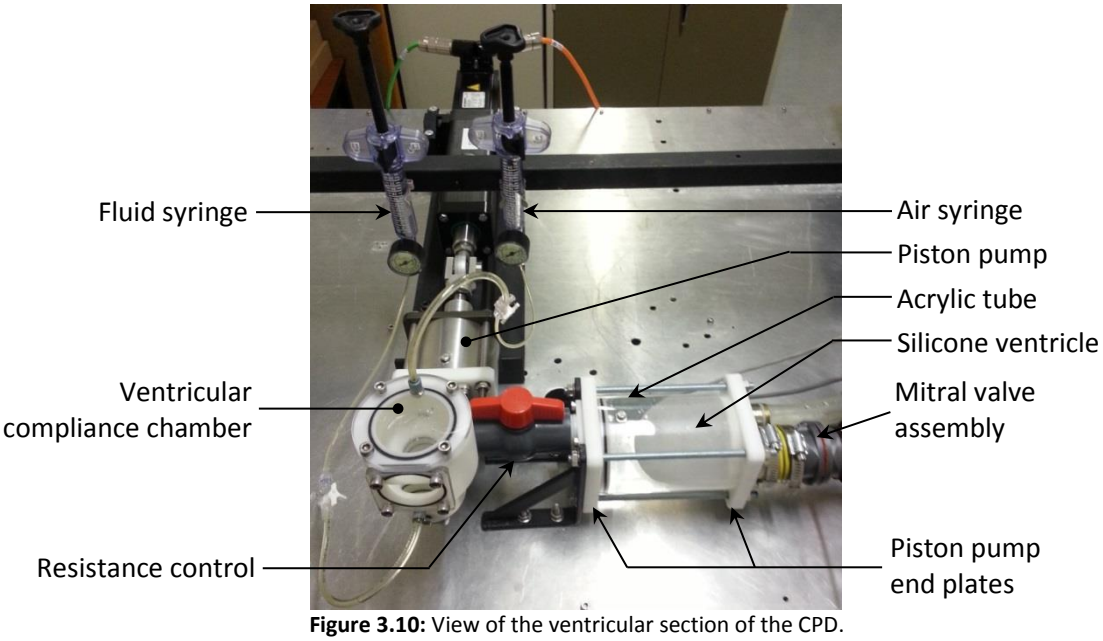

Figure 3.10: View of the ventricular section of the CPD.

3.2.3 Mechanical overview

Figure 3.11 is a diagrammatic representation of the CPD's new layout while Figure 3.12 shows the final embodiment of the CPD (in the image a PIV system is set up to visualise flow through the aortic tube). One of the old compliance chambers was repurposed as the reservoir. This greatly reduced the required test fluid volume (from approximately 26 L to 3 L) and heating time (from approximately 35 minutes to 18 minutes for a temperature change of 17 ^{o}C with the system running). This solution also allows the height of volume within the reservoir to be changed easily which can be used to adjust the mean atrial pressure. The number of heaters was reduced to one and since it is placed in an area of constant flow, the agitators were eliminated completely.

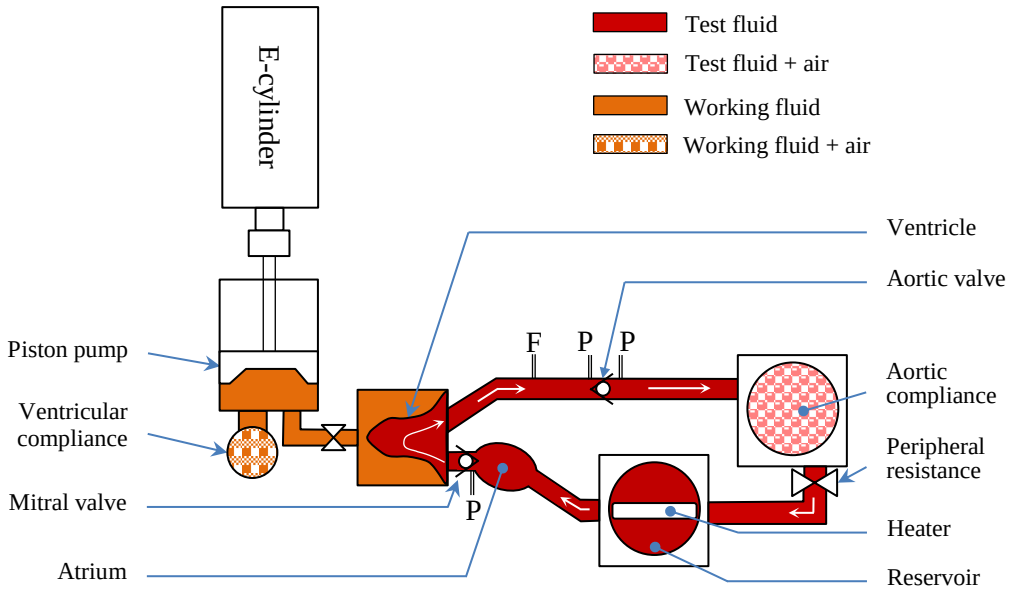

Figure 3.11: Physical layout of the CPD. F = flowmeter; P = pressure sensor.

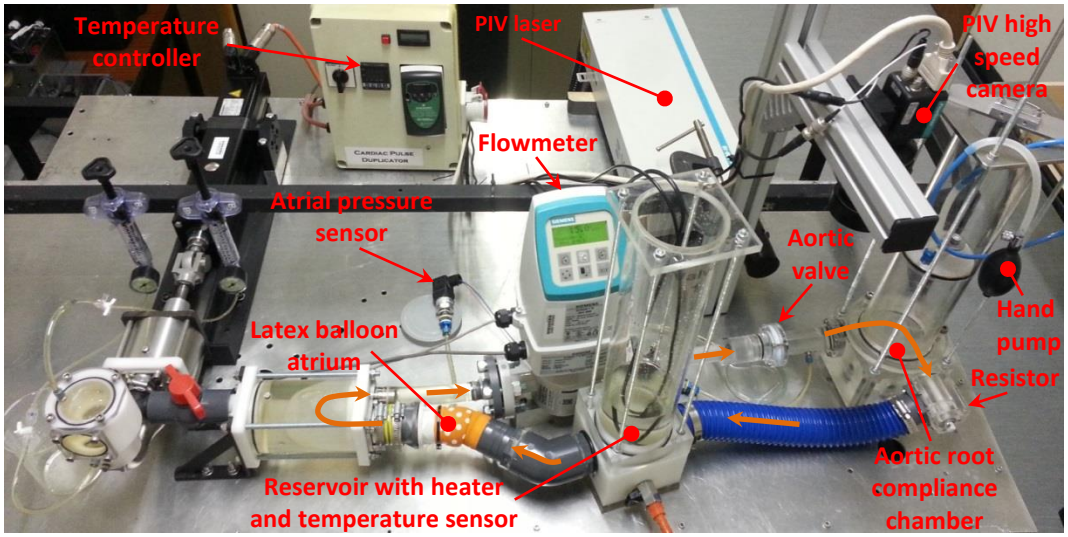

Figure 3.12: Final state of the redesigned CPD.

An atrium fashioned from a conventional latex balloon was positioned immediately before the mitral valve assembly. This acts as a buffer by quickly collapsing and supplying the ventricle with test fluid during diastole, reducing the inertial effects of the volume of fluid between the reservoir and the mitral valve. While the mitral valve is closed, the atrium fills at a rate determined by the height of fluid in the reservoir (mean atrial pressure). The mean atrial pressure can also be used to alter ventricular preload.

The electric cylinder's rod drives the original piston pump which pumps the working fluid. The pressure generated by the pump is manipulated through the ventricular compliance settings before it acts on the outer surface of the silicone ventricle. The volume by which

the ventricle collapses is the effective SV. The volume ejected through the aortic valve is dependent on the efficiency of the mechanical mitral valve (St Jude Regent 25AGFN-756, St Jude Medical, Minnesota, USA) so it may differ from the demanded SV. To compensate for this, a magnetic flowmeter (Siemens Sitrans Mag 5100W DN15 with a Siemens Mag 5000 signal converter, Siemens AG, Berlin, Germany) located between the ventricle and the aortic valve measures flow rate from which the actual volume ejected is calculated. After circulating through the aortic valve, aortic root compliance chamber and resistor the test fluid returns to the reservoir where the heater and temperature sensor reside.

3.2.4 Control strategy and software

Using an electric cylinder provided the opportunity to gain full control of the heart rate, SV and the shape of the ventricular discharge waveform so that the behaviour of different valve sizes under various operating conditions could be investigated. Modifying the ventricular discharge waveform not only allows a more realistic simulation of arbitrary cardiac conditions but also extends the functionality of the CPD beyond PHV testing to investigate, for example, the repercussions of some ventricular pathologies such as fibrillation or other types of arrhythmias.

To achieve the requirements set out in Section 3.2.1 it was decided to use National Instruments (NI) LabVIEW 2015 Full Development System (National Instruments, TX, USA) as the development software. The reason for this choice is manifold:

- LabVIEW integrates control, logging and process visualisation functions very well so it is ideal for this application which requires immediate visual feedback for tuning, logging of various process variables for analysis and fine control over a highly dynamic process demanding complex calculations.
- LabVIEW provides efficient communication mechanisms to facilitate interaction between the computer and the real time controller used for controlling the electric cylinder. From the available real time controllers a NI myRIO-1900 running LabVIEW RT (real time) was selected.
- LabVIEW has been used numerous times as the software platform for CPDs, both academically [89, 94, 95] and commercially [62, 96].

LabVIEW is a graphical programming language created and maintained by National Instruments which has been designed to enable easy interaction with data capturing and control devices as well as the creation of rich user interfaces. A program created in LabVIEW consists, in its most basic form, of a front panel and a block diagram. The block diagram is used to graphically code the processing by intuitively wiring functional nodes while the front panel serves as the user interface allowing the display of relevant data and user input. The front panel and the block diagram are intended to replicate a hardware instrument (for example, an oscilloscope) which has a front panel and internal processing hardware components connected by wires so LabVIEW programs are called virtual instruments (VIs). The software developed for controlling the CPD consists of a number of VIs residing both in the real time controller and a personal computer (PC).

3.2.4.1 Software Overview

Figure 3.13 gives an overview of how information flows between the various devices and helps understand the software architecture described in the following sections. The general design principle from a user point of view is PC based control so the PC runs the main user interface.

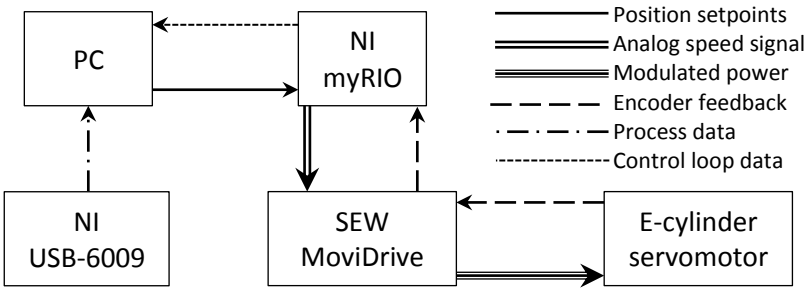

Figure 3.13: Information flow between the physical components of the system.

The PC and the real time controller communicate over a virtual Ethernet network using LabVIEW's Shared Variable Engine (SVE). This engine facilitates efficient and guaranteed data transfer thanks to both network and real time first-in-first-out (FIFO) buffers. The parameters used to describe the cylinder's motion, among other things, are transferred to the RT controller using this facility. The primary function of the RT controller is to coordinate motion timing and handle hardware controls. The software has been broken down into functional components for the purposes of discussion and each one is described in more detail in the following sections.

3.2.4.2 Ventricle pump control

The ventricle pump's motion was achieved through a cascaded feedback control loop approach consisting of two control loops: a speed control loop executed by a SEW MoviDrive (SEW MDX61B0015-5A3-4-00) following a position control loop developed for a NI myRIO[7] (myRIO 1900, National Instruments, TX, USA). The user can graphically design the motion pattern that the position control loop will perform. In the following subsections the software architecture related to the motion control is discussed. Figure 3.14 provides the framework for the discussion and highlights the data exchange that takes place to enable the ventricular pump motion. Each thick rectangle represents a hardware entity while the thin rectangles represent VIs running within those entities. Each major loop running inside a VI was assigned a descriptive name according to its function and is listed within its corresponding thin rectangle. The flow of data within and between loops is represented by arrows. Data communication crossing the boundaries of VIs was achieved through the SVE.

[7] The NI myRIO is a real time (RT) embedded controller incorporating an FPGA (Field Programmable Gate Array). The RT operating system has direct access to the FPGA which controls all hardware inputs and outputs. This facilitates the development of high speed, complex control applications as well as high speed data acquisition tasks.

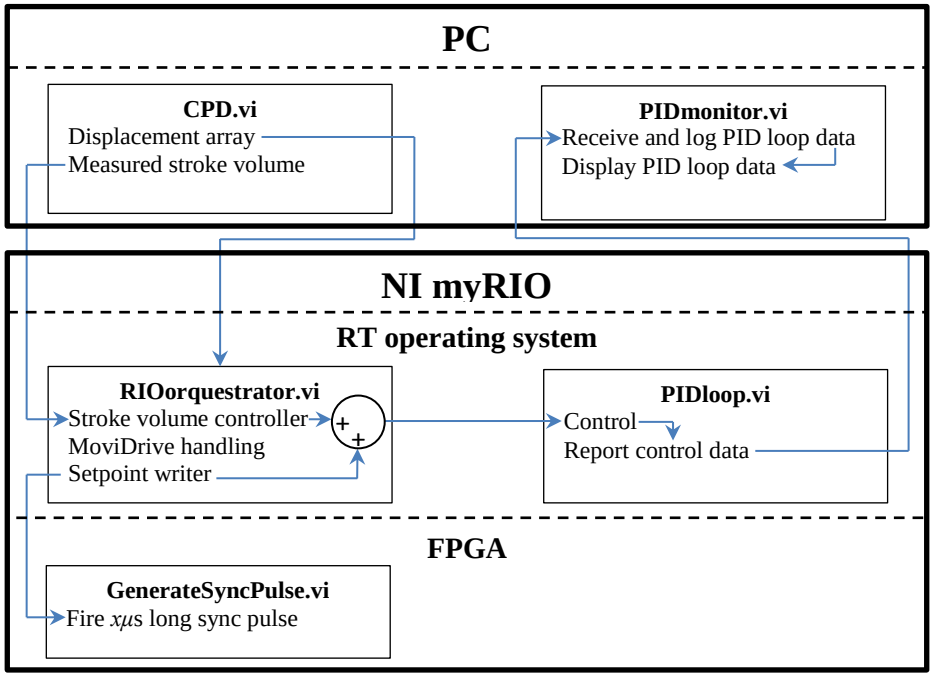

Figure 3.14: Data exchange pertinent to motion control.

Motion design

Motion design takes place on the PC through a graphical user interface. Here the user can describe the electric cylinder's motion profile by adjusting 16 sliders (refer to Figure 3.15 and Appendix E for a more detailed image) or loading a cam profile file. The resting position of the pump's piston (zero displacement) corresponds to a ventricle in complete diastolic state. Thus, the beginning of motion marks the start of the systolic phase of the cardiac cycle and the sliders control the displacement of the piston in a positive direction (generating positive pressure inside the pump). To ensure the piston's motion always begins and ends at the same position, one zero is inserted at the beginning of the array of values from the 16 sliders and another at the end. The motion described by cam profile files must adhere to this philosophy.

The values of the sliders (or those read from a cam profile file) represent discrete positions separated by a constant time period that define the travel of the piston for one heartbeat. These values are normalised so they affect only the morphology of the control waveform. A control for SV defines the maximum amplitude of the waveform and the array is scaled. When using the sliders, the array is then interpolated into a waveform with a number of positions selected by the user. The interpolation is done using a spline method, ensuring a continuous and smooth waveform. The enforcement of continuity means that this operation can result in an interpolated waveform with values that exceed those stipulated by the user which would result in larger SVs than requested. In order to guarantee the SV, the error between the requested and maximum volume resulting from the interpolation operation is calculated. The waveform is then rescaled by this error. Prior to rescaling, the waveform is checked for negative values and positive displacement is enforced by means of substitution. The graph at the bottom of the user interface shows both the sliders array and the fully processed waveform that is sent to the real time controller. Two buttons

allow the user to save and retrieve previously configured waveforms providing the ability to switch waveforms instantly, even while running. This feature provides the ability to easily expand the functionality of the CPD by automating the loading of motion profiles from cycle to cycle to perform tests where heartbeats are not identical to previous ones, as in the case of missing heartbeats.

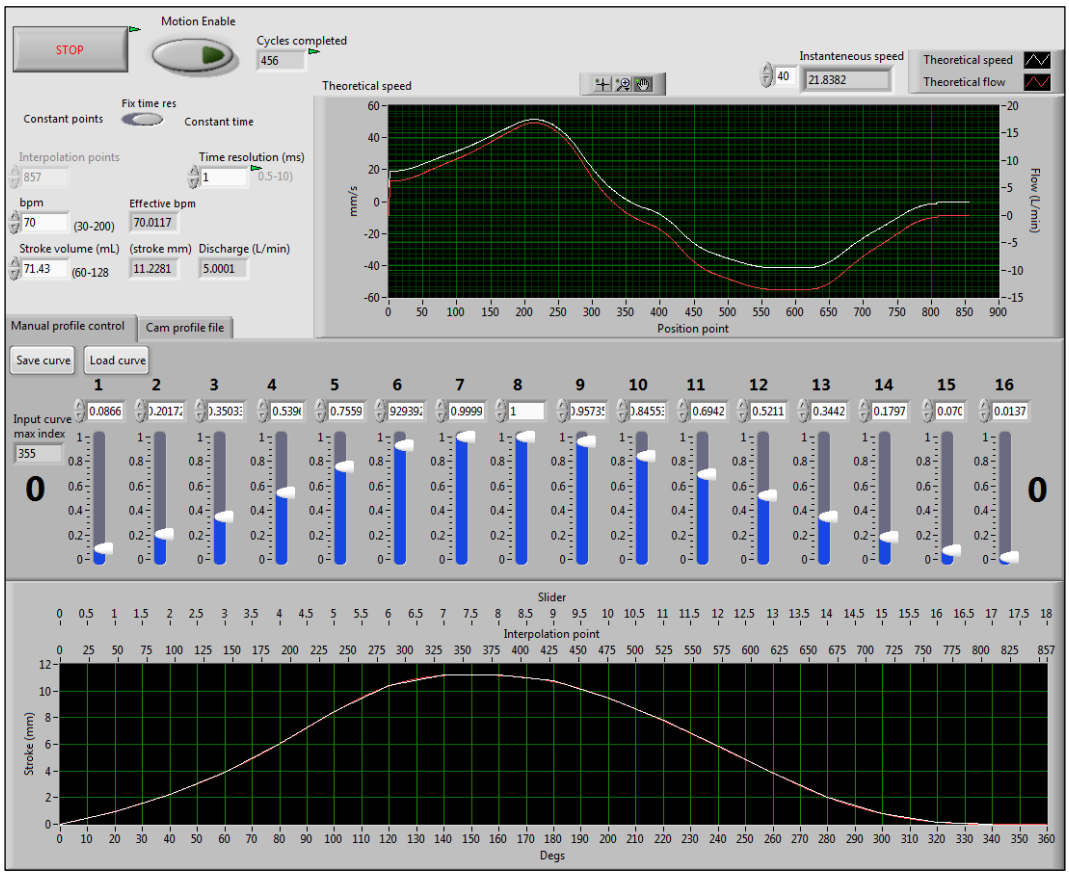

Figure 3.15: Main user interface showing motion design controls.

A control allowing the user to set the heart rate dictates the time period over which the complete waveform must be executed. The selected heart rate, together with the number of points into which the waveform is discretised, determines the rate at which the individual positions are fed to the position controller (hereafter called time resolution). An option to switch from a fixed number of interpolation points to a fixed time resolution is included. Having direct control over the time resolution can lead to improved motion controller accuracy and smoother response, overcoming some limitations of the SEW MoviDrive related to sampling time (see Section 5.1). Cam profile files are not interpolated and the extracted array is sent to the RT controller after scaling it for SV so the time resolution is determined by the number of positions in the file and the selected heart rate. The above design philosophy means that heart rate, SV and the ventricle discharge profile are completely independent of each other and can be adjusted in any order or at any time. Also, all parameters can be adjusted during motion allowing for real time fine tuning of the ventricular action while monitoring its effect on pressure and flow. Figure 3.16 shows the flow diagram for the algorithm used in generating the control

waveform for the manual user input; this algorithm only runs when the parameters describing motion are modified.

An important feature of the user interface is a graphical display of the piston's theoretical linear speed derived from the fully described motion control waveform (SV and time). This is a valuable tool when fine tuning the motion and is useful to detect high accelerations which may lead to pressure spikes. These data are further used to ensure that a control waveform containing instantaneous speeds in excess of 275 mm/s cannot be sent to the controller. The pump's theoretical flow rate, which is closely related to the linear speed, is indicated in the same graph. A button for enabling motion also forms part of the motion design window. Figure 3.15 shows the graphical user interface where motion design takes place.

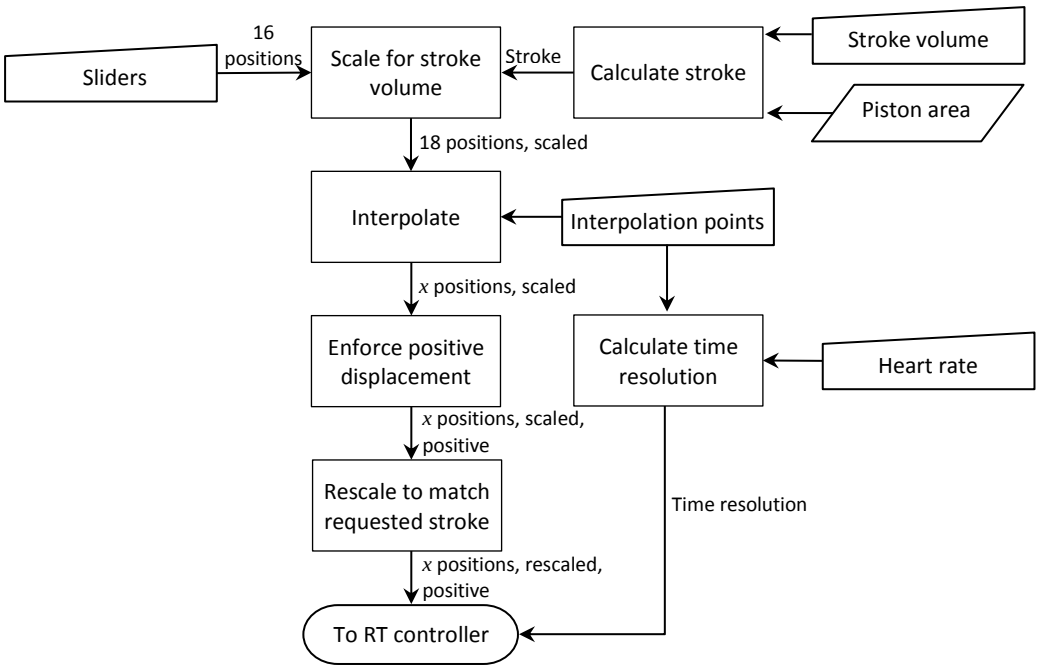

Figure 3.16: Flow diagram for waveform generation in the CPD.

Speed controller

The speed of the electric cylinder's servomotor is directly controlled by the SEW MoviDrive which was configured for servo speed control, with the setpoint based on a -10 V – 10 V analog input. The analog input is read every 1 ms and the setpoint it represents passed onto the speed control loop, which iterates every 0.5 ms. The MoviDrive's speed control loop was configured with aggressive parameters aiming to optimise tracking of a rapidly changing setpoint (see Section 3.4.1.1 for details related to the tuning of the speed controller). Speed feedback is provided to the MoviDrive by the servomotor's built-in 2-pole resolver. In order to perform external position control, the MoviDrive was configured to digitise this signal and instead output it as an emulated 1024 lines per revolution incremental rotary encoder signal. This emulated output was connected to the NI myRIO and interpreted as a quadrature encoder signal yielding a

resolution of 4096 pulses per revolution. With the electric cylinder's screw pitch of 5 mm this results in a linear resolution of 1.22 μm per pulse. Both the MoviDrive and the NI myRIO have a resolution of 12 bits on their analog interfaces and both were configured with a range of -10 V – 10 V, translating to a linear speed resolution of 0.183 mm/s. In order to successfully exchange these two sensitive signals, filtering capacitors (10 nF) needed to be installed at the receiving end of the signals to absorb electrical noise created by the high frequency (16 kHz) pulsing of the MoviDrive.

Position controller

The NI myRIO computes the position of the cylinder from the emulated encoder signal and uses this information as the feedback input to the position PID control loop it executes every 1 ms, in the PIDloop VI. The speed of the loop was limited to 1 ms due to this being the MoviDrive's sampling speed of its analog inputs. The setpoint for the PID control loop is provided by the setpoint writer loop, which runs in the RIOorquestrator VI and iterates at a variable rate, equal to the control waveform's time resolution. The main purpose of the setpoint writer loop is to feed the correct position setpoint extracted from the control waveform to the PID control loop at the right time. However, it also performs other functions related to motion, including:

- ensuring that an entire heartbeat cycle is completed before committing changes made by the user mid-cycle. This prevents sudden and unpredictable changes of the control output.
- handling the starting and stopping of motion, as commanded by the user from the PC's user interface. This function is related to first point above in that the loop will ensure the cycle is completed before stopping the motion, thus preventing a dead stop and returning the cylinder to its home position.
- controlling the firing of a configurable synchronisation pulse, which is useful to synchronise external measuring equipment such as high speed cameras, pressure and flow transducers or any other instrumentation that needs to acquire data at an exact point of the heartbeat. This pulse can be configured to fire at the start of the heartbeat (once per cycle), for each position in the displacement array or at a specified multiple of positions.
- detecting internal errors and having the ability to set the output of the PID control loop to zero. This is important because the output of the position controller maps to a speed so if an internal error occurs in the PID loop, its output may be left set to a non-zero value which will cause the cylinder to continue moving at a constant speed and crash.

The PIDloop VI runs two synchronised timed loops: one for the controller itself and one to report the control data to the PC which allows the monitoring and logging of both controller performance and process status without burdening the real time controller with graphics or saving data. Separating these two functions was done to remove the burden of communications from the controller loop. Data are passed from the controller loop to the reporting loop using fast, local variables. The reporter loop then compiles the variables into a single package that is posted to the SVE from where the PC collects it. This package includes the controller loop's iteration count which, since the iteration period is deterministic, can be used to ensure that no data points are missed during transfer between loops or devices.

The controller loop includes all the functions necessary to run the positioning PID controller as well as for self-monitoring (the generation of a heartbeat or stay-alive signal reported to the RIOorquestrator VI every loop). The implemented PID controller is of the academic type, described by Equation 2:

$$u(t) = K_p\left(e + \frac{1}{T_i}\int_0^t edt + T_d\frac{de}{dt}\right) \quad (2)$$

where

u = controller output
e = error
K_p = Proportional gain
T_i = Integral action time constant
T_d = Derivative action time constant

The output of the controller was scaled to the range of the analog interfaces so that it could be written directly to the output of the NI myRIO and easily mapped to the servomotor's maximum speed. Provision was made to run the controller in both automatic and manual modes. When in manual mode the PID constants are automatically adjusted to enable smooth, slower positioning as the parameters used during normal operation are too aggressive, resulting in overcurrent errors in the MoviDrive.

An important part of the controller loop is the PID constants scheduling feature. This enables the controller to operate optimally over a wide range of conditions, in this case cardiac output. The reason for using cardiac output as a reference is that the velocity of the cylinder for a given waveform is a product of heart rate and stroke volume. Running the CPD at 3.5 L/min with constants that provide satisfactory performance at 20 L/min results in jerky operation. Conversely, when the controller is configured with constants that enable smooth operation at 3.5 L/min, it cannot track the steep speed gradients introduced by the rapidly changing setpoint at 20 L/min. To ensure optimal performance through the entire range of cardiac output, a linear PID constant scheduling system was implemented. Since the heart rate used for most tests is 70 bpm (termed the base), the controller was tuned for best performance using a sine wave with this frequency and a peak to peak amplitude of 11.23 mm, corresponding to a cardiac output of 5 L/min (see Section 3.4.1.1 for details related to the tuning of the position controller). The proportional gain (K_p) and integral time constant (T_i) obtained from this tuning point were regarded as the base constants. The process was then repeated but with a cardiac output corresponding to 24.2 L/min, the maximum designed combination of heart rate and stroke volume. The constants recorded from these two tuning points were used to calculate the optimal performance gradient for K_p and T_i. Equation 9 and Equation 11 are used within the controller loop to calculate the effective constant values whenever the heart rate is adjusted. These equations arise from a linear function (Equation 3). The result of Equation 3 is added to the base constant allowing K_{p_eff} to be adjusted proportionally such that $K_{p\_eff@CO<CO_{base}} < K_{p\_base} < K_{p\_eff@CO>CO_{base}} < K_{p\_max}$ (Equation 6). Figure 3.17 helps to understand the variables used in the equations. It also shows the recorded optimal K_p and T_i values at 5 L/min and 24.2 L/min. Although all the equations reflect variables labelled for K_p, they apply to T_i as well.

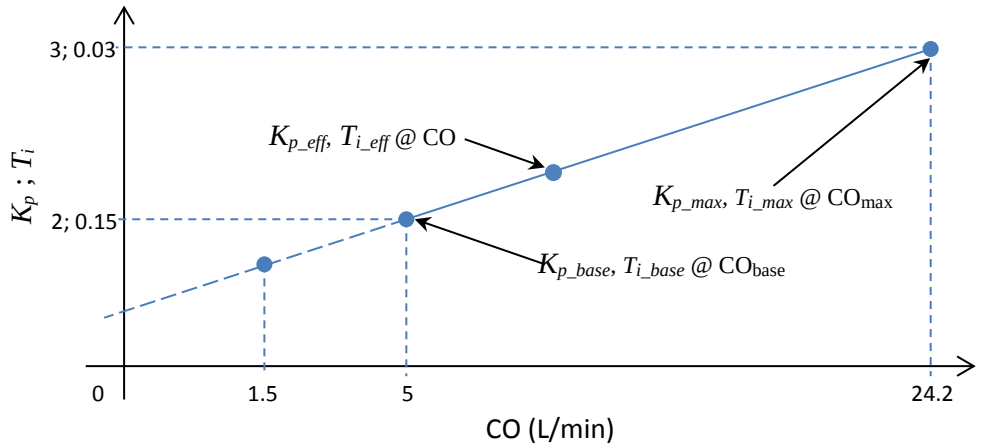

Figure 3.17: Values used in the determination of the optimal performance gradient for constants K_p and T_i.

$$y = mx + c \;\; => \;\; K_{p\_add} = m.CO + c \tag{3}$$

where

$$m = \frac{\Delta y}{\Delta x} = \frac{K_{p\_max} - K_{p\_base}}{CO_{max} - CO_{base}} = \frac{K_{p\_max} - K_{p\_base}}{19.2} \tag{4}$$

$$c = -mx_{base} = -m.CO_{base} \tag{5}$$

where

K_{p_add} = the proportional part of the K_p gain that must be added to K_{p_base}
K_{p_max} = K_p gain for best performance at 24.2 L/min
K_{p_base} = K_p gain for best performance at 5 L/min

$$K_{p\_eff} = K_{p\_base} + (mCO + c) \tag{6}$$

$$K_{p_{eff}} = K_{p_{base}} + \left[\left(\frac{K_{p_{max}} - K_{p_{base}}}{19.2}\right)CO - \left(\frac{K_{p_{max}} - K_{p_{base}}}{19.2}\right)CO_{base}\right] \tag{7}$$

$$K_{p\_eff} = 2 + \frac{1}{19.2}CO - \frac{1}{19.2}CO_{base} \tag{8}$$

$$K_{p\_eff} = 1.73958 + \frac{1}{19.2}CO \tag{9}$$

where

K_{p_eff} = effective proportional gain

Following from Equation 7, for T_i:

$$T_i = 0.15 - \frac{0.12}{19.2}CO + \frac{0.12}{19.2}CO_{base} \tag{10}$$

$$T_{i\_eff} = 0.18125 - \frac{0.12}{19.2} CO \quad (11)$$

where

T_{i_eff} = effective integral time constant

It should be noted that while the derivative term is implemented in this controller, in practice its constant is normally kept to zero so it was not incorporated in the scheduling system. The flow diagram for the PIDloop VI is shown in Figure 3.18. The front panel of the PIDloop VI (refer to Appendix E) makes the controller's parameters available to the user although in general these parameters do not need to be changed and are used for development or tuning.

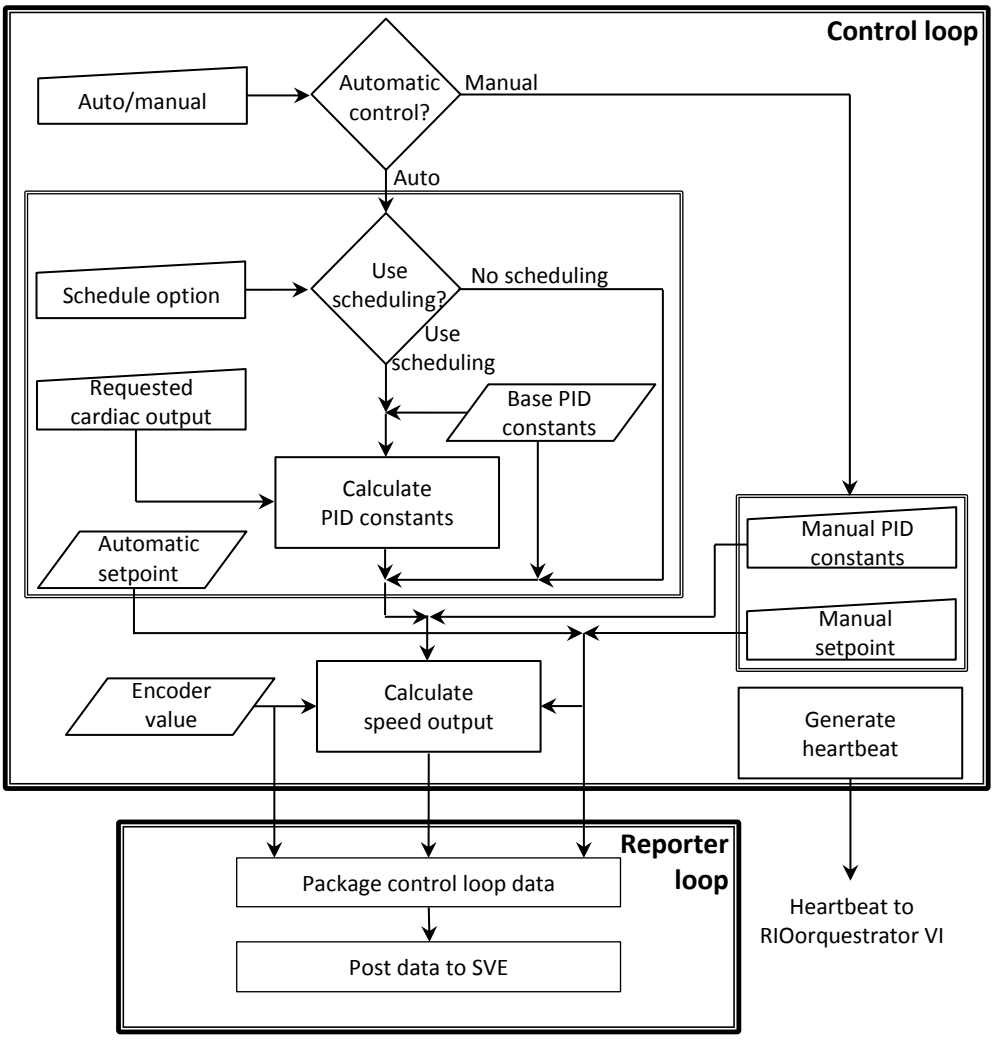

Figure 3.18: Flow diagram for the PIDloop VI.

Stroke volume controller

When ventricular compliance is introduced, the requested SV may no longer be an accurate indication of the volume ejected through the aortic valve due to the compressibility of air in the ventricular compliance chamber. Since the working fluid's

pressure is not monitored, there is no way of establishing the effective SV. To maintain an accurate cardiac output, a closed loop system (using the flow meter reading as feedback) was implemented to automatically adjust the piston pump's stroke to match the effective SV to the requested SV. The algorithm described below is presented as a flow diagram in Figure 3.19.

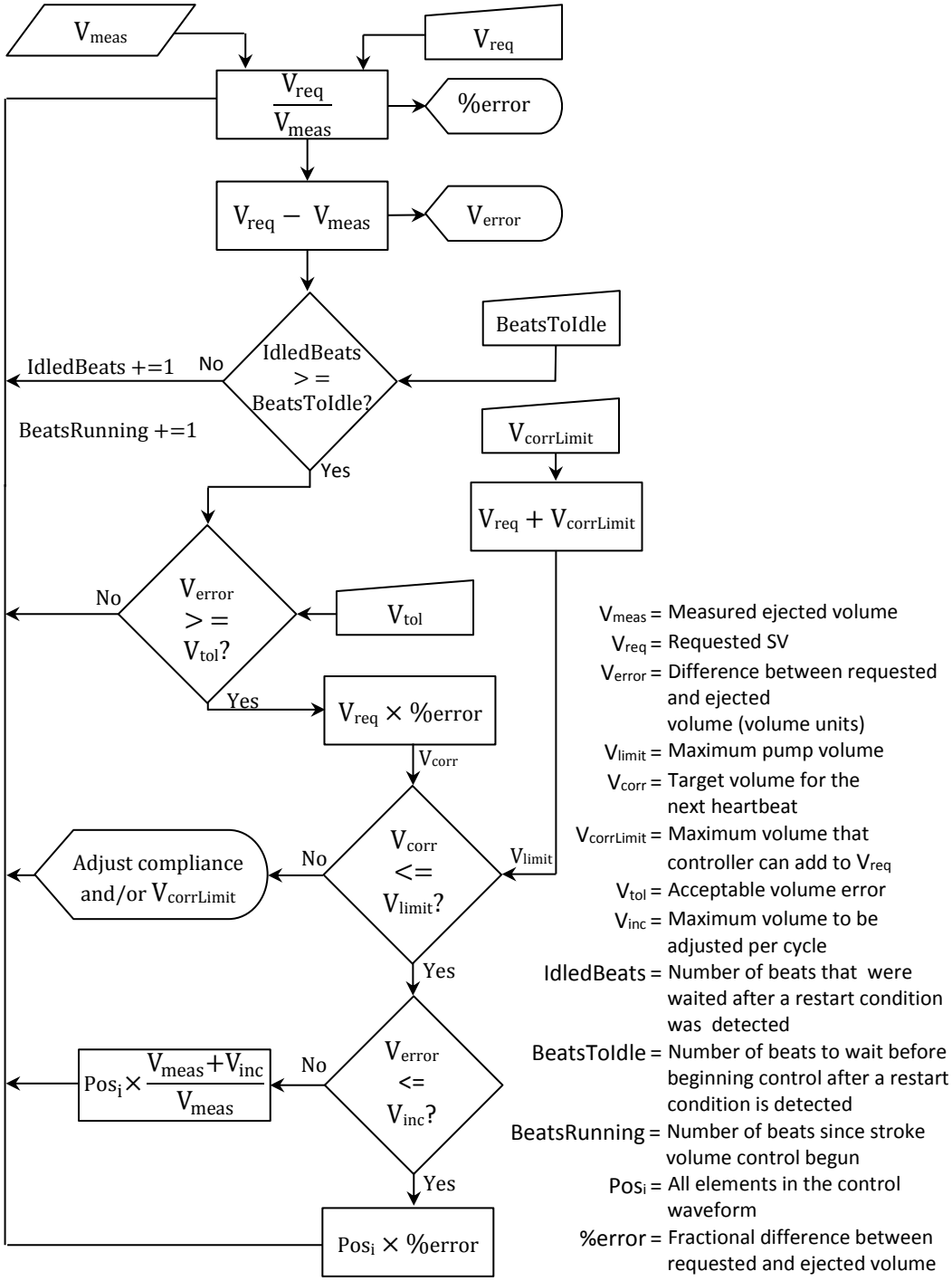

Figure 3.19: Flow diagram for the stroke volume controller's algorithm.

The system works on a cycle by cycle basis and is activated for an adjustable number of cycles after any changes to the motion descriptors are detected, allowing the system to settle. The volume discharged during the previous cycle is calculated by integrating the positive region of the instantaneous flow rate curve. The controller compares this volume to the requested SV, computes percentage and volume errors and uses these values to rescale the control waveform for the next cycle. The algorithm is designed in such a way that the original requested volume is never affected and the PC supplying the control waveform is unaware of any modifications to it. Prior to modifying the control waveform, the controller checks if the initial error is within acceptable limits. If the initial error is beyond the defined limit, the ventricular compliance settings or the limit must be adjusted. The limit is pre-set to a safe value that will prevent the piston from being driven too far in an attempt to reach the correct SV, should the ventricular compliance chamber contain too much air or volume measurement errors arise.

To prevent sudden changes which could destabilise the controller when errors are large, the maximum volume by which the controller can increase or decrease the control waveform is limited for each cycle, allowing a progressive change. Further, in order to enable steady state measurements, the volume error is checked against a dead zone value and if the error is smaller than the dead zone value the controller does not make any adjustments. The dead zone value represents a convergence tolerance and prevents the controller from making adjustments indefinitely, which could result in cycle to cycle variations for pressure and flow measurements. To illustrate the above-mentioned functions, if the total error to be corrected is 9 mL and the cycle to cycle volume change is limited to 2 mL, the controller will increase the volume by 2 mL one cycle at time until the error is below this limit and then continue to adjust the volume proportionally until the error is within the dead zone.

3.2.4.3 Data acquisition

The NI myRIO was found to have insufficient resolution on its analog inputs to meet the ISO5840:2005 specifications stipulated in Table 2.2 for pressure and flow measurements. This led to the need for a separate data acquisition (DAQ) card (National Instruments USB-6009) to record the data.

The variables measured by the DAQ card are ventricular, aortic and atrial pressures as well as aortic flow rate. All transducers were set up for current output and each is measured by the DAQ via a 500 Ω precision resistor (PAPTF56500R00BYEK, Vishay Intertechnology, Inc., PA, USA). A facility to input calibration data for the pressure transducers has been included in the acquisition window, making it possible to automatically calibrate all measurements as they are acquired. By default, data from all transducers is acquired at 1000 Hz although this can be changed in the data acquisition window.

The data acquisition window (refer to Appendix E) provides graphical feedback of the variables being measured, valve performance indicators, options for logging acquired data and controls for the acquisition parameters. Both raw and filtered plots of pressure and flow measurements are displayed as they are acquired.

3.3 Reproduction of cam profile

One of the main challenges encountered during preliminary tests with the CPD in its original configuration was determining the source of abnormal pressure waveforms. After ruling out other factors such as the geometry of the hydraulic loop, it was suspected that the shape of the ventricular discharge waveform was not appropriate because there was no numerical information available for the cam being used.

To obtain a numerical profile for the cam, the experiment shown in Figure 3.20 was set up. It consisted of a vertically mounted HBM 1-WA/50MM-L (Hottinger-Baldwin-Messtechnik GmbH, Darmstadt, Germany) linear variable differential transformer (LVDT) (*a*) contacting the cam (*b*) which was mounted on the shaft of a SEW DT90S4 motor (*e*). On the other side of the motor's shaft, a shaft encoder (*f*) with 1024 pulses per revolution (SEW ES1R) was attached and used to trigger the readings of the LVDT. The LVDT was connected to a NI USB-6212 data acquisition card (*d*) via an instrumentation amplifier (HBM Clip A501) (*c*). A SEW MoviDrive (SEW MDX61B0015-5A3-4-00) (*g*) was used to rotate the motor at 2 rpm. Two separate LabVIEW programs were used to acquire and post process the data.

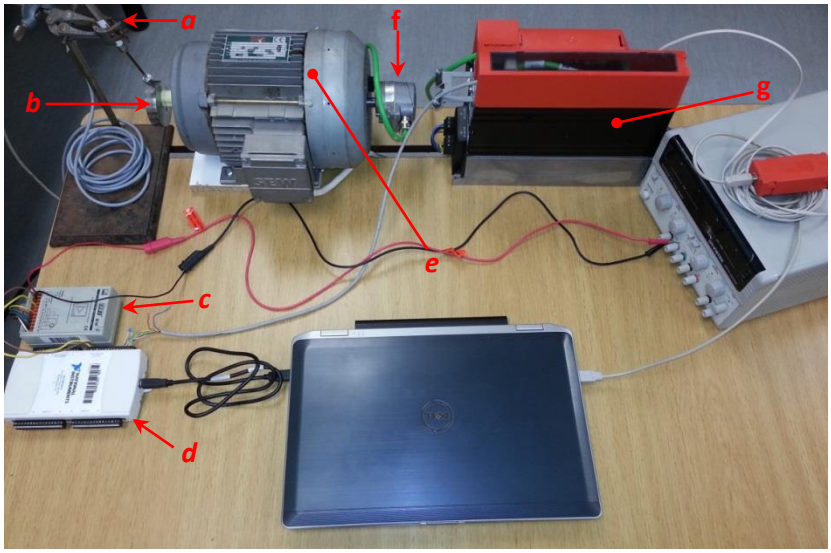

Figure 3.20: Experimental setup used to obtain cam profile. a) LVDT; b) cam; c) instrumentation amplifier; d) data acquisition card; e) motor; f) encoder; g) SEW MoviDrive motor controller.

A number of steps were taken to help minimise measurement errors:

- A tip cut at 20° was attached to the end of the LVDT core to help eliminate errors while measuring the steep gradients of the cam.
- The axis of displacement of the LVDT was aligned with the centre of the motor shaft's diameter to prevent errors due to the cosine effect.
- The LVDT was calibrated using gauge blocks. Only 20 mm of the LVDT were calibrated (because the cam's maximum displacement was measured at 15.55 mm) but this was the only part of the LVDT's core that was used in the experiment and this section was chosen because it was identified as having the lowest electrical error in the factory calibration certificate (see Appendix A).

- For every encoder pulse, 20 measurements were taken at a sampling frequency of 1000 Hz. These measurements were then averaged, eliminating errors caused by electromagnetic interference (EMI) because a single data point was measured over an entire period of mains power frequency (50 Hz).
- Five full rotations of the cam were recorded and the data smoothed using a moving average filter with a half-width of five data points.
- The point-by-point average of the five rotations was used to produce a curve representative of the cam profile (each data point in the final curve represents the average of the corresponding points in the five rotations).

The final combined curve generated by this process was interpolated into an array with a user-defined number of data points and saved to a file. This file could then be directly read by the CPD's control program and used to simulate the original cam profile (with any SV) in the hydrodynamic tests (see Section 3.4.3).

3.4 Calibration and testing

This section describes the methods used for calibration of the various components of the CPD as well as tests carried out to validate the accuracy and overall performance of the CPD as a complete system. For details related to the calibration of the instrumentation, refer to Appendix A. Thanks to the design approach, calibration and assessment of the motion control system could be done independently of the rest of the CPD. The rest of the performance aspects of the CPD (Section 3.4.2) needed to be assessed by means of testing a reference valve and commercially available PHVs were used for this. Finally, as part of this project, the hydrodynamic performance of two PHVs was investigated following the procedures recommended in ISO5840:2005 as proof that the CPD can achieve all the required test conditions. The details of the tests used for this purpose are presented in Section 3.4.2.4.

3.4.1 Ventricular motion control

3.4.1.1 MoviDrive servomotor speed controller

Owing to the electric cylinder's limited range of motion the MoviDrive's speed controller could only be tuned using a sine wave as speed input. To measure actual speed, the servomotor's encoder pulses were counted and differentiated using the sampling frequency. The measured speed was plotted together with the speed setpoint wave and the position of the cylinder. The speed controller's parameters were adjusted with the process running so that the effect of changes in the parameters could be seen immediately in graphical form.

The sine wave was initially configured with an amplitude of 1 V and a frequency of 1.16 Hz (70 bpm), resulting in a displacement of 10.3 mm which corresponds to a CO of approximately 4.5 L/min. The controller was then tuned at this operating point. When configured for servo speed control the MoviDrive uses a mixed feedback/feedforward control scheme which improves setpoint tracking and regulation. Thanks to this, the MoviDrive can maintain the servomotor's speed to within 0.01% error of a stationary

setpoint, provided that both the motor and the MoviDrive are correctly sized for the load demands of the application [97]. From the position controller's point of view, this means that the speed is essentially guaranteed regardless of the load applied to the motor. Nevertheless, to verify the accuracy of the speed controller, its response was tested by configuring the sinusoidal wave with various maximum speeds and frequencies. This exercise also served to assess the operational range (frequency and magnitude response) of the system. Table 3.3 shows the operating points that were verified and indicates the equivalent CO. The maximum speed tested was 300 mm/s. While many of the operating points tested represent non-physiological conditions they were tested regardless to verify the behaviour of the system at that speed since the control waveform could cause the position controller's output to contain such velocity values.

Table 3.3: Operating points tested during speed calibration.

Frequency / Max amplitude	1 Hz (60 bpm)	1.167 Hz (70 bpm)	1.5 Hz (90 bpm)	2 Hz (120 bpm)	3 Hz (180 bpm)	3.333 Hz (200 bpm)
1 V (37.5 mm/s)	~4.6 L/min					
2 V (76 mm/s)	~9.25 L/min					
3 V (112.5 mm/s)	~13.85 L/min					
5 V (187.5 mm/s)	~23.88 L/min					
7 V (262.5 mm/s)	~32.16 L/min					
8 V (300 mm/s)	~36.85 L/min					

3.4.1.2 LabVIEW position controller

The position controller was tuned once the speed controller was considered to be performing optimally. To safely obtain a controller that was stable but responsive to step inputs, the PID constants were initially adjusted by loosely following the Ziegler-Nichols ultimate sensitivity method of PID tuning as well as guidelines provided by Franklin *et al* [98]. The controller's parameters were subsequently fine-tuned experimentally using a control waveform derived from the cam profile obtained through the experiment described in Section 3.3. The amplitude and frequency of the control waveform were set to simulate physiological conditions using data from Table 3.4 as a reference, to realistically match HR to SV.

Table 3.4: Cardiovascular response to exercise in adults. (Adapted from [99]).

	Rest	Exercise (moderate)	Exercise (maximal)
HR (bpm)	71 ±15	146 ±12	189 ±12
SV (mL)	81 ±23	119 ±22	128 ±23
CO (L/min)	5.72 ±2.22	17.61 ±3.28	24.26 ±4.62

In order to implement the PID constant scheduling system discussed in Section 3.2.4.2, the system needed to be tuned at two operating points. A frequently used point (70bpm) and the upper limit of the speed range (200 bpm) were chosen. The optimal PID constants were first determined for the rest conditions by adjusting them until the tracking error

could no longer be improved. The process was then repeated for the operating point corresponding to maximal exercise, using the same control waveform.

The stroke volume controller could not be tested due to the poor performance of the flowmeter used. In order to fulfil its purpose the controller requires accurate feedback, especially in terms of determining flow reversal, and this could not be achieved with the available instrumentation. The algorithm was presented as part of this project's contribution to the field but it should be noted that its performance is untested. The limitations experienced as a result of the flowmeter's performance are summarised under Section 4.5.

3.4.1.3 Ventricle pump accuracy and resolution

Evaluation of the overall ventricular motion performance was carried out once both controllers were tuned. This involved assessing the resolution, accuracy and effective tracking error of the controller. While performing analyses of the system's positioning ability it is important to note that due to the type of controller used and the nature of the system the process will always lag the control signal by a small amount. Part of the objective of this section was to establish this lag time. However, in this application, the ability to closely reproduce the control signal is more important than the lag time. Therefore, emphasis is placed on analysing the morphology and magnitude of the process value instead of phase so when performing analyses related to tracking, the process value and the control signal are time aligned. Further, for this application accuracy does not only refer to magnitude but it also contains a time component: for the controller to be accurate it has to attain a position at the correct time. Given this and the fact that the process lags the setpoint by a certain amount of time, the measurable accuracy is dependent on motor speed because of the fixed sampling rate (at high speeds the setpoint may be attained but not picked up during sampling). Nevertheless, accuracy is evaluated at a given practical speed as described below.

The system's theoretical linear displacement resolution is 1.22 μm but while this is achievable with a step input, it does not necessarily reflect the controller's ability to go through a position of this multiple during motion. Preliminary testing showed that pressures are highly sensitive to even minute changes in the control waveform so it was deemed relevant to know the smallest change in position that the system can achieve because this would help to fine tune pressure curves. To test resolution and accuracy a 500 point, 60 bpm control waveform was setup with a stroke of 10 mm and the electric cylinder's displacement was recorded as a baseline. One control point was then modified to effect a change of +0.1 mm. Subsequent tests were carried out, reducing the amount of change until it became imperceptible. The difference in position between the baseline and modified cylinder displacements were computed and plotted together.

Tracking ability was quantified by computing the root mean square error (RMSE) between the control waveform and the electric cylinder's measured position. This was done beat-to-beat for five consecutive heartbeats and the standard deviation for the individual RMSEs calculated. Using this approach instead of calculating a single RMSE for five beats provides a more reliable indication of random beat fidelity. Three operating points, based on Table 3.4, were verified using this process.

3.4.2 Hydrodynamic verification

Tests intended to validate the CPD's hydrodynamic performance were done using commercially available aortic PHVs, described in Table 3.5. Note that there are two identical St Jude Medical Epic 21 mm PHVs and they are referred as SJME V1 or SJME V2. PHVs of different designs were used to demonstrate that the CPD can produce the required test conditions irrespective of the sample being assessed. The valves tested are aortic models and were tested in the aortic position.

To allow comparisons between two separate measurements, the recordings were synchronised using the closing of the aortic valve as the reference event. For the purposes of these tests compliance is characterised by the volume of air present in the respective chamber once the system reached steady state. All measurements were recorded once the system had settled (reached steady state) which was regarded to have been achieved once changes in the systolic pressure trace were no longer observable from cycle to cycle. The settling time was dependent on cardiac output and the extent of changes in lump parameter controls but steady state was typically achieved within five to 25 heartbeats.

Table 3.5: Commercially available aortic PHVs used for the verification of the CPD's hydrodynamic performance.

Valve	SJME V1/V2 St Jude Medical Epic 21 mm (SJM E100-21A; St Jude Medical, Inc., Minnesota, USA)	SJME V3 St Jude Medical Epic 23 mm (SJM E100-23A; St Jude Medical, Inc., Minnesota, USA)	SJMR St Jude Medical Regent Aortic 25 mm (SJM 25AGFN-756, St Jude Medical, Inc., Minnesota, USA)
Tests	V1: • ISO tests (all) • Comparison to original CPD V2: • ISO tests (all) • Adjustment of lump parameter controls • Effect of changes in control waveform on pressure • Repeatability and fidelity	• Tests for comparison to published data	• ISO Test 1 • Ventricular compliance
Description	Bioprosthetic stented trileaflet from porcine aortic valve cusps		Mechanical bileaflet from pyrolytic carbon
Dimensions[8] (mm)	Nominal size: 21 Tissue annulus diameter: 21.1 Internal diameter: 15.7 Geometric orifice area: 1.94cm^2	Nominal size: 23 Tissue annulus diameter: 23.1 Internal diameter: 17.9 Geometric orifice area: 2.52 cm^2	Nominal size: 25 Tissue annulus diameter: 26.4 Internal diameter: 23.0 Geometric orifice area: 4.02 cm^2
Image	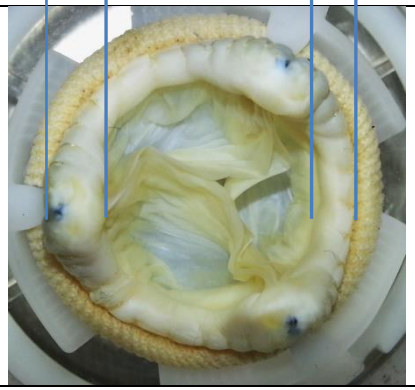	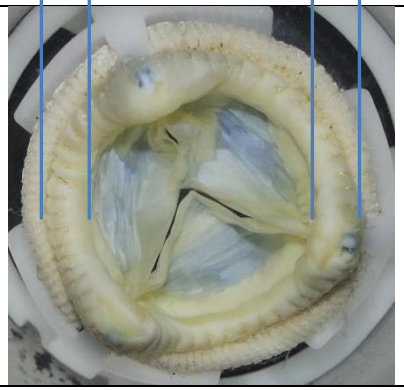	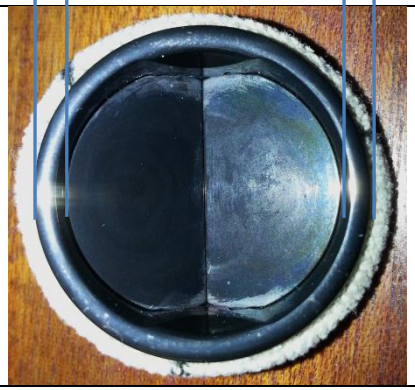

[8] All dimensions are measured, except for the geometric orifice area of the SJMR PHV which is quoted from the manufacturer.

3.4.2.1 Adjustment and effect of compliance and resistance controls

Aortic root compliance and peripheral resistance

The principle of operation of these controls has been described and the tests performed in this section serve the purposes of verifying that the design being presented behaves as expected and is capable of producing the operating conditions required for testing of PHVs according to ISO5840:2005 guidelines. As such, this section is not intended to present exhaustive tests to investigate the effect of compliance and resistance at various combinations of HR and SV but rather to evaluate the design of the controls. Achieving all the required test conditions set out in Section 3.4.2.4 represents the ultimate test of performance.

The SJME V1 PHV was used for these tests. Aortic compliance was initially set to approximately 650 mL, based on the recommendation for the Vivitro CPD [46]. Sufficient fluid was introduced into the compliance chamber to ensure that air would not enter the aorta or the resistance element during pumping, which was set to 70 bpm with CO = 5 L/min. Based on widely accepted physiological values, a target of 120/80 mmHg was set for the arterial pressure. The effect of the controls is demonstrated by comparing the pressures and flow before any adjustments were made and once the target values were reached, quantifying the changes made at the controls. No changes related to the ventricular action were made and no ventricular compliance was used.

Ventricular compliance

The effect of ventricular compliance on pressures (ventricular, aortic and atrial), as well as flow rate was investigated by means of the two tests described in Table 3.6, using the SJMR PHV. A mechanical valve was used for this test as its rigidity makes it easier to demonstrate the effect of ventricular compliance. The conditions for Test 2 were chosen based on the fact that PHVs are seldom studied *in vitro* at cardiac outputs exceeding 7 L/min. Laske *et al* [100] present a review of eight *in vitro* studies for the SJM bileaflet PHV, none of which exceed 7.5 L/min for the 25 mm model. For tests involving other PHV sizes where the cardiac output is above 7.5 L/min, the heart rate is above 70 bpm. This led to the decision of using a heart rate of 90 bpm and a cardiac output of 7.5 L/min since physiologically it is more plausible to reach 7.5 L/min at 90 bpm than at 70 bpm.

To perform these tests, first arterial pressure was stabilised through the adjustment of the aortic root compliance and peripheral resistance controls. Initially no ventricular compliance was used. After recording baseline pressure and flow variables, the ventricular compliance controls were manipulated to eliminate as much as possible of the high frequency oscillations highlighted in Figure 2.7. Measurements were taken again once the system had settled. All other variables were kept constant for the duration of this process.

Table 3.6: Test conditions for the ventricular compliance experiment. (HR: heart rate; CO: cardiac output; SV: stroke volume; P_{sys}: arterial systolic pressure; P_{dias}: arterial diastolic pressure; MAP: mean arterial pressure).

Test	HR	CO	SV	P_{sys}/P_{dias}	MAP
T1	70 bpm	5 L/min	71.43mL	120/80 mmHg	100 mmHg
T2	90 bpm	7.5 L/min	83.33mL	140/80 mmHg	110 mmHg

3.4.2.2 Effect of changes in control waveform on pressure

The ability to modify the control waveform during operation and observe the effects of the change on the process through immediate graphical feedback greatly simplifies the task of fine tuning the system for pressure, the main variable being controlled. This section presents a set of tests devised to demonstrate how the cylinder's path affects pressure, with all other settings (HR, SV, ventricular compliance, aortic compliance, peripheral resistance and mean atrial pressure) being equal. All tests in this section were performed using the SJME V1 PHV.

Response to changes in a single control point

The effect of changes to one control point was investigated with the aim of better understanding how to tune the pressure profile. Using a control waveform of 500 positions the chosen control point, affecting the waveform at location 140 (of 500), was increased by 0.1 mm per heartbeat for 7 heartbeats. The test was performed at a HR of 60 bpm and a SV of 63.62 mL (this combination results in a stroke of 10 mm and 2 ms per position). Arterial pressure was set to 120/80 mmHg with a MAP of 100 mmHg.

Tuning the pressure profile

The aim of this test was to improve the shape of the pressure profile by changing only the control waveform. A pressure profile produced by a given 500 position control waveform and exhibiting systolic pressure spikes was used as the base for the comparison. All parameters were identical to those used in the previous test.

3.4.2.3 Repeatability and fidelity

Repeatability

Basic cylinder repeatability is indirectly proved and presented in Section 4.1.4. Repeatability of the CPD as an instrument was assessed hydrodynamically rather than from the perspective of a controller's response. Two repeatability notions are employed: intra-test and inter-test repeatability. Intra test repeatability is based on pressure measurements of 5 consecutive heartbeats. It is established by calculating the standard deviation (SD) of the RMSEs between the differential pressures of a baseline heartbeat and the following five individual heartbeats. To evaluate inter-test repeatability it is necessary to perform another test, a large number of heartbeats after the first test (without adjusting any parameters) and determine a second intra-test repeatability value using the original baseline heartbeat as reference. Inter-test repeatability is then determined by the average of the two standard deviations. Therefore, an inter-test repeatability value of zero indicates perfect repeatability. Repeatability within a group of consecutive heartbeats can be ascertained from the individual SD values. Figure 3.21 explains the concept diagrammatically.

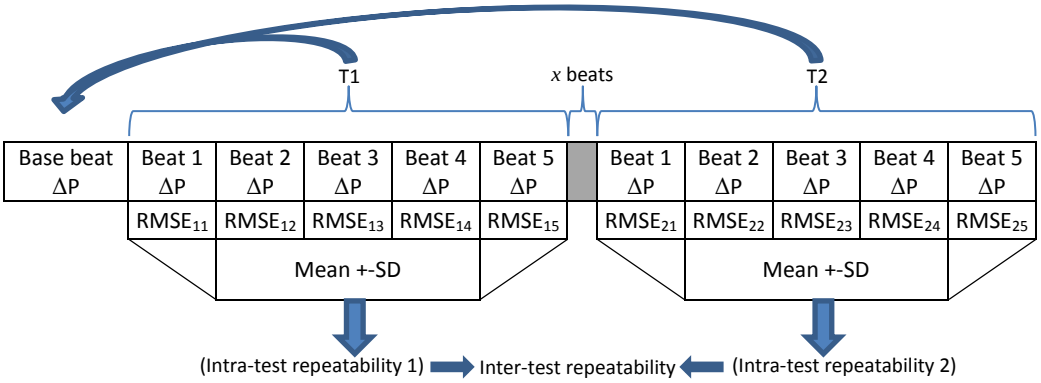

Figure 3.21: The concept used to evaluate repeatability of the CPD.

The repeatability experiment was performed with the SJME V2 PHV. Arterial pressure was set to 120/80 mmHg with HR = 70 bpm and CO = 5 L/min. Two measurements were taken, approximately 30 minutes apart, without having modified any test parameters.

Fidelity

As repeatability cannot account for accuracy, the idea of fidelity is introduced in an effort to provide a single metric that can be used to judge the CPD's performance in terms of both of these properties. This is a challenge due to the fact that accuracy contains an element of time (the correct amplitude must be generated at the correct time within a cycle) and this must then be evaluated over multiple cycles. Since pressure is not controlled directly, there is no setpoint to which measurements can be compared so certain features of the arterial pressure trace were chosen as reference: systolic (maximum), diastolic (minimum) and mean values. The systolic and diastolic pressures are used in conjunction with the theoretical time at which they should occur within a heartbeat. Together, these five measurements provide a good indication of arterial pressure conditions and morphology. The theoretical time, in terms of arterial pressure, where a maximum or minimum pressure should occur was estimated from the piston speed (derived from the control waveform) and phased by using the beginning of systole as a reference.

The following equations were constructed to quantify fidelity:

$$\mathcal{F}_{P_{syst}} = \frac{\frac{\left|P_{syst\_target} - P_{max}\right|}{P_{syst\_target}} + \frac{\left|Index_{P_{syst\_target}} - Index_{P_{max}}\right|}{Index_{P_{syst\_target}}}}{2} \quad (12)$$

$$\mathcal{F}_{P_{diast}} = \frac{\frac{\left|P_{diast\_target} - P_{min}\right|}{P_{diast\_target}} + \frac{\left|Index_{P_{diast\_target}} - Index_{P_{min}}\right|}{Index_{P_{diast\_target}}}}{2} \quad (13)$$

$$\mathcal{F}_{P_{MAP}} = \frac{\left|P_{MAP\_target} - P_{MAP}\right|}{P_{MAP\_target}} \quad (14)$$

where:

$\mathcal{F}_{P_{syst}}$, $\mathcal{F}_{P_{diast}}$, $\mathcal{F}_{MAP}$ = Fidelity value for systolic, diastolic and mean pressures, respectively.

P_{syst_target}, P_{diast_target}, MAP_{target} = Target systolic, diastolic and mean pressures, respectively.

P_{max}, P_{min}, MAP = Measured systolic, diastolic and mean pressures, respectively.

$Index_{P_{syst\_target}}$, $Index_{P_{diast\_target}}$ = Theoretical location within heartbeat when systolic and diastolic pressures, respectively, should occur (sample number).

To prevent negative values (which could bias the results towards zero when calculating the difference between the target and the measurement) the absolute value of the difference is used before normalising the result. This ensures that the error is centred on the target and negative values do not skew the result. Summing both terms ensures that if the target for one of the measurements is achieved but the other is not, an error is still registered. Equation 12 and Equation 13 contain two normalised terms so they are divided by 2 to give a range of 1, where 1 means that the magnitude of each of the errors is as large as the target itself and 0 indicates perfect fidelity.

Equation 12 to Equation 14 yield a fidelity value for each heartbeat. To obtain a fidelity figure over time, the single heartbeat fidelity values for each type of pressure are accumulated in an array, resulting in three arrays. The fidelity figure for each type of pressure is expressed as the 90th percentile. Finally, the average of the three percentiles yields a single value expressing the overall fidelity of the CPD. This method can be applied to any measurement (arterial pressure, ventricular pressure or flow rate) provided that target locations can be established for the measurement in question.

The fidelity test was carried out with the SJME V2. Standard operating conditions were used: HR = 70 bpm, CO = 5 L/min and arterial pressure set at 120/80 mmHg (MAP = 100 mmHg). 100 heartbeats were recoded and analysed.

3.4.2.4 ISO testing

The hydrodynamic testing protocol was based on Annex L.4 of the ISO5840:2005 standard which provides guidelines for pulsatile flow testing procedures. All tests were performed for the two SJME 21 mm PHVs. The reason for using this valve was not only due to two identical samples being available but also because it is from a manufacturer with a long history of PHV development and it has FDA approval [101]. Test 1 was also performed for the SJM Regent PHV.

For each of the tests in Table 3.7, ten cycles were analysed and results reported in SD format (mean, range and SD). Table 3.7 indicates the operating conditions for each test, as stipulated in ISO5840:2005.

Table 3.7: Test matrix for the assessment of valve hydrodynamic performance. (CO: Cardiac Output (L/min); HR: heart rate (bpm); MAP: Mean arterial pressure (mmHg); $-\Delta P_{mean}$: mean back pressure (mmHg); ΔP: differential pressure; Reg vol: regurgitant volume; Rep Wave: representative pressure and flow waveforms; T1-T7: test number).

CO \ HR	MAP = 100	$-\Delta P_{mean}$ = 80	$-\Delta P_{mean}$ = 120	$-\Delta P_{mean}$ = 160
	70	45	70	120
2	**T2:** ΔP			
3,5	**T3:** ΔP			
5	**T1:** Rep Wave; ΔP	**T5:** Reg vol	**T6:** Reg vol	**T7:** Reg vol
7	**T4:** ΔP			

- Representative wave: Pressure and flow waveforms, representative of normal operating conditions, intended to graphically present an overall picture of the PHV's performance. A systolic fraction of 35% is used. EOA is calculated based on the measurements from this test.
- Differential pressure: Performed at a fixed heart rate and MAP, the CO is increased by altering the SV. This test evaluates the performance of the PHV in terms of the pressure drop across it during the forward flow phase.
- Regurgitant volume: Performed at a fixed CO, these tests are used to measure regurgitant volume at three mean back pressures corresponding to a range of heart rates. Mean back pressure refers to the differential pressure measured across a closed valve.

The pressure drop across the open PHV (tests 1-4) is denoted as ΔP while the differential pressure across the closed PHV (tests 5-7) is denoted as $-\Delta P$. Crucial to many of the measurements presented in the sections concerning ISO testing is establishing when the valve opens and closes. The opening and closing events were determined using landmark features on the pressure trace, indicated in Figure 3.22.

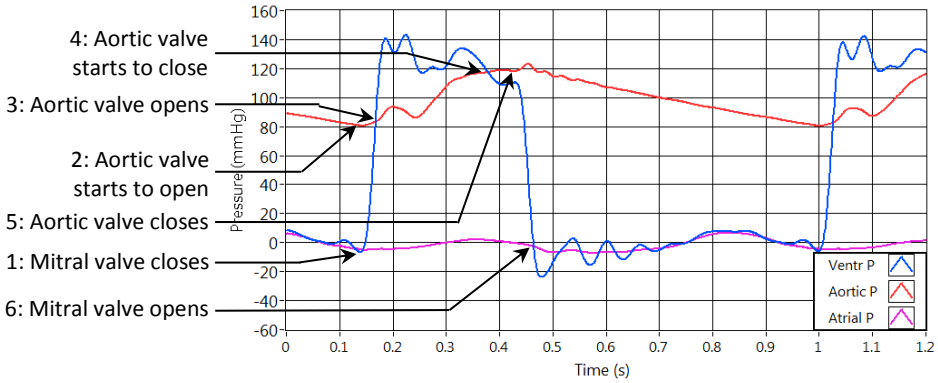

Figure 3.22: Heart valve events.

The following expands on the events highlighted in Figure 3.22:

1. Ventricular pressure overcomes atrial pressure and rises rapidly.
2. Reversal of pressure on aortic trace, momentary dip in ventricular trace.
3. Ventricular pressure overcomes aortic pressure, forward flow is established.
4. Ventricular pressure falls below aortic pressure, flow is reversed.
5. Closure of the aortic valve is signalled by a slight momentary increase in pressure due to fluid inertia (the dichrotic notch).
6. Ventricular pressure falls below atrial pressure.

Using the data obtained from the above tests, the following variables were calculated:

- Duration of the forward flow phase: The amount of time taken by the systolic phase expressed as a percentage of the heartbeat period. Also known as systolic fraction.
- Mean flow rate: The average flow rate measured over a heartbeat.
- Effective Orifice Area: EOA should not be confused with the geometric area of the valve orifice. It is a performance based indication of a PHV's flow area which is calculated from flow rate and pressure data under pulsatile conditions as per Test 1 above. The ISO5840:2005 suggests using the following equation to calculate EOA based on the volumetric flow rate and Bernoulli equations:

$$EOA = \frac{q_{v_{RMS}}}{51{,}6 \times \sqrt{\frac{\Delta P_{mean}}{\rho}}} \qquad (15)$$

where

EOA = effective orifice area (cm^2)

ΔP_{mean} = mean positive pressure difference during the forward flow phase (mmHg)

ρ = test fluid density (g/cm^3)

and

$$q_{v_{RMS}} = \sqrt{\frac{\int_{t_1}^{t_2} q_v(t)^2 dt}{t_2 - t_1}} \qquad (16)$$

$q_{v_{RMS}}$ = root mean square forward flow (mL/s)

$q_v(t)$ = instantaneous flow rate

t_1 = time at start of forward flow (s)[9]

t_2 = time at end of forward flow (s)[9]

- Total regurgitant volume, discretised into closing and leakage volumes:

$$V_{reg\_total} = V_{closing} + V_{leakage} \qquad (17)$$

- MAP: arterial pressure, averaged over the entire heartbeat

3.4.3 Comparative tests

3.4.3.1 Comparison to original CPD

Having obtained the pump's discharge profile given by the original cam, it was tested on the new CPD to compare the pressure measurements against those obtained with the old

[9] Due to the flowmeter's poor performance during pulsatile conditions, the times used correspond to the positive differential pressure period, which is as recommended in ISO5840-1:2015.

setup. To enable comparisons to be made as directly as possible the heart rate and pressure conditions were matched to the available data, which had been acquired at 72 bpm. For tests that were run using the CPD in its final state the stroke volume was set to 100mL to match the cam's discharge.

3.4.3.2 Comparison to published data

ViVitro SuperPump

ViVitro Labs' SuperPump is at the core of the ViVitro Pulse Duplicator System and it is the most popular commercial pump for generating cardiac flows [102]. The most important performance criterion quoted in the SuperPump's datasheet is the waveform accuracy. To be able to make a direct comparison, two tests were carried out since values are quoted for two different heart rates: 70 bpm and 200 bpm with a stroke volume of 75 mL. The control waveform was the same as that used for the ISO tests.

The accuracy for the BERG CPD was calculated based on the RMSE between the setpoint and the measured waveforms (as described in Section 3.4.1.3). The RMSE was then multiplied by the area of the piston pump to obtain a volumetric error indicative of accuracy throughout the entire heartbeat. The error was derived from the accuracy and expressed as a percentage of the stroke volume at a given heart rate.

Commercial CPD

Testing of commercial PHVs was done in order to prove the CPD's capabilities. However, it is also important to compare the results obtained with the CPD to those published in the scientific literature so as to establish how this apparatus performs in relation to its ISO-certified counterparts. To make direct comparisons to the data available for the equivalent model and size of PHV, the tests described in Table 3.8 were performed using the SJME 23 mm PHV.

Table 3.8: Tests for comparison to published data. (HR: heart rate; CO: cardiac output; SV: stroke volume; P_{sys}: arterial systolic pressure; P_{dias}: arterial diastolic pressure).

Test	HR (bpm)	CO (L/min)	SV (mL)	P_{sys}/P_{dias} (mmHg)
1	70	2	28.57	120/80
2	70	4	57.14	120/80
3	70	5	71.43	120/80
4	70	7	100.00	120/80

The measurements of interest were the pressure readings across the valve during the forward flow phase of the systolic period. An auxiliary measurement is the stroke work loss (SWL) which is expressed as a percentage of the ratio between mean systolic arterial pressure and mean systolic ventricular pressure:

$$SWL = \left(1 - \frac{P_{sys\_mean\_art}}{P_{sys\_mean\_vent}}\right) \times 100 \qquad (18)$$

where

$P_{sys\_mean\_art}$ = mean systolic arterial pressure

$P_{sys\_mean\_vent}$ = mean systolic ventricular pressure

Together with the peak and mean systolic pressure difference, SWL represents a good metric of valve performance during the forward flow period. As with the previous tests, ten cycles were recorded, analysed and the results reported as mean, range and SD.

4 Results

4.1 Cylinder and controller performance

4.1.1 Speed controller

Figure 4.1 presents the results of the magnitude/frequency speed tests for the electric cylinder (as set out in Table 3.3). Each bar represents the difference between the setpoint and the measured speed for each frequency (equivalent to HR) for one maximum speed at a time. The error is positive when the cylinder extends and negative when it retracts.

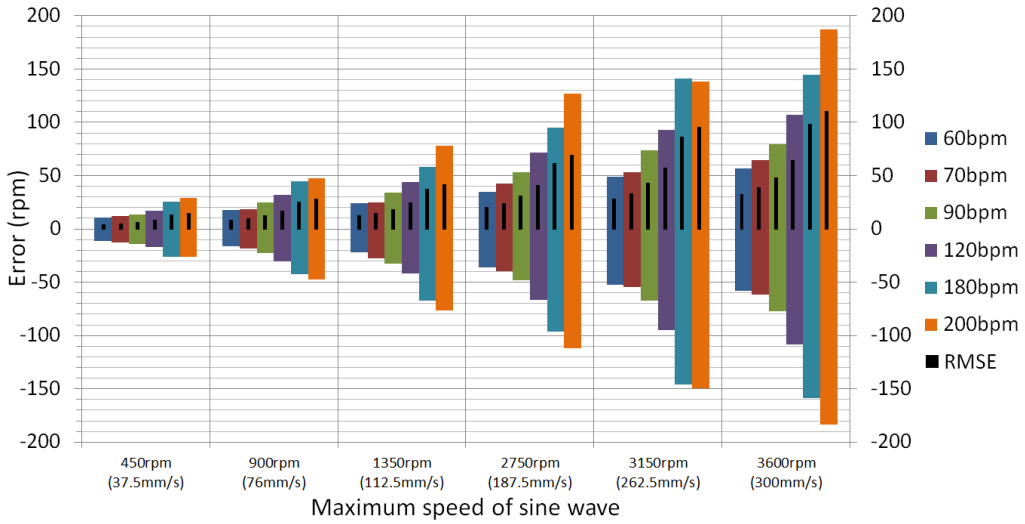

Figure 4.1: Dynamic speed tracking error.

4.1.2 Position controller

Figure 4.2 (CO = 5 L/min) and Figure 4.3 (CO = 24.2 L/min) depict the controller's behaviour after experimental fine tuning for two vastly different operating conditions (although the control waveform is morphologically identical for both cases). The tuning parameters determined through this experiment and used in each case are recorded in Table 4.1 which is related to Figure 3.17. To highlight the drastic difference in the demands of the setpoint and how the controller behaves in these situations, the span of all the graphs' axes has been kept equal for corresponding graphs across both figures. A total of three plots are displayed per graph: the setpoint, the measured position and the measured position phased in post-processing. The phasing time is highly dependent on the PID constants. Further details about phasing time and error are presented in Section 4.1.4.

Table 4.1: Tuning parameters used in the PI position controller.

CO	HR (bpm)	SV (mL)	K_p	T_i
5 L/min	70	71.43	2	0.15
24.2 L/min	189	128	3	0.03

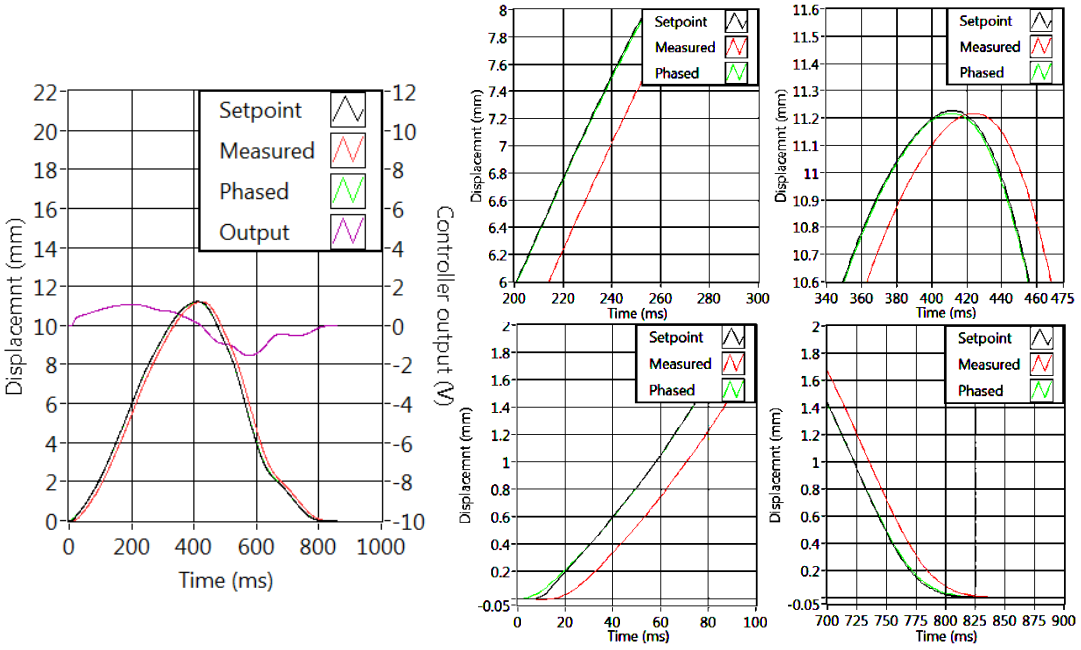

Figure 4.2: Position controller response at HR = 70 bpm and SV = 71.43 mL.

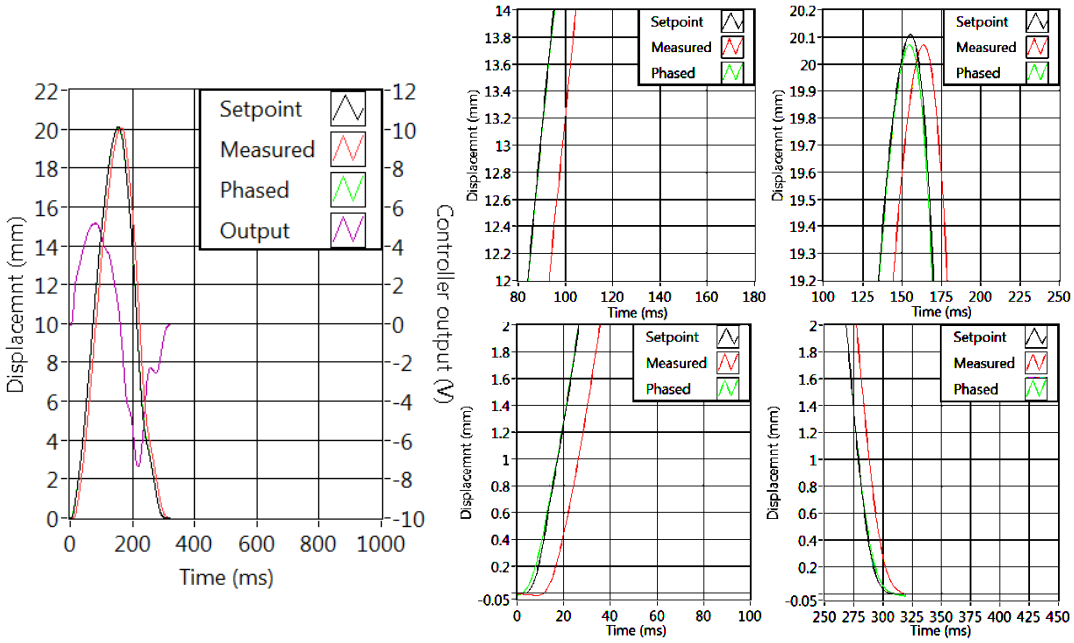

Figure 4.3: Position controller response at HR = 189bpm and SV = 128mL.

4.1.3 Accuracy and resolution

The results of these tests are presented graphically in Figure 4.4. The plotted difference is with respect to a baseline measurement (bottom graph) where the red circle indicates the area upon which the modified control point has the largest effect on the control waveform. The velocity shown in the figure is included to provide an indication of the range at which the tests took place. Although the quoted repeatability accuracy for the

electric cylinder is ±0.05 mm [103], only changes below 0.005 mm did not produce a noticeable difference.

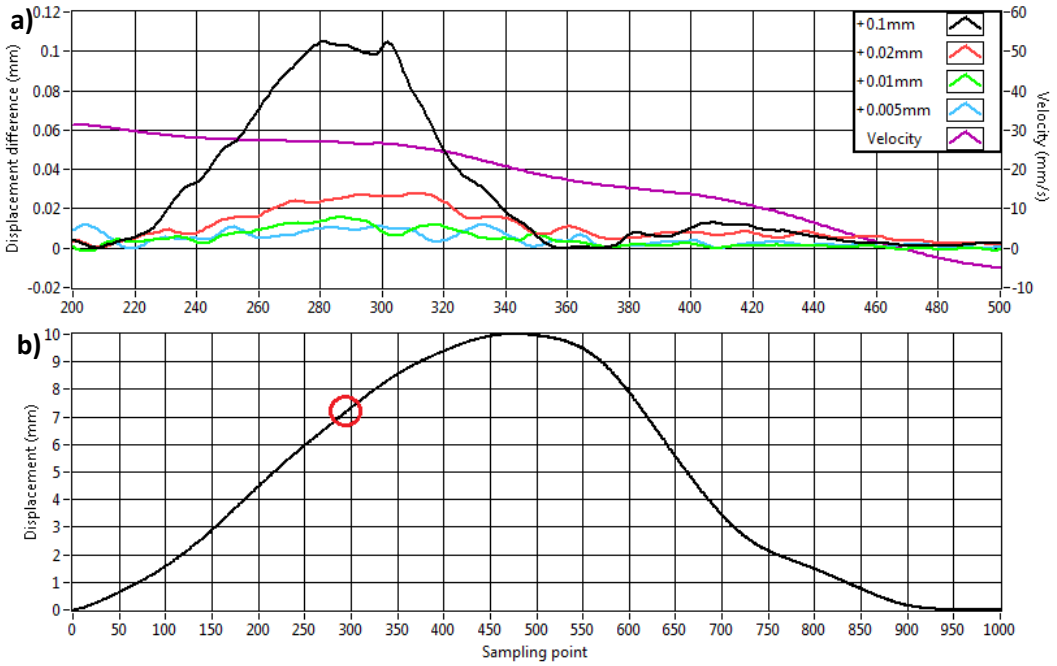

Figure 4.4. a) Extract of the measured positions plotted as the difference to the baseline. b) Overview of the baseline measured position.

4.1.4 Tracking

Table 4.2 presents the results of the tracking tests with "RMSE, phased" indicating the effective tracking error. "Lag" is the amount of time by which the position feedback was shifted to obtain the phased RMSE.

Table 4.2: Results for overall tracking tests.

Operating point / Beat	HR = 70 bpm, SV = 71.43 mL			HR = 140 bpm, SV = 120 mL			HR = 189 bpm, SV = 128 mL		
	RMSE (mm)	RMSE, phased (mm)	Lag (ms)	RMSE (mm)	RMSE, phased (mm)	Lag (ms)	RMSE (mm)	RMSE, phased (mm)	Lag (ms)
Beat 1	0.405	0.016		1.059	0.064		1.334	0.044	
Beat 2	0.403	0.016		1.064	0.063		1.327	0.048	
Beat 3	0.406	0.016		1.068	0.059		1.326	0.049	
Beat 4	0.404	0.018	13	1.067	0.069	10	1.330	0.049	9
Beat 5	0.403	0.029		1.065	0.095		1.328	0.052	
Mean	0.404	**0.019**		1.065	**0.070**		1.329	**0.048**	
±SD	0.001	**0.006**		0.003	**0.014**		0.003	**0.003**	

4.2 Cam profiling

The results of the cam profiling experiment can be seen in Figure 4.5. The upper graph indicates the recorded raw voltage from the LDVT for each encoder pulse. The lower graph is the average of the first five revolutions and shows scaled values representing the displacement of the cam. In this case the selected number of points for the output curve is 500. Using the scanned image of the cam shown in the inset of Figure 4.5 as reference, the lower graph corresponds to the profile of the cam starting approximately at 12 o'clock and moving clockwise. To generate a basic control waveform that could be easily modified from the motion design interface of the CPD's control program, a 16 point curve was also generated. Each interpolated data point could then be used as the value for the respective control point. The 16 point output is shown in Table 4.3.

Analysis of the 500 point numerical model enabled the extraction of the cam's basic parameters. The maximum displacement (lift) recorded was 15.57 mm, corresponding to a SV of 99.07 mL. Assuming a combined error of 1% arising from manufacture, wear and measurement, it can be deduced that Krynauw most likely designed the cam to produce a SV of 100 mL which makes this cam useful only for one of the ISO tests. The profile yielded a systolic fraction of 38% with 1% (3.6°) dwell at full lift and 13% (46.8°) dwell at base circle. Appendix B contains a 500 point numerical model of the cam and a 6th order polynomial fit function describing the same experimental results. The polynomial function achieves a summed square error of 3.786 and a RMSE of 0.087.

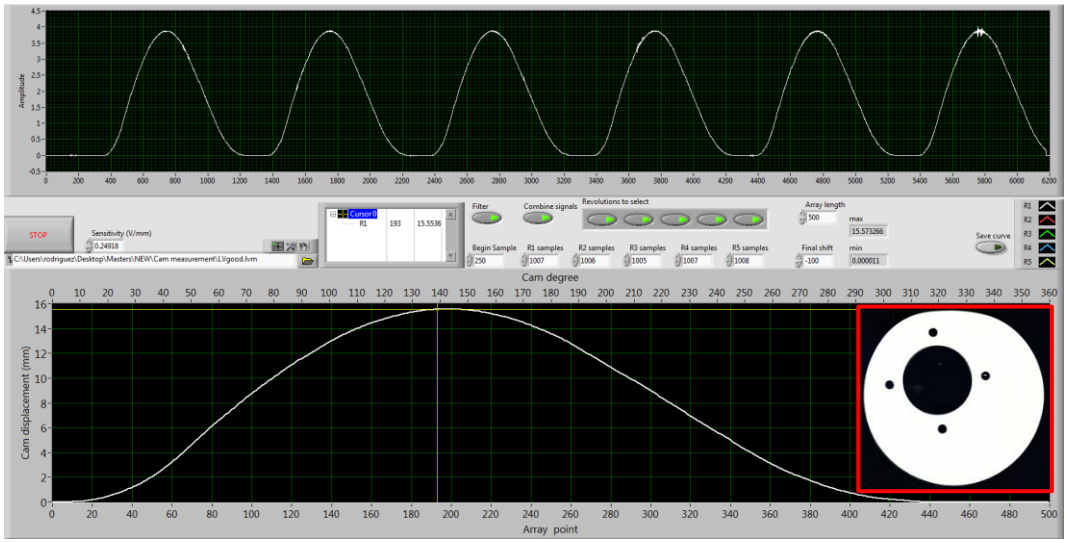

Figure 4.5: Interface of the processing program used to extract the cam profile. The upper graph displays experimental raw data and the lower graph the resultant cam profile. Inset: processed scan of the actual cam.

Table 4.3: Control points used to describe the original cam's profile.

Control point	**1**	**2**	**3**	**4**	**5**	**6**	**7**	**8**
Value (scaled to mm)	*0.017*	*0.614*	*3.085*	*7.050*	10.528	13.312	15.080	15.719
Control point	**9**	**10**	**11**	**12**	**13**	**14**	**15**	**16**
Value (scaled to mm)	15.159	13.511	10.912	8.191	5.411	2.825	1.103	0.216

4.3 Hydrodynamic results

4.3.1 Adjustment of lump parameter controls

Aortic root compliance and peripheral resistance

The target pressure was achieved by setting the resistor at approximately 90° from its fully closed position. The area open to flow for this position is 16.4 mm^2 at the entrance of the resistor. An increase in peripheral resistance increases overall arterial pressure while increasing the aortic root compliance volume raises only the diastolic pressure. Diastolic pressure was found to be directly proportional to the volume of air in the compliance chamber for a given heart rate. Figure 4.6 shows pressure and flow plots of the three steps in this test. Table 4.4 contains the lump parameter control values used to achieve the target pressures as well as numerical results of the test. Note the systolic pressure listed in Table 4.4 for the centre and right plots indicates the maximum arterial pressure before the dichrotic notch. All pressures are arterial.

Table 4.4: Effect of aortic root compliance and peripheral resistance on pressure. (C: compliance; R: resistance; P_{sys}: systolic arterial pressure; P_{dias}: diastolic arterial pressure; MAP: mean arterial pressure.)

	Figure 4.6, left	**Figure 4.6, centre**	**Figure 4.6, right**
Test conditions	C and R unspecified	R changed to achieve target (P_{sys} = 120 mmHg)	C changed to achieve target (P_{dias} = 80 mmHg)
C (mL air)	~650	~650	~1208
R (qualitative)	Unrestrictive	~90° from fully closed	~90° from fully closed
P_{sys} (mmHg)	23.48	121.62	117.91
P_{dias} (mmHg)	-11.81	43.71	78.01
MAP (mmHg)	2.30	80.45	99.00

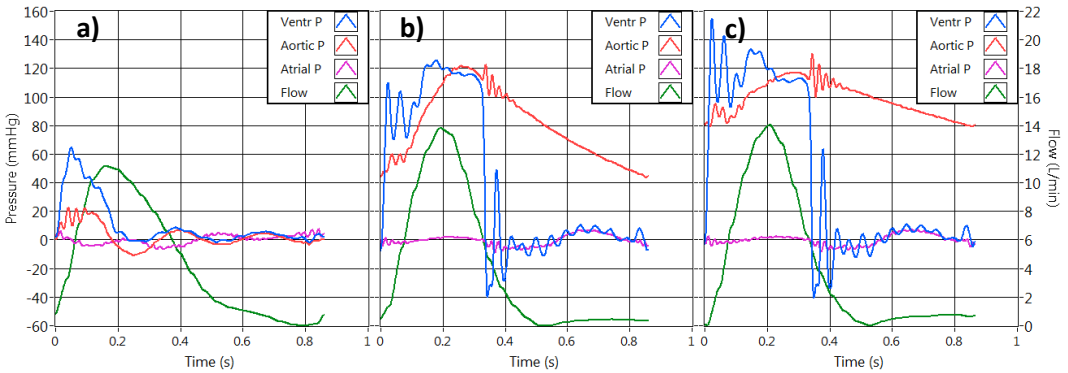

Figure 4.6: Pressure response to lump parameter adjustments. a) No resistance set; b) resistance set for target systolic pressure; c) aortic root compliance set for target diastolic pressure

Ventricular compliance

Adjustment of the ventricular compliance controls produced acceptable results for the first test. Under these conditions, the controls were effective in reducing ventricular pressure oscillations after closure of the aortic valve (this is made evident in Figure 4.7 between 0.4 s and 0.5 s). A portion of these oscillations' amplitude can be seen to be

transmitted to the arterial pressure, especially immediately after the aortic valve closes. It was found that 6 mL of air in the ventricular compliance chamber was the ideal volume and any further increase in volume had a detrimental effect regardless of the resistance setting. Resistance only had an evident effect when using a high setting. To demonstrate the effects of compliance and resistance separately, an extra set of data was acquired after having adjusted the controls. This set of data was recorded with the final compliance volume but with no resistance and it corresponds to the centre panel on Figure 4.7. Table 4.5 contains the most relevant pressure values related to each panel of Figure 4.7.

Table 4.5: Effect of ventricular compliance controls on pressure. HR = 70 bpm, CO = 5 L/min. (C: compliance; R: resistance; P_{sys}: systolic arterial pressure; P_{dias}: diastolic arterial pressure; MAP: mean arterial pressure; -ΔP_{mean}: mean back pressure.

		Figure 4.7, left	Figure 4.7, centre	Figure 4.7, right
	C (mL air)	0	6	6
	R (qualitative)	Unrestrictive	Unrestrictive	ball valve 7/10 closed
Arterial	P_{sys} (mmHg)	12.32	118.48	121.16
Arterial	P_{dias} (mmHg)	79.63	77.90	76.86
Arterial	**MAP** (mmHg)	99.79	99.14	97.93
Vent	P_{max} (mmHg)	363.14	189.14	163.48
Vent	P_{min} (mmHg)	-50.73	-49.09	-42.05
	-ΔP_{mean} (mmHg)	83.87	86.13	95.68

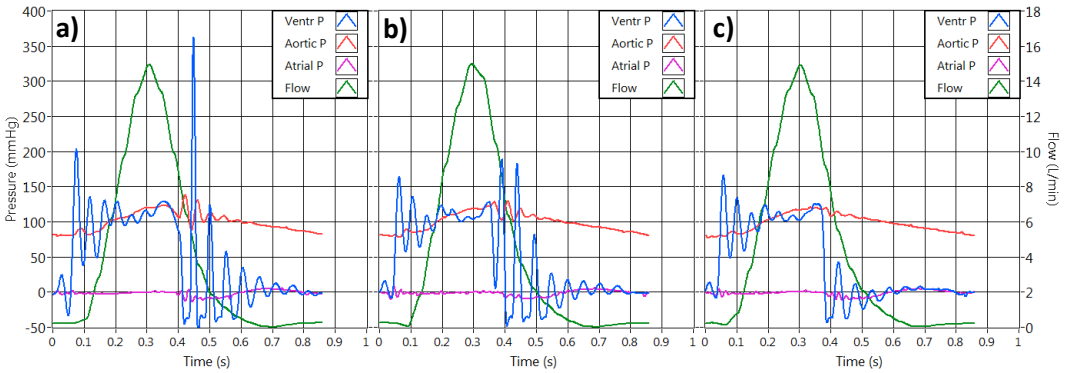

Figure 4.7: Pressure response to ventricular compliance adjustments for test 1. a) No resistance or compliance; b) compliance only; c) compliance with resistance.

The performance of the ventricular compliance feature was not satisfactory for the second test. Any volume of air in the ventricular compliance chamber, up to 50 mL, resulted in an increased peak ventricular pressure during diastole. Various resistance settings were tested with no significant changes being observed. The measurements in Table 4.6 show an overall decrease in arterial pressure as a result of the reduced effective SV caused by the air in the ventricular compliance chamber being compressed. This agrees with the findings from the test at 70 bpm. However, the peak to peak amplitude of the ventricular pressure oscillations increased. Figure 4.8 shows a trend of increased diastolic

peak pressure with increased compliance volume, suggesting a resonance or reflecting wave problem (see Section 5.1.2).

Table 4.6: Effect of ventricular compliance controls on pressure. HR = 90 bpm, CO = 7.5 L/min. (C: compliance; R: resistance; P_{sys}: systolic arterial pressure; P_{dias}: diastolic arterial pressure; MAP: mean arterial pressure; $-\Delta P_{mean}$: mean back pressure.

		Figure 4.8, left	Figure 4.8, centre	Figure 4.8, right
	C (mL air)	0	12	24
	R (qualitative)	Unrestrictive	ball valve 7/10 closed	ball valve 7/10 closed
Arterial	P_{sys} (mmHg)	142.22	140.106	137.39
Arterial	P_{dias} (mmHg)	83.29	77.10	75.79
Arterial	**MAP** (mmHg)	112.44	111.15	109.08
Vent	P_{max} (mmHg)	320.85	405.08	512.91
Vent	P_{min} (mmHg)	-47.15	-52.92	-60.22
	$-\Delta P_{mean}$ (mmHg)	96.86	95.10	85.31

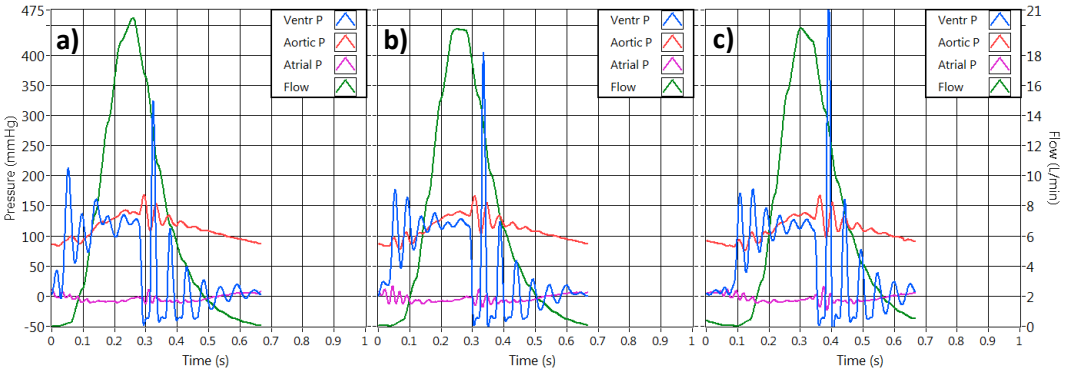

Figure 4.8: Pressure response to ventricular compliance adjustments for test 2. a) No resistance or compliance; b) compliance only; c) compliance with resistance.

Based on these results, it was concluded that the current ventricular compliance model is inadequate for the desired quality of data at elevated heart rates. The ventricular compliance model used, with a single compliance chamber, did not provide the ability to control systolic and diastolic pressure features independently. A simple modification to incorporate an extra compliance element is proposed in Section 6.2.

4.3.2 Response to changes in a single control point

Figure 4.9 shows the resultant ventricular pressure for each of the changes made to the control point. This panel also demonstrates the effect of the interpolation method used: notice the small decrease in path around locations 100 and 175. A well-defined relationship between ventricular pressure and the control waveform can be observed. The results of this test highlighted how a small change in the path of the cylinder affects fluid inertia and consequently pressure, supporting the findings in Section 4.1.3.

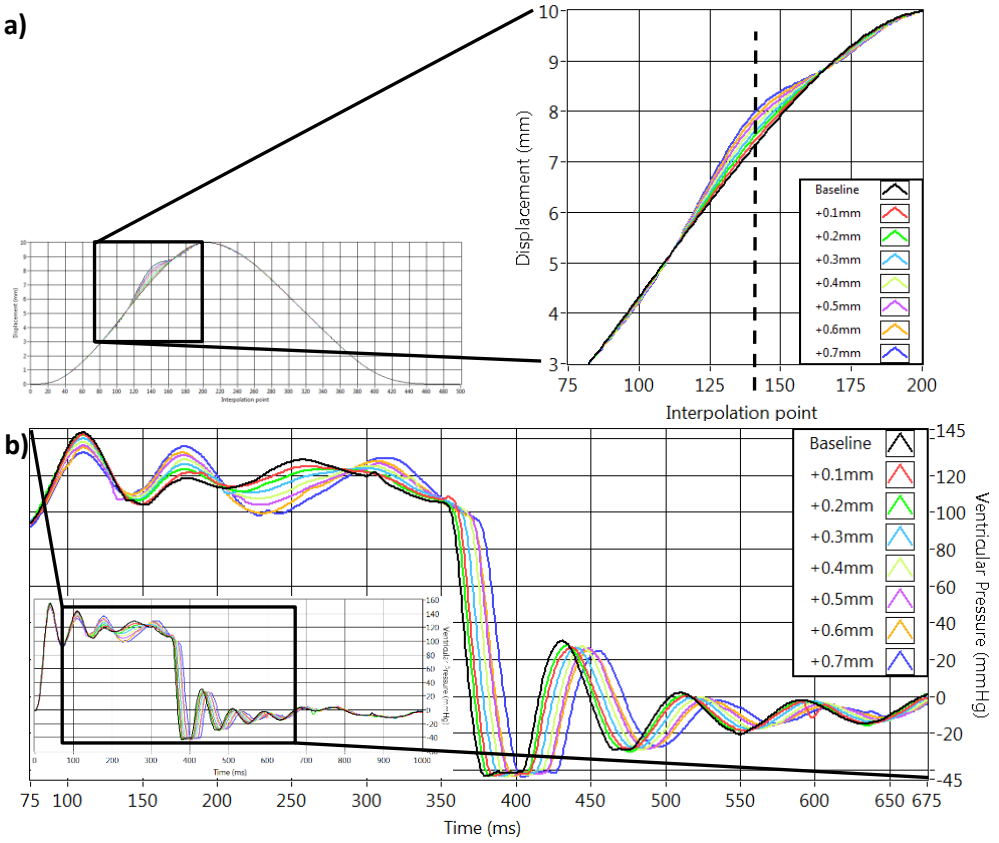

Figure 4.9: a) Control waveform used for each heartbeat. b): Corresponding ventricular pressure.

4.3.3 Tuning the pressure profile

This experiment illustrates the practical application of the tests carried out in Section 4.1.3 and Section 4.3.2, demonstrating the fine control offered by the system. Through subtle manipulation of the first five control points the systolic pressure spikes were eliminated. Table 4.7 contains the scaled values of the control points that describe the two waveforms used in this test. Grey values were unchanged. Figure 4.10 shows the resultant changes in pressures as well as a depiction of the control waveform. It can be seen that the displacement difference (blue line in the right panel) closely resembles the original pressure spikes and as a result has a direct counteracting effect upon them.

Table 4.7: Control points used for tuning the pressure profile. Scaled values are in mm.

Original control waveform	Control point	**1**	**2**	**3**	**4**	**5**	**6**	**7**	**8**
	Value (scaled)	0.209	1.335	3.101	5.211	7.241	8.961	10.000	9.879
	Control point	**9**	**10**	**11**	**12**	**13**	**14**	**15**	**16**
	Value (scaled)	8.981	7.561	5.911	4.241	2.631	1.230	0.381	0.060
Modified control waveform	Control point	**1**	**2**	**3**	**4**	**5**	**6**	**7**	**8**
	Value (scaled)	*0.519*	*1.345*	*3.071*	*5.121*	*7.421*	8.961	10.000	9.879
	Control point	**9**	**10**	**11**	**12**	**13**	**14**	**15**	**16**
	Value (scaled)	8.981	7.561	5.911	4.241	2.631	1.230	0.381	0.060

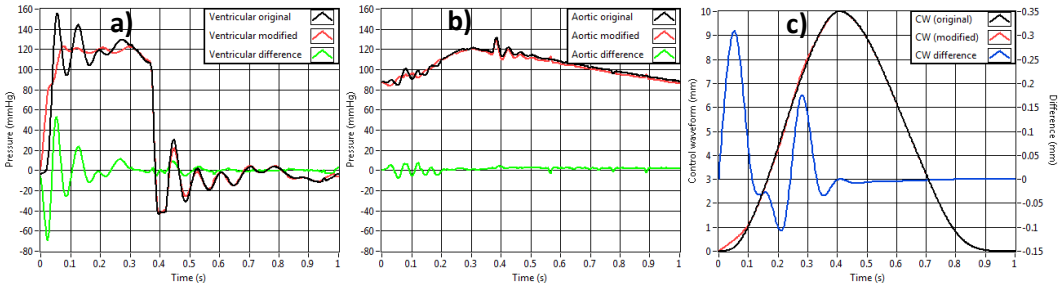

Figure 4.10: Measurements before tuning (black) and after tuning (red) for a) ventricular pressure, b) aortic pressure and c) control waveform.

4.4 Repeatability and fidelity tests

4.4.1 Repeatability

Intra-test and inter-test results are presented in Table 4.8 which is organised in the same fashion as Figure 3.21 to help in visualising the flow of data leading to the inter-test repeatability value. The baseline heartbeat used to obtain these results is part of the first test (T1). The second set of data (T2) was acquired 2500 heartbeats after the initial recording.

Table 4.8: Hydrodynamic repeatability results. All values are in mmHg.

	T1					T2				
	Beat 1	Beat 2	Beat 3	Beat 4	Beat 5	Beat 1	Beat 2	Beat 3	Beat 4	Beat 5
ΔP RMSE	3.375	1.638	1.257	2.193	1.139	2.776	1.968	3.087	1.789	2.467
Intra-test mean	**1.921**					**2.417**				
Intra-test ±SD	**0.911**					**0.542**				
Inter-test mean	**2.169**									
Inter-test ±SD	**0.727**									

4.4.2 Fidelity

To analyse fidelity it helps to visualise the history of the entire process rather than concentrate on a single point of interest. The left panel in Figure 4.11 depicts arterial pressure for 100 heartbeats. The XY view on the right panel is useful to visualise how the location of a specific area of pressure (systolic or diastolic) changes in magnitude and phase from one heartbeat to the next.

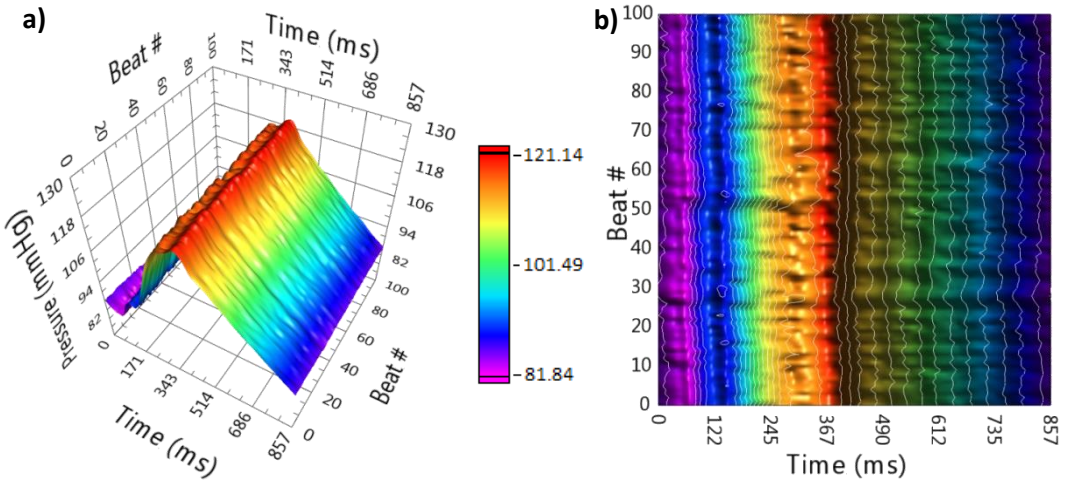

Figure 4.11: a) Surface plot of arterial pressure for 100 heartbeats. b) XY plane view (with contour lines) of the surface plot showing the location of highest pressure (red) and lowest pressure (purple) for 100 heartbeats.

While Figure 4.11 provides an easier way to display the whole dataset and is more effective at visually presenting the results over time, the combination graph in Figure 4.12 shows only information pertinent to the variables of interest. Table 4.9 complements the combination graph with statistical results. This constitutes supporting information that leads to the quantification of fidelity.

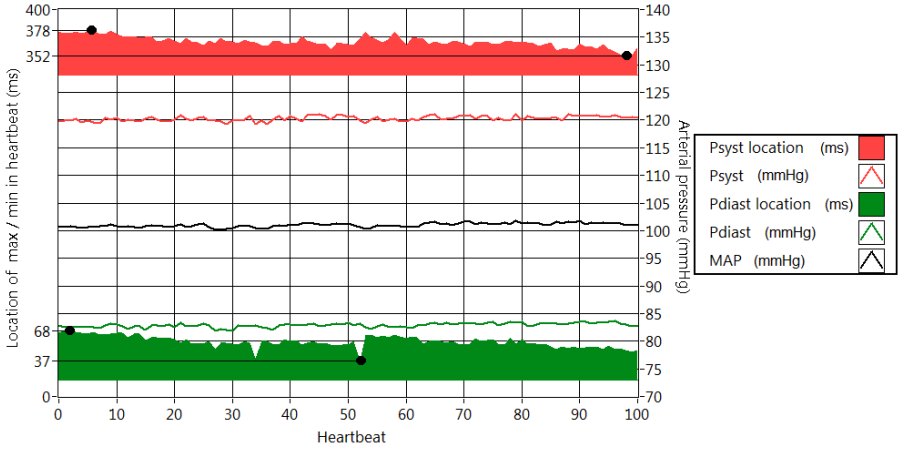

Figure 4.12: Graphical results for the variables of interest.

Table 4.9: Statistical results to supplement Figure 4.12.

	Systolic		Diastolic		MAP (mmHg)
	Pressure (mmHg)	Location (ms)	Pressure (mmHg)	Location (ms)	
Target	120	356	80	58	100
Max	121.14	378	83.70	68	101.75
Min	119.25	352	81.84	37	100.13
Mean	120.25	367	82.88	57	100.99
SD	0.46	5.5	0.39	5.7	0.37

Table 4.10 shows the individual fidelity values leading to the final statement of fidelity for the machine. These results indicate that the combination of pressure and its location (where applicable) is within 4.6% of the individual targets for 90% of the heartbeats.

Table 4.10: Fidelity description of the CPD.

	$\mathcal{F}_{P_{syst}}$	$\mathcal{F}_{P_{diast}}$	$\mathcal{F}_{MAP}$	$\boldsymbol{\mathcal{F}_{P_{arterial}}}$
90th percentile	0.028	0.094	0.015	**0.046**

4.5 ISO5840:2005 tests

Table 4.11 to Table 4.17 contain statistical results for each of the ISO tests. These results are derived from the analysis of ten consecutive heartbeats (refer to Appendix C for the complete dataset). Columns in bold are the measurements requested by each test, as per Table 3.7. The rest of the columns are supporting measurements included as proof of the test conditions under which the main measurement was obtained.

The flowmeter was found the have very poor performance during pulsatile flow conditions. Measurements were always under the expected value but the error was partly dependant on heart rate and stroke volume. In an effort to overcome this problem, an attempt was made to produce a calibration map for a combination of HRs and SVs by connecting the flowmeter directly to the pump and although results were better, they were variable. One major problem was that the flowmeter could not accurately identify flow reversal and this was exacerbated when valves were included in the flow loop. Most of these problems were attributed to the flowmeter's integral time constant which could not be removed from the software (it was set to its minimum value of 0.1 s) and the 25 Hz (40 ms) update rate which for this application is very slow. Unfortunately, no suitable flowmeters were available. Therefore, the flow and volume measurements presented in the following sections are not representative of actual conditions but are included as they can still show trends.

4.5.1 Pressure drop

This section presents the results of the pressure drop tests with Table 4.11 to Table 4.14 showing statistical information for each test. Effective orifice area (EOA) was calculated for all pressure drop tests. The representative wave (part of Test 1) of each PHV can be seen in Figure 4.13.

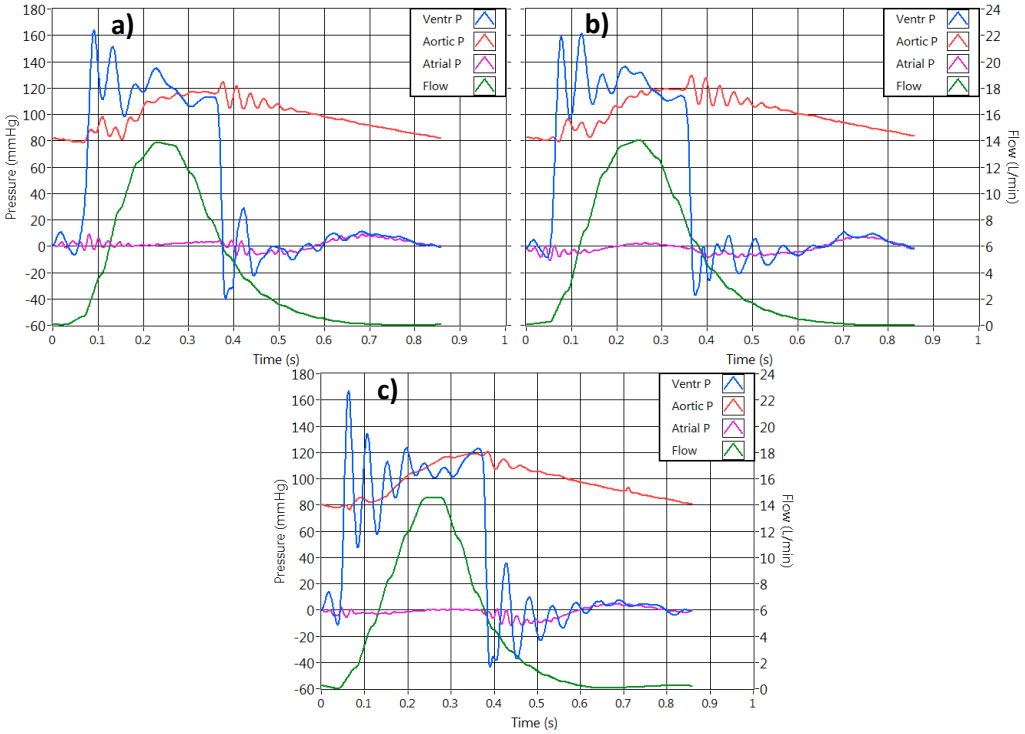

Figure 4.13: Representative waves showing ventricular, aortic and atrial pressures, as well as aortic flow rate. a) SJM Epic valve 1; b) SJM Epic valve 2; c) SJM Regent valve.

Table 4.11: Statistical results for Test 1. (HR = 70 bpm; CO = 5 L/min; MAP = 100 mmHg).

		EOA (cm^2)	**ΔP_{mean} (mmHg)**	MAP (mmHg)	Q_{mean} (L/min)	Systole (%)	T_{sys} (ms)
SJME V1	Mean	**0.86**	**17.47**	98.86	4.69	36.1	309.8
	SD	± **0.01**	± **0.33**	± 0.32	± 0.04	± 0.4	± 3.0
	Max	**0.87**	**18.20**	99.38	4.76	36.6	314
	Min	**0.85**	**17.16**	98.22	4.63	35.4	304
SJME V2	Mean	**0.81**	**20.04**	100.59	4.69	35.2	301.8
	SD	± **0.01**	± **0.21**	± 0.34	± 0.03	± 0.2	± 1.2
	Max	**0.82**	**20.34**	101.40	4.76	35.5	304
	Min	**0.80**	**19.56**	100.18	4.65	35.0	300
SJMR	Mean	**1.83**	**3.57**	98.08	3.97	37.1	317.7
	SD	± **0.03**	± **0.08**	± 0.45	± 0.05	± 0.6	± 5.2
	Max	**1.88**	**3.71**	98.57	4.00	38.0	326
	Min	**1.78**	**3.43**	97.27	3.84	36.1	309

Table 4.12: Statistical results for Test 2. (HR = 70 bpm; CO = 2 L/min; MAP = 100 mmHg).

		EOA (cm^2)	**ΔP_{mean} (mmHg)**	MAP (mmHg)	Q_{mean} (L/min)	Systole (%)	T_{sys} (ms)
SJME V1	Mean	**0.56**	**7.36**	100.23	1.92	34.8	298.6
	SD	± **0.01**	± **0.17**	± 0.41	± 0.03	± 0.5	± 4.3
	Max	**0.57**	**7.57**	100.72	1.95	35.6	300
	Min	**0.55**	**7.10**	99.47	1.87	34.3	294
SJME V2	Mean	**0.50**	**5.49**	100.22	1.43	34.9	298.9
	SD	± **0.01**	± **0.10**	± 0.24	± 0.04	± 0.3	± 2.9
	Max	**0.51**	**5.65**	100.74	1.49	35.6	305
	Min	**0.48**	**5.32**	99.96	1.37	34.3	294

Table 4.13: Statistical results for Test 3. (HR = 70 bpm; CO = 3.5 L/min; MAP = 100 mmHg).

		EOA (cm^2)	**ΔP_{mean} (mmHg)**	MAP (mmHg)	Q_{mean} (L/min)	Systole (%)	T_{Sys} (ms)
SJME V1	Mean	**0.70**	**11.10**	99.08	3.05	35.4	303.5
	SD	± **0.01**	± **0.12**	± 0.47	± 0.03	± 0.3	± 2.8
	Max	**0.71**	**11.28**	99.62	3.08	36.1	309
	Min	**0.69**	**10.93**	98.30	3.00	34.9	299
SJME V2	Mean	**0.71**	**11.23**	98.46	3.10	35.5	304.2
	SD	± **0.00**	± **0.10**	± 0.32	± 0.02	± 0.4	± 3.2
	Max	**0.71**	**11.42**	98.99	3.13	36.2	310
	Min	**0.71**	**11.03**	97.86	3.08	35.1	301

Table 4.14: Statistical results for Test 4. (HR = 70 bpm; CO = 7 L/min; MAP = 100 mmHg).

		EOA (cm^2)	**ΔP_{mean} (mmHg)**	MAP (mmHg)	Q_{mean} (L/min)	Systole (%)	T_{Sys} (ms)
SJME V1	Mean	**0.93**	**29.53**	101.13	6.98	36.2	310.1
	SD	± **0.01**	± **0.80**	± 0.25	± 0.05	± 0.50	± 4.4
	Max	**0.94**	**30.88**	101.52	7.09	37.0	317
	Min	**0.91**	**28.72**	100.69	6.91	35.5	304
SMJE V2	Mean	**0.91**	**31.26**	96.48	6.97	35.7	306.2
	SD	± **0.01**	± **0.40**	± 0.21	± 0.07	± 0.30	± 2.9
	Max	**0.92**	**31.87**	96.81	7.06	36.3	311
	Min	**0.90**	**30.63**	96.01	6.86	35.00	300

4.5.2 Regurgitation

This section presents the results for the regurgitation volume tests. Table 4.15 to Table 4.17 contain statistical results for the two PHVs that underwent these tests. Bearing in mind the limitations of the flowmeter, these results are included to show trends rather than actual values.

Table 4.15: Statistical results for Test 5. (HR = 45 bpm; CO = 5L/min;–ΔP_{mean} = 80 mmHg).

		V_{reg_total} (mL)	$V_{closing}$ (mL)	$V_{leakage}$ (mL)	Q_{mean} (L/min)	$-\Delta P_{mean}$ (mmHg)	MAP (mmHg)
SJME V1	Mean	**25.91**	**13.27**	**12.63**	4.39	79.21	93.11
	SD	± **0.81**	± **0.53**	± **0.72**	± 0.03	± 0.61	± 0.64
	Max	**26.88**	**14.00**	**14.28**	4.44	80.04	94.11
	Min	**24.37**	**12.39**	**11.38**	4.34	78.40	92.43
SJME V2	Mean	**25.11**	**12.62**	**12.49**	4.40	80.15	93.81
	SD	± **0.86**	± **0.42**	± **1.10**	± 0.03	± 0.50	± 0.25
	Max	**26.18**	**13.29**	**14.22**	4.44	80.81	94.19
	Min	**23.92**	**11.96**	**11.10**	4.35	79.16	93.38

Table 4.16: Statistical results for Test 6. (HR = 70 bpm; CO = 5L/min; –ΔP_{mean} = 120 mmHg).

		V_{reg_total} (mL)	$V_{closing}$ (mL)	$V_{leakage}$ (mL)	Q_{mean} (L/min)	$-\Delta P_{mean}$ (mmHg)	MAP (mmHg)
SJME V1	Mean	**22.87**	**9.61**	**13.26**	3.92	119.59	142.10
	SD	± **1.02**	± **0.37**	± **0.90**	± 0.06	± 0.38	± 0.28
	Max	**23.99**	**10.27**	**14.50**	3.99	120.18	142.61
	Min	**21.64**	**9.17**	**11.79**	3.84	118.84	141.75
SJME V2	Mean	**23.65**	**9.86**	**14.06**	4.10	118.34	131.53
	SD	± **1.22**	± **0.525**	± **1.19**	± 0.07	± 0.41	± 0.74
	Max	**25.21**	**10.26**	**15.58**	4.19	119.01	132.22
	Min	**21.55**	**8.68**	**12.13**	4.00	117.80	130.45

Table 4.17: Statistical results for Test 7. (HR = 120 bpm; CO = 5L/min; –ΔP_{mean} = 160 mmHg).

		V_{reg_total} (mL)	$V_{closing}$ (mL)	$V_{leakage}$ (mL)	Q_{mean} (L/min)	$-\Delta P_{mean}$ (mmHg)	MAP (mmHg)
SJME V1	Mean	**16.37**	**5.91**	**10.44**	3.04	154.18	194.51
	± SD	± **0.960**	± **0.191**	± **0.799**	± 0.119	± 0.759	± 0.70
	Max	**17.95**	**6.29**	**11.65**	3.21	155.25	195.64
	Min	**14.95**	**5.63**	**9.30**	2.86	152.68	193.83
SJME V2	Mean	**12.89**	**5.06**	**7.83**	2.35	156.68	193.94
	SD	± **0.94**	± **0.26**	± **0.90**	± 0.13	± 1.10	± 0.99
	Max	**14.14**	**5.67**	**9.22**	2.53	157.96	194.90
	Min	**11.30**	**4.73**	**6.18**	2.10	153.85	191.47

4.6 Comparative results

4.6.1 Comparison to original CPD

This section presents results in such a way as to allow comparisons to be made between results obtained at the various stages of the CPD starting from the initial design, followed

by its second iteration, then by improvements made as part of this work and eventually by the final state of the apparatus. In the left panel of Figure 4.14 are results obtained by Krynauw at 72 bpm. This is compared to unfiltered data recorded in the original configuration of the CPD under similar conditions (right panel), in order to establish the similarities. Although the measurements shown correspond to dissimilar PHVs, a good correlation can be observed between the two, particularly in terms of the morphology of the arterial pressure traces during systole, which do not exhibit physiological characteristics. It should be noted that Krynauw did not use the same valve chamber that was used for obtaining the measurements on the right panel (which constitutes part of the second iteration of the CPD, implemented prior to the start of this project) and this could be the reason for the high pressure differential seen in the ventricular trace between 0.2 s and 0.3 s. The remainder of the ventricular pressure profile follows the same tendency, notably the pressure spike at the beginning of systole at 0.05 s.

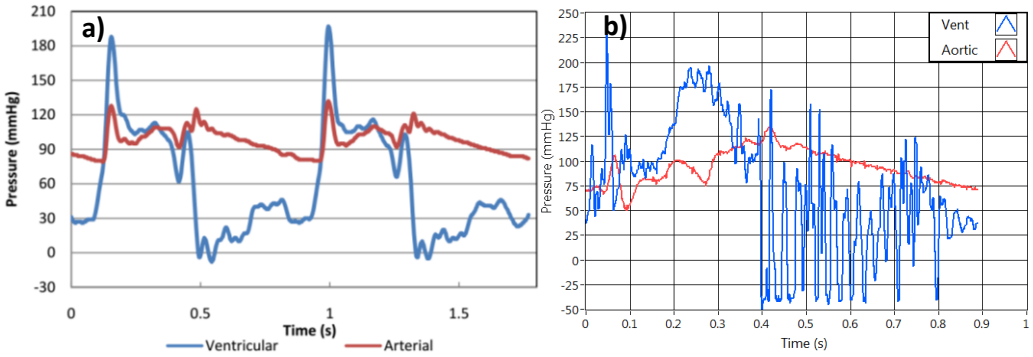

Figure 4.14: a) Pressure measurements obtained by Krynauw (adopted from [28]). b) Pressure measurements obtained with the original CPD configuration.

Figure 4.15 displays the results obtained after implementing the new compliance chamber and LVOT but still using the mechanical cam and the old resistance ball valve. The trends remain the same as with the old configuration for both ventricular and arterial pressure traces but the amplitude of the ventricular pressure spikes was reduced. Further, the large rise in ventricular pressure during the systolic phase was no longer present, suggesting smoother flow through the PHV.

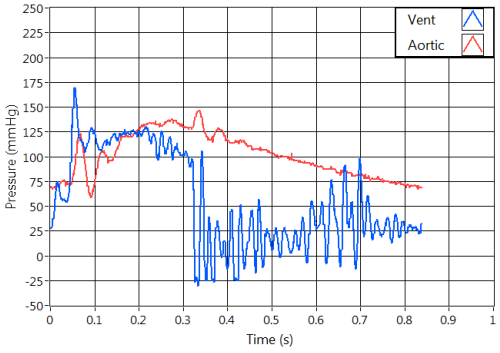

Figure 4.15: Pressure measurements obtained using the new compliance chamber and LVOT.

Results obtained with the system in its final configuration are shown in Figure 4.16. The left panel shows the pressures produced by the cam profile discussed in Section 4.2 (numerically described in Table 4.3). The ventricular trace still exhibits a systolic ventricular pressure spike (between 0 and 0.1 s) with the same features as those seen in Figure 4.14 and Figure 4.15, consistently affecting the arterial pressure trace. However, the frequency of the oscillations is drastically reduced as an effect of the compliant ventricle. The right panel shows the pressure produced by a modified control waveform. Only the first four control points were adjusted to eliminate the pressure spike (see Table 4.18); the remainder of the control points were as per Table 4.3. Eliminating the systolic pressure spike had the effect of making the arterial pressure rise more progressively and as a result, the pressure drop across the PHV is more constant, indicating smoother flow. The mean systolic pressure difference produced by the original cam was 31.46 mmHg and 23.33 mmHg after adjusting the control waveform. This pressure drop is characteristic of a stenotic valve presenting moderate stenosis.

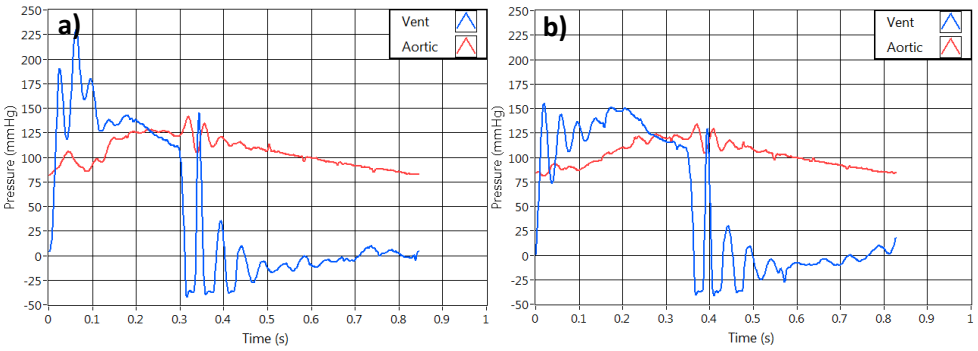

Figure 4.16: Results obtained from the system in its final state with a) unmodified cam profile showing systolic ventricular pressure spike between 0 and 0.1 s and b) modified cam profile showing reduced peak systolic ventricular pressure.

Table 4.18: Control points used to eliminate the ventricular pressure spike during systole.

	Control waveform (original cam)				Control waveform (modified cam)			
Control point	1	2	3	4	1	2	3	4
Value (scaled to mm)	*0.017*	*0.614*	*3.085*	*7.050*	*1.297*	*2.704*	*4.689*	*7.427*

4.6.2 Results used for comparison to published data

This section only reports results obtained from the tests intended to produce data to be compared against that of a commercial CPD (see Table 5.1 in Section 5.2.2 for the ViVitro Labs SuperPump comparison). The results presented here are for parameters that provide useful points of comparison against the data in the available literature. Thus, the outcomes of the test were the following: peak systolic pressure difference (ΔP_{peak}), mean systolic pressure difference (ΔP_{mean}) and stroke work loss. Table 4.19 presents the results for all the relevant parameters, including the systolic fraction which is reported as proof of the test conditions.

Table 4.19: Statistical results for SJME 23 mm PHV. (CO: cardiac output; ΔP_{peak}: peak systolic pressure difference; ΔP_{mean}: mean systolic pressure difference; SWL: stroke work loss)

CO	Parameter	Mean	SD	Max	Min
2 L/min	ΔP_{mean} (mmHg)	5.91	± 0.15	6.19	5.6
	ΔP_{peak} (mmHg)	11.17	± 0.90	13.56	10.34
	SWL (%)	6.03	± 0.14	6.30	5.81
	Systole (%)	33.0	± 0.2	33.1	32.4
4 L/min	ΔP_{mean} (mmHg)	12.48	± 0.23	12.7	12.05
	ΔP_{peak} (mmHg)	24.92	± 0.63	25.81	23.53
	SWL (%)	11.62	± 0.19	11.87	11.26
	Systole (%)	34.6	± 0.2	35.1	34.4
5 L/min	ΔP_{mean} (mmHg)	14.49	± 0.21	14.92	14.1
	ΔP_{peak} (mmHg)	24.39	± 0.47	25.62	23.81
	SWL (%)	13.41	± 0.19	13.79	13.06
	Systole (%)	35.8	± 0.2	36.1	35.5
7 L/min	ΔP_{mean} (mmHg)	19.17	± 0.29	19.54	18.68
	ΔP_{peak} (mmHg)	45.16	± 1.68	49.48	44
	SWL (%)	16.95	± 0.23	17.22	16.48
	Systole (%)	37.3	± 0.4	37.9	36.3

5 Discussion

Previous sections described the development, testing and performance of the CPD. In particular, Section 4 presented the results of the tests designed to evaluate specific aspects of the CPD. Some points related to these results are worth noting and are discussed in the section that follows. Section 4 also presented results obtained from tests stipulated by the ISO5840:2005 which were performed using commercially available PHVs. In contrast, Section 5.1 aims to assess the CPD beyond these isolated tests by using these data and comparing it to the results published in the literature, thus placing the CPD in context with similar devices described in scientific publications. Owing to the poor performance obtained from the flowmeter, this section will not discuss flow or volume measurements in detail but rather concentrate on pressure readings.

5.1 Hydrodynamic analysis

The hydrodynamic analysis is founded on the proven performance of the motion control system, whose accuracy compares favourably against ViVitro Labs' SuperPump, the pump regarded as the gold standard for producing cardiac flows. A comparison is made in Table 5.1 for the conditions for which data is available from the SuperPump's datasheet [102]. The "Phased" column indicates the error obtained after shifting the position feedback waveform to align it with the setpoint waveform. The quoted error and accuracy correspond to a stroke volume of 75 mL. Note that the accuracy and error values refer to displaced volume.

Table 5.1: Comparison of waveform accuracy for BERG CPD and ViVitro Labs SuperPump at SV = 75 mL.

HR	BERG CPD				ViVitro Labs SuperPump [102]	
	Unphased		Phased			
	Error	Accuracy	Error	Accuracy	Error	Accuracy
70 bpm	< 3.56 %	± 2.67 mL	< 0.15 %	± 0.11 mL	< 4 %	± 3 mL
200 bpm	< 6.71 %	± 5.04 mL	< 0.27 %	± 0.21 mL	< 5 %	± 3.8 mL

The repeatability and accuracy of the pressure readings were demonstrated in Section 4.4 and this, combined with the above mentioned performance, gives good credibility to the data produced by the BERG CPD and allows meaningful comparisons to be made based on pressure. However, while a great deal of data is available for the SJME PHVs, most of it relates to *in vivo* studies published in medical journals as post-implantation follow up investigations. Given the nature of these studies, the conditions under which the measurements are taken are difficult to control. This means that the range of testing conditions is very limited which has the added disadvantage of reducing the results to a very narrow band. Further, echocardiography continues to be the method of choice to assess PHV performance post-implantation and there is evidence showing that pressure values obtained through *in vivo* studies do not match the data acquired *in vitro* [100]. A factor contributing to this may be the fact that valve replacements often take place in the presence of comorbidities which affect the hydrodynamics around the PHV. The

combination of all these facts means that it is not possible to compare the data acquired from the CPD to *in vivo* data and reputable *in vitro* studies for the PHVs that were available were found to be scarce. Gerosa *et al* [88] used the well-known Sheffield Pulse Duplicator (D'Avenio *et al* [104] provide a description) to perform an *in vitro* assessment of the SJM Epic Supra 21mm PHV. Thanks to an improved mounting style, the orifice area of the SJM Epic Supra model corresponds to that of a standard SJM Epic model one size larger for a given tissue annulus diameter [105]. Thus, a 21 mm SJM Epic Supra corresponds (hydrodynamically) to a standard 23 mm SJM Epic. Consequently, Table 5.2, which summarises Table 4.19, is a comparison of pressure data between measurements obtained for the SJM Epic 23 mm PHV and data published by Gerosa *et al* for the 21 mm SJM Epic Supra.

Table 5.2: Measured and published pressure data for the SJME 23 mm PHV. (CO: cardiac output; ΔP_{mean}: mean systolic pressure difference; ΔP_{peak}: peak systolic pressure difference; SWL: stroke work loss).

CO	Parameter	Measured SJME	Gerosa *et al* [88]
2 L/min	ΔP_{mean} (mmHg)	5.91 ± 0.15	7.41 ± 1.80
	ΔP_{peak} (mmHg)	11.17 ± 0.90	13.50 ± 2.32
	SWL (%)	6.03 ± 0.14	9.36 ± 2.70
4 L/min	ΔP_{mean} (mmHg)	12.48 ± 0.23	13.06 ± 1.50
	ΔP_{peak} (mmHg)	24.92 ± 0.63	24.90 ± 2.30
	SWL (%)	11.62 ± 0.19	14.75 ± 2.16
5 L/min	ΔP_{mean} (mmHg)	14.49 ± 0.21	17.37 ± 1.80
	ΔP_{peak} (mmHg)	24.39 ± 0.47	36.20 ± 4.60
	SWL (%)	13.41 ± 0.19	19.10 ± 2.80
7 L/min	ΔP_{mean} (mmHg)	19.17 ± 0.29	27.50 ± 1.37
	ΔP_{peak} (mmHg)	45.16 ± 1.68	50.50 ± 3.80
	SWL (%)	16.95 ± 0.23	27.13 ± 2.50

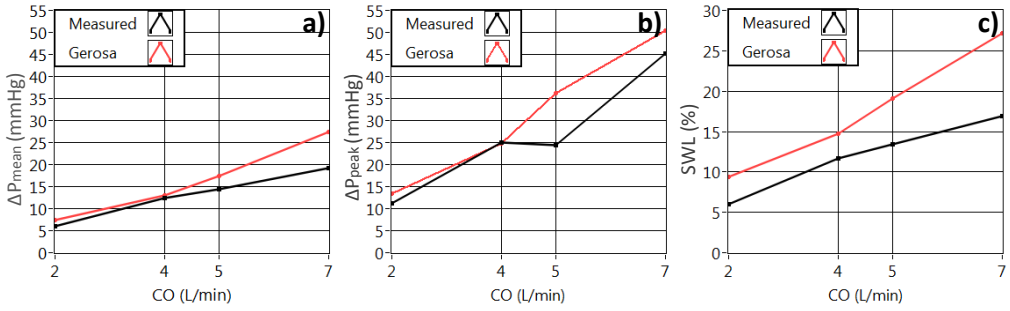

Figure 5.1: Graphical comparison between measured and published hydrodynamic data. a) Mean systolic pressure difference; b) peak systolic pressure difference; c) stroke work loss.

It can be seen from Figure 5.1 that the values obtained by Gerosa's group are consistently higher than those measured. Starting in very close agreement at 2 L/min, the results from the two studies tend to converge at 4 L/min. However, they diverge at higher cardiac outputs, with the peak systolic pressure difference (Figure 5.1 (b)) exhibiting a crucial difference at 5 L/min. Although the two sets of data follow the same general trend, some

points need to be considered to identify the reasons for the deviations and these will be discussed in the sections that follow. It should be noted that since the SJME is a bioprosthetic valve, some variation in hydrodynamic performance is to be expected from sample to sample and Gerosa *et al* tested three identical PHVs to account for this. However, only one sample was available for this study.

5.1.1 The sinuses of Valsalva

D'Avenio *et al* [104] noted that the same PHV produces different flow fields in different CPDs. Differences in the flow field have the potential to alter the perceived characteristic resistance of the PHV which would lead to differences in pressure values. The flow field and perceived characteristic resistance can be affected by the presence and geometry of the sinuses of Valsalva[10] (see Figure 5.2). Bottio *et al* [106] speculated that the sinuses of Valsalva have a significant effect on the hemodynamic behaviour of the PHV during both the systolic and diastolic phases, suggesting that a lack of sinuses could impact valve durability due to higher stresses. Recently, Salica *et al* [107] proved that the presence of sinuses of Valsalva lead to improved flow through a reduced pressure drop across the PHV, especially at higher flow rates, confirming that the sinuses are responsible for minimising energy losses.

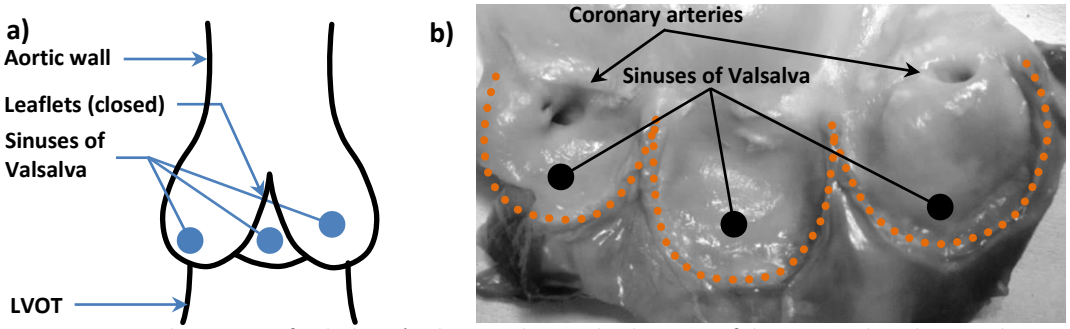

Figure 5.2: The sinuses of Valsalva. a) Schematic longitudinal section of the aortic valve, showing the location of the sinuses. b) Aortic root cut lengthwise with leaflets removed to show the sinuses of Valsalva, defined by the basal leaflet attachment (marked by the dotted orange line).

Taking the above into consideration, the divergence seen in Figure 5.1 for both mean pressure drop and SWL at higher cardiac outputs could be attributed to the differences in the geometry of the aortic root immediately after the valve. The CPD used in Gerosa's study has a glass aorta with anatomically modelled sinuses of Valsalva whereas the surgical aortic valve holder used for this study (refer to Figure 3.6) uses a 28 ^{o} taper as pseudo sinuses (due to the cost and manufacturing complexity of including sinuses of Valsalva in the design this consideration was outside the scope of this project). Pisani *et al* [108] present clear evidence that the sinuses modify the leaflets' movement resulting in reduced pressure gradients during the systolic phase. To explain this they hypothesise that flow past the valve creates an area of low pressure within the sinuses allowing the leaflets to open wider, effectively increasing the geometric orifice area. Following this rationale, it is likely that having a ring of low pressure around the leaflets, instead of three

[10] A sinus of Valsalva is an enlargement of the aortic root defined by the basal attachment of a leaflet, forming an oval cavity between the aortic wall and the leaflet.

distinct sinuses, is the cause for lower pressure differences across the PHV since the effect would be magnified.

5.1.2 Pulse wave velocity

Pulse wave velocity (PWV) refers to the speed at which the pressure wave generated by the ventricle travels through the arterial system. PWV is dependent on both the compliance of the system and the arterial pressure. Achieving the same arterial pressure at various cardiac outputs demands modifications to the resistance and compliance, in turn affecting PWV. PWV also contributes to the shape of the arterial pulse because the latter is influenced by the pressure wave reflected from the periphery of the arterial system [109, 110]. Since the location where the pressure wave is reflected back to the source is constant in a CPD, the overall time taken by it to return to a given measurement point can be affected through PWV without changing the heart rate. This means that the peak systolic pressure difference is susceptible to resonance which would manifest itself at different cardiac outputs for a given heart rate. Burattini *et al* [44] studied this phenomenon using a viscoelastic model and experimental data from dogs, concluding that the viscoelasticity of the aorta and nearby arteries is key in governing the magnitude of resonance. Therefore, a logical explanation for the peak systolic pressure difference obtained at 5 L/min being significantly lower than Gerosa's measurements is that the reflection points of the two CPDs are at different distances from the source of the pressure wave and that the compliance required for achieving the correct pressure at 5 L/min in the BERG CPD minimises the effects of resonance. Figure 5.3 is useful to explain the effect of this phenomenon.

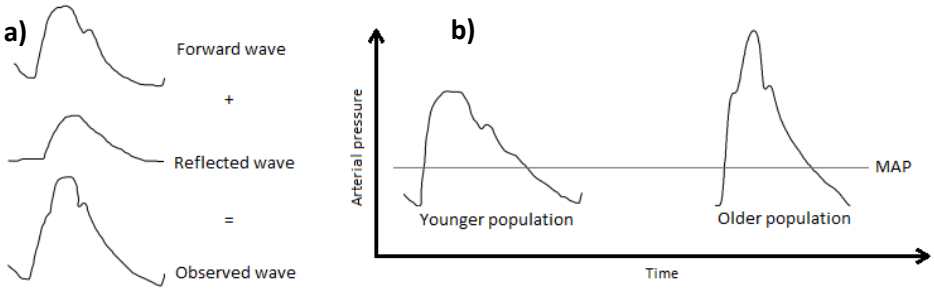

Figure 5.3: a) Pressure components of the arterial pressure curve. b) Effect of reduced compliance on arterial pressure due to age. (Adapted from [109])

Analysis of five heartbeats yielded an average PWV of 9.35 m/s during the systolic phase for a CO of 5 L/min (see Appendix C: SJM Epic 23 mm, for graphical results). This fits well into the 50-59 years of age category within the normal population [111] indicating that, although towards the upper limit (likely due to the rigid tubes comprising the LVOT), the PWV is within physiological limits. Since the reflected wave contributes to the characteristic shape of the arterial waveform, the distance between the source and reflection point of the pressure wave should be physiological too. This is necessary in order for the reflected wave to contribute to the forward wave at the right time. Deviations will cause the shape of the arterial pressure wave through different heart rates and mean pressures to not follow a physiological response.

5.1.3 Nature and operation of the CPD

The phenomena described in the previous two sections relate to the physical design and operating conditions of the CPD. The diameter, length and path, as well as the choice of material for the hydraulic loop play an important role in shaping the pressure wave. Sugawara *et al* [110] used a dog model to explain how fluid inertia affects ventricular pressure, especially at the end of the systolic period. They hypothesise that, due to its inertia, blood can continue moving forward for longer than the ventricle is in systole. Therefore, the ventricle must stop blood flow by going into diastole (before the aortic valve closes), rather than diastole starting after blood flow has decayed significantly. Their theory explains the negative pressure spike observed at 0.38 s in all panels of Figure 4.13, suggesting that this feature is likely linked to the large volume of fluid subject to pulsatile flow after the ventricle. Nonetheless, this feature also has been observed, in varying degrees, in commercial devices such as the ViVitro CPD [46].

In terms of the material used for the hydraulic loop, interaction between the pressure wave and its surroundings creates or eliminates certain features in the pressure and flow measurements. The stiffness of the wetted material influences the magnitude of the reflected pressure wave, affecting how the observed wave is constructed. Furthermore, the locations where these variables are measured also influence the perceived test results since the formation of the observed pressure wave has a time component due to interaction with the reflected pressure wave.

Section 4.3.3 demonstrated that small changes to the control waveform (small enough to be unperceivable without precise measuring aids) can effect significant changes in pressure measurements that directly affect a PHV's commonly reported performance indicators. This highlights the need for the motion control system to be highly dynamic and accurate. However, it also proves the susceptibility of the tests to manipulation (for example, adjusting the control waveform when testing the same PHV sample in different CPDs, to reduce the peak systolic pressure difference that arises due to different inertance characteristics). In the comparison between the Sheffield Pulse Duplicator and the BERG CPD, the CPDs' different abilities to track a control waveform could also account for the disparities observed at 5 L/min, given the dynamic nature of the pressure wave and the components that contribute to its formation (the forward pressure wave and the reflected pressure waves from all possible reflection points).

Through the above observations it becomes apparent that every aspect of the CPD, including its fundamental design, contributes to the perceived performance of a PHV raising the need to establish well defined performance criteria covering all systems involved: electrical, mechanical, hydraulic and software (control, data acquisition and analysis). Without appropriate CPD performance quantification it is impossible to accurately reproduce results of PHV performance tests for comparison or independent analysis. Although the CPD performance assessment methods developed for this project have limitations, they should provide valuable information about a CPD's abilities that can be used to establish to what extent the CPD influences PHV performance. It should be noted that to obtain a CPD's performance baseline a universal valve (such as a simple spring loaded disc valve) should be used as this will provide consistent performance regardless of the test platform.

5.2 Limitations affecting system performance

A few limitations played a role in the development of the CPD. This section discusses the compromises that had to be made during the design process, the rationale behind the decisions made and the measures taken to mitigate the effects on performance.

5.2.1 Mechanical

The main constraint governing mechanical design was that all modifications and upgrades had to be backwards compatible with the existing setup which required the new design's dimensions to be adjusted, particularly at the subsystem interfaces. This resulted in the CPD's hydraulic loop being larger than necessary. The flowmeter also contributed to the size of the hydraulic loop due to the length of its flow tube. The electromagnetic probe is housed at the middle of a flow tube which is used to form laminar flow and ensure consistent readings. This flow tube has a length of 200 mm and installation is by means of flanges integral to the tube. Besides the space required to accommodate the instrument's overall length, the diameter of the flanges (95 mm) also demanded that the left ventricular outflow tract be extended. The need for this additional length can be seen in Figure 3.12, where it is evident that the mitral valve assembly and atrium prevent the flowmeter from being mounted closer to the ventricle due to the size of its inlet flange. The size of the hydraulic loop plays an important role on the hydrodynamic behaviour of the system since the inertial effects of the increased volume of fluid that the ventricle must set in motion affect the dynamics of the entire system (see Section 5.1.3). Although the above-mentioned constraints meant that the volumetric size of the hydraulic loop was largely out of the control of the design, every effort was made to keep the volume of the section experiencing pulsatile flow within a realistic limit.

5.2.2 Motion control

One of the limitations in terms of controller performance was hardware related. The electric cylinder that was used was a general purpose actuator instead of one tailored specifically for the application of the CPD. This means it is larger than necessary which results in higher inertia, reducing dynamic response. While the electric cylinder can easily achieve its maximum speed of 375 mm/s during longer strokes, the sudden acceleration and deceleration to which it is subjected in order to track the control waveform precisely within such short strokes can damage the screw assembly. Therefore, following the general architecture of the system, a three layered approach was taken to protect the electric cylinder:

1. at the motion design level, the maximum speed component that a control waveform can contain in order to be sent to the position controller was limited to 275 mm/s,
2. at the position controller level, the maximum transient output (the maximum speed the controller can request) was limited to 300 mm/s (equivalent to 8 V out of a maximum of 10 V) and,
3. at the speed controller level, the peak current to the motor was limited to 100 %, effectively limiting torque (a value of 150 % is typical for this type of servomotor).

The MoviDrive itself imposed some limitations on the control system due to its fixed maximum sampling rate of 1 kHz for its analog inputs. This means that to prevent aliasing the maximum rate at which the position control loop can send speed values to the MoviDrive is limited to 1 ms. Sending speed values at a rate faster than 1 ms introduces jitter as some of the values may be completely missed by the MoviDrive causing the position controller to overreact during the following iteration. This happens because the MoviDrive will continue moving the electric cylinder at a constant speed for longer than the position controller expects, undershooting or overshooting the target position. A similar situation arises when the position controller sends speed values at a rate slower than the MoviDrive reads them. In this case the MoviDrive has too much time to attain the requested speed between speed commands from the position controller, again overshooting or undershooting the target position, causing the controller to overcompensate during subsequent iterations. Figure 5.4 shows the behaviour of the position controller at a heart rate of 70 bpm and a stroke volume of 71.43 mL using (a) a fixed time resolution of 1 ms (857 positions) and (b) a fixed number of positions (500 positions resulting in a time resolution of 1.71 ms). It can be seen that the main areas affected by jitter are those characterised by high velocity while the piston is half way through its travel.

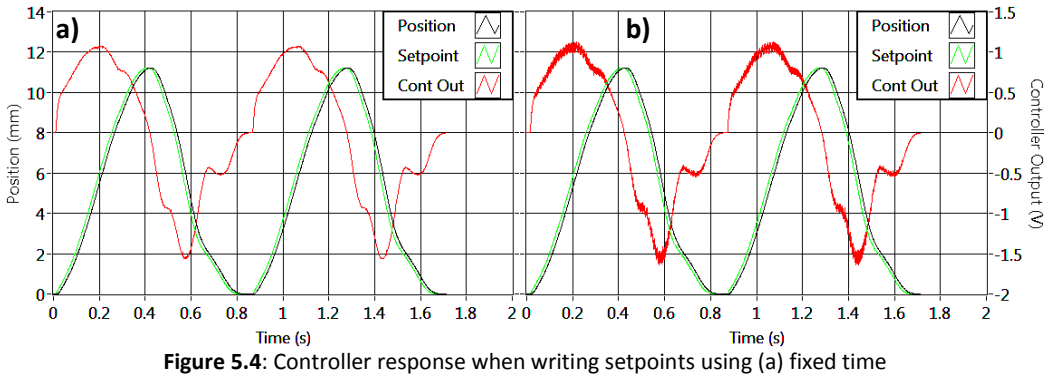

Figure 5.4: Controller response when writing setpoints using (a) fixed time resolution and (b) fixed number of positions.

It should be noted that the behaviour observed in Figure 5.4 (b) is still that of a PI controller, with an inactive T_d term which is notorious for introducing this type of high frequency oscillation. The oscillation introduced by the position controller's overcompensation manifests itself on the motor both audibly and tangibly and at heart rates above 180 bpm it translates to large changes in instantaneous speed values between iterations, causing the MoviDrive to experience overcurrent errors. To avoid this instability and take full advantage of the benefits of smooth operation, the control waveform's time resolution is normally kept fixed to 1 ms but this has two drawbacks:

1. To enforce a period of 1 ms for writing the setpoint value, the heartbeat duration must be rounded off to the nearest millisecond. This means that Figure 5.4 (b) has a heart rate of exactly 70 bpm because it was produced with a fixed number of positions in the control waveform which allows for adjustment of the time resolution. However, Figure 5.4 (a) has a heart rate of 70.011 bpm because a fixed time resolution was used. This difference tends to increase together with the heart rate: at 192 bpm, where it would be necessary to have a smooth controller output to prevent overcurrent errors, the actual heart rate is 191.69 bpm.

2. As the heart rate increases, the number of points in the control waveform must decrease, resulting in a reduction of temporal resolution of the control waveform.

To provide the determinism of control with a fixed number of points per heartbeat or the better performance offered by a fixed time resolution, both functions were coded and can be switched while the CPD is running.

Table 4.2 shows that the typical RMSE for setpoint tracking under the operating conditions used in Figure 5.4 is below 0.02 mm. To complement this, the RMSE for the position waveform between the two heartbeats shown in Figure 5.4 (a) is 0.001 mm, indicating excellent repeatability and controller behaviour. By comparison, the same analysis yielded an RMSE of 0.009 mm for Figure 5.4 (b). While 0.009 mm does not represent a significant error, it is 9 times more than with a well-timed controller and it serves to show how jitter can introduce variability to the process. The effect of jitter becomes more pronounced as cardiac output increases because higher speeds increase the amplitude of the oscillations. In contrast, a fixed time resolution of 1 ms results in smooth controller behaviour across the full range of operating conditions. Thus, despite the afore-mentioned limitations, the CPD performs on par with commercial systems.

5.3 Cost overview

A detailed breakdown of the hardware and manufacturing costs for the CPD is available in Appendix D. Table 5.3 provides a summary of these costs, given in 2015 South African Rand (ZAR). The costs shown represent retail prices and exclude Value Added Tax. Other costs excluded from the estimation are those related to assembly, programming, testing and tuning of the apparatus.

While this CPD has certain limitations and would benefit from some improvements beyond the scope of this project, the overall estimated cost of R 161 000 is approximately 8 times less than the retail price of a leading commercial device, depending on the selected hardware and software features of the latter. Therefore, the functionality offered by this custom-built CPD has a good cost-to-benefit relationship when compared to commercial devices. Understandably, a large component of the cost of commercially available CPDs relates to recovering development costs. The costs reported for this project include only hardware, raw materials and manufacturing but this project fulfils one of its aims by detailing the architecture of the system (for both hardware and software) so that these costs can be reduced to a minimum. A further benefit of the custom-built CPD is that its software is customisable since the source code is accessible. Modifying or expanding the software can lead to greater flexibility during testing and more in-depth real-time analysis of PHV performance.

Table 5.3: Summary of hardware and manufacturing costs.

	BERG CPD	Commercial CPD
Instrumentation and control	R 113 651	**~R 1 250 000**
Materials	R 10 200	
Manufacturing	R 37 100	
TOTAL	**R 160 951**	

6 Conclusion and Recommendations

6.1 Conclusion

A CPD was redesigned, constructed and tested following ISO5840:2005 recommendations. This thesis represents a collection of information intended to aid those wishing to develop a custom-built CPD to produce a successful design, based on the good results obtained from the apparatus presented in this work. This investigation resulted in an in-house CPD that produces performance measures on par with commercial equivalents.

The need for the above follows from the rationale that PHVs are most needed in areas of the world that cannot afford them. Reducing development costs to encourage local PHV development is an effective way to increase the availability of PHVs in resource constrained areas. One of the means to accomplish this is through the use of developing and testing equipment built in-house. One such piece of equipment is a CPD and the literature review was used, among other things, to describe their theory of operation, role in the development of PHVs and challenges surrounding their design and implementation. The key areas presenting the major challenges related to the development of CPDs were discussed and later shown to have a direct impact on the performance of the machine. While this project started off with an existing apparatus, the extent of the modifications actually gave birth to a new device, the design of which is documented in this text. A number of tests were devised and carried out to evaluate the performance of the machine. The tests worked well to highlight both its good characteristics and certain flaws.

With the exception of the limitations imposed by the flowmeter, overall performance of the CPD was found to be satisfactory. Pressure measurements obtained from reputable PHVs under a range of operating conditions showed expected trends and good agreement with published data. Achieving the specified test conditions which allowed comparison of results to values found in literature was made possible through a series of hardware improvements as well as extensive software development. Despite these good outcomes, some aspects of the CPD require further work and the section that follows provides some advice on how to overcome the problems encountered during testing.

While many works present methods and data for the validation of CPDs, no reference could be found in the literature in terms of approaches to quantify CPD performance. Further, no literature could be found that directly compares two CPDs to each other by using the same PHV samples and test parameters. The lack of a standardised assessment for the performance of CPDs means that the evaluation of a few specific parameters (such as P_{sys}/P_{dias} and MAP) could allow a CPD to pass a simple validation test. However, it is thoroughly proven, overall CPD performance (perceived only through more subtle parameters, or their combination), that yields credible and unbiased PHV performance results. As a consequence, skewed or biased PHV performance results could go unnoticed without the use of more complex CPD performance indicators (such as those discussed in Section 3.4.2.3). This leaves a gap in the domain of heart valve testing and led to the development of new techniques to evaluate and present performance metrics which should prove useful in assessing and comparing CPDs, irrespective of design. In

connection to this contribution, a proposal for a standardised system of evaluating CPD performance is made and the approach discussed in this document is presented as a first step toward this goal.

6.2 Recommendations

As the CPD is expected to be used in further investigations, future work is needed to address the main drawbacks encountered during testing. The recommendations presented here should contribute not only towards maximising the functionality but also the reliability of the CPD.

The sourcing and installation of a flowmeter capable of measuring pulsatile flow more accurately is of highest importance and necessary to perform detailed analyses on the PHVs being tested. However, widely cited modern flowmeters (Carolina Medical Electronics CME 500 Series [67, 95], Transonic Systems ultrasonic probes [79, 89]) are not affordable in the local context, making this a challenging task. An unrestrictive and low profile probe will be greatly advantageous as it will eliminate a significant volume of fluid between the ventricle and the aortic valve. Beyond the aortic valve, it is highly recommended that sinuses of Valsalva be included. The original design of the LVOT is meant to accept sinus inserts so that the effect of different size sinuses can be studied.

The integration of an accurate means of measuring the peripheral resistance setting is recommended. While this will not have a direct effect on the performance of the CPD, it will make inter-test repeatability more accurate and easily achieved. This could be accomplished by attaching a graded dial to the resistor's shaft and referencing it to the housing of the resistor.

Fabrication of a thinner (~1 mm thick) and more elastic moulded ventricle is advised, primarily for durability reasons. Having a mould will allow easy manufacture of identical replacement parts. The CNC-machined PVC mould in Figure 6.1 (left panel) produces a silicone ventricle with a wall thickness of 1mm. In relation to ventricular compliance, a more effective system to improve the performance at elevated HRs should be implemented. The diagrams on Figure 6.1 (right panel) depict the old and proposed configurations. The proposed model is similar in design to a commercially available system [84] and the current configuration of the CPD's ventricular section can easily accommodate this modification.

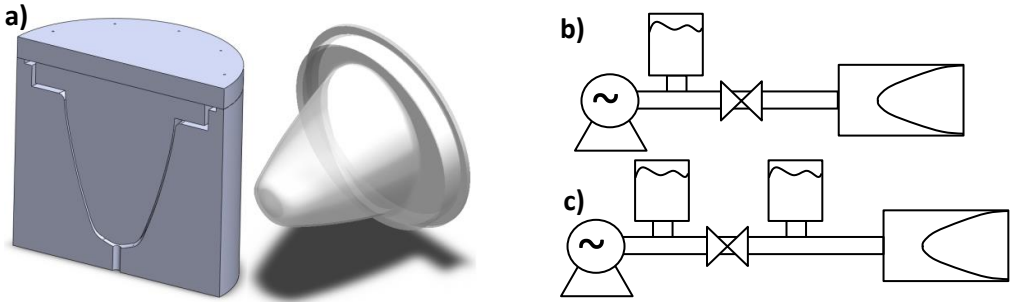

Figure 6.1: a) Ventricle mould to be manufactured and resultant silicone model. b) Current ventricular compliance setup; c) proposed ventricular compliance setup.

7 References

1. World Health Organization. *"Rheumatic fever and rheumatic heart disease*." Report of a WHO expert consultation (Technical Report Series, No. 923). Geneva, Switzerland. 2001.

2. Marijon E, Ou P, Celermajer DS, Ferreira B, Mocumbi AO, Jani D, Paquet C, Jacob S, Sidi D, Jouven X. *"*Prevalence of rheumatic heart disease detected by echocardiographic screening." *N Engl J Med* 2007; 357(5):470-6.

3. Sliwa K, Carrington M, Mayosi BM, Zigiriadis E, Mvungi R, Stewart S. "Incidence and characteristics of newly diagnosed rheumatic heart disease in Urban African adults: insights from the Heart of Soweto Study." *Eur Heart J* 2010; 31:719–27.

4. National heart, lung and blood institute. "What causes heart valve disease?" Retrieved April 22, 2016, from https://www.nhlbi.nih.gov/health/health-topics/topics/hvd/causes

5. British heart foundation. "Heart valve disease." Retrieved April 22, 2016, from https://www.bhf.org.uk/-/media/files/publications/heart-conditions/his11_0414_heart-valve-disease_a6.pdf

6. Burke A, Tavora F. *Practical cardiovascular pathology.* 1st Edition. Philadelphia, Pennsylvania, USA: Wolters Kluwer | Lippincott Williams & Wilkins, 2011.

7. Anderson RH, Becker A, Piazza N. "The anatomy of the aortic valvar complex". In *Transcatheter Aortic Valve Implantation: Tips and tricks to avoid failure*, edited by Serruys PW, Piazza N, Cribier A, Webb JG, Laborde JC, de Jaegere, 1-17. New York, USA: Informa Healthcare USA, Inc., 2010.

8. Visible heart lab. "Left atrium, mitral valve." Retrieved March 30, 2016, from http://www.vhlab.umn.edu/atlas/left-atrium/mitral-valve/index.shtml

9. Visible heart lab. "Aorta, aortic valve." Retrieved March 30, 2016, from http://www.vhlab.umn.edu/atlas/aorta/aortic-valve/index.shtml

10. Sliwa K, Zilla P. "Rheumatic heart disease - The tip of the iceberg." *Circulation* 2012; 125:3060-2.

11. Zühlke L, Mirabel M, Marijon E. "Congenital heart disease and rheumatic heart disease in Africa: recent advances and current priorities." *Heart* 2013; 99:1554-61.

12. Remenyi B, ElGuindy A, Smith SC Jr, Yacoub M, Holmes DR Jr. "Valvular aspects of rheumatic heart disease." *Lancet* 2016; 387:1335-46.

13. Carapetis JR. “Rheumatic heart disease in developing countries.” *N Engl J Med* 2007; 357(5):439-41.

14. Carapetis JR, Beaton A, Cunningham MW, Guilherme L, Karthikeyan G, Mayosi BM, Sable C, Steer A, Wilson N, Wyber R, Zühlke L. “Acute rheumatic fever and rheumatic heart disease.” *Nat Rev Dis Primers* 2016; 2: Article number 15084. Accessed May 1, 2016. DOI:10.1038/nrdp.2015.84.

15. Pick A. “How much do heart valve replacements cost?” Retrieved March 30, 2016, from http://www.heart-valve-surgery.com/heart-surgery-blog/2010/09/20/mechanical-tissue-valve-replacements-cost/

16. Mabin TA, Candolfi P. “An analysis of real-world cost-effectiveness of TAVI in South Africa.” *Cardiovasc J Afr* 2014; 25(1):21–6.

17. Yacoub MH, Takkenberg JJM. “Will heart valve tissue engineering change the world?” *Nat Clin Pract Cardiovasc Med* 2005; 2(2):60-1.

18. Edmunds LH Jr. “Evolution of prosthetic heart valves.” *Am Heart J* 2001; 141:849-855.

19. Gott VL, Alejo DE, Cameron DE. “Mechanical heart valves: 50 years of evolution.” *Ann Thorac Surg* 2003; 76:S2230–9.

20. Esterhuyse A. “Structural design of a stent for a percutaneous aortic heart valve.” MSc (Mechanical Engineering) thesis, Stellenbosch University, South Africa, 2009.

21. Smuts AN. “Design of tissue leaflets for a percutaneous aortic valve.” MSc (Mechatronic Engineering) thesis, Stellenbosch University, South Africa, 2009.

22. Van Aswegen K. “Dynamic modelling of a stented aortic valve.” MSc (Mechanical Engineering) thesis, Stellenbosch University, South Africa, 2008.

23. Kemp IH. “Development, testing and fluid–structure interaction simulation of a bioprosthetic valve for transcatheter aortic valve implantation.” MSc (Mechanical Engineering) thesis, Stellenbosch University, South Africa, 2012.

24. Smuts AN, Blaine DC, Scheffer C, Weich H, Doubell AF, Dellimore KH. “Application of finite element analysis to the design of tissue leaflets for a percutaneous aortic valve.” *J Mech Behav Biomed Mater* 2011; 4(1): 85–98.

25. Van Aswegen KHJ, Smuts AN, Scheffer C, Weich HSV, Doubell AF. “Investigation of leaflet geometry in a percutaneous aortic valve with the use of fluid–structure interaction simulation.” *J Mech Med Biol* 2012: 12(1):1–15.

26. Kemp I, Dellimore K, Rodriguez R, Scheffer C, Blaine D, Weich H, Doubell AF. "Experimental validation of the fluid-structure interaction simulation of a bioprosthetic aortic heart valve." *Australas Phys Eng Sci Med* 2013: 36(3):363-73.

27. Dellimore K, Kemp I, Rodriguez R, Scheffer C. "In vitro characterization of an aortic bioprosthetic valve using Doppler echocardiography and qualitative flow visualization." In *Conf Proc IEEE Eng Med Biol Soc* 2012; 2012:6641-4.

28. Krynauw H. "Design and implementation of an apparatus for hydrodynamic and fatigue testing of prosthetic aortic valves." MSc (Biomedical Engineering) thesis, University of Cape Town, South Africa, 2008.

29. International Organization for Standardization. *Cardiovascular implants – Cardiac valve prostheses. ISO5840:2005*. Geneva, Switzerland. 2005.

30. McMahon Biovisuals. "The heart." Retrieved April 19, 2016, from http://www.mcmahonbiovisuals.com/the-heart

31. Yoganathan AP. "Cardiovascular fluid mechanics." PhD thesis, California Institute of Technology, USA, 1978.

32. Vincent JL. "Understanding cardiac output." *Crit Care* 2008; 12(4):174.

33. Dobrin PB. "Vascular mechanics." In *Handbook of physiology, Section 2: The cardiovascular system; Volume III: Peripheral circulation and organ blood flow, Part 1*, edited by Shepherd J and Abboud F, 65-102. Baltimore, Maryland, USA: Waverly Press, Inc., 1983.

34. Snyder MF, Rideout VC, Hillestad RJ. "Computer modelling of the human systemic arterial tree." *J Biomechanics* 1968; 1(4):341-53.

35. Berne RM, Levy MN. "The arterial system." In *Physiology of sport and exercise*, edited by Berner R and Levy M, 453-464. St Louis, Missouri, USA: Mosby-Year Book Inc., 1993.

36. Segers P, Dubois F, De Wachter D, Verdonck P. "Role and relevancy of a cardiovascular simulator." *Cardiovascular Engineering* 1998; 3(1):48-56.

37. Arimon JA. "Numerical modelling of pulse Wave propagation in the cardiovascular system: development, validation and clinical applications." PhD thesis, University of London, UK, 2006.

38. Stergiopulos N, Westerhof BE, Westerhof N. "Total arterial inertance as the fourth element of the windkessel model." *Am J Physiol* 1999; 276(1):H81-8.

39. Frank O. "Die Grundform des arteriellen pulses." *Z Biol* 1899; 37:483–526.

40. Kokalari I, Karaja T, Guerrisi M. “Review on lumped parameter method for modeling the blood flow in systemic arteries.” *J Biomed Sci Eng* 2013, 6:92-9.

41. Westerhof N, Lankhaar JW, Westerhof BE. “The arterial Windkessel.” *Med Biol Eng Comput* 2009; 47:131–41.

42. Westerhof N, Elzinga G, Sipkema P. “An artificial arterial system for pumping hearts.” *J Appl Physiol* 1971; 31(5):776-81.

43. Burattini R, Natalucci S. “Complex and frequency-dependent compliance of viscoelastic Windkessel resolves contradictions in elastic Windkessels.” *Med Eng Phys* 1998; 20(7):502-14.

44. Burattini R, Natalucci S, Campbell KB. “Viscoelasticity modulates resonance in the terminal aortic circulation.” *Med Eng Phys* 1999; 21:175–85.

45. Grant BJB, Paradowski LJ. “Characterization of pulmonary arterial input impedance with lumped parameter models.” *Am J Physiol* 1987; 252:H585-93

46. Pulse duplicator system user manual. ViVitro Labs Inc., Victoria, BC, Canada, 2015.

47. Chew YT, Chew TC, Low HT, Lim WL. “Techniques in the determination of the flow effectiveness of prosthetic heart valves.” In *Biomechanical Systems: Techniques and Applications, Volume II: Cardiovascular Techniques*, edited by Leondes C, 2.1-2.48. Boca Raton, Florida, USA: CRC Press LLC, 2001.

48. Davila J, Trout R, Sunner J, Glover R. “A simple mechanical pulse duplicator for cinematography of cardiac valves in action”. *Ann Surg* 1956; 143(4): 544–51.

49. Goodale F Jr, Shaw R. “Functional examination of the heart at autopsy.” *N Engl J Med* 1955; 253:719-21

50. McMillan IKR, Daley R, Matthews MB. “The movement of aortic and pulmonary valves studied post mortem by colour cinematography.” *Br Heart J* 1952; 14(1):42–6.

51. Kelley RR, Goodale F Jr, Castleman B. “The dynamics of rheumatic and calcific aortic valve disease.” *Circulation* 1960; 22:365-75.

52. Bjork VO, Intonti F, Meissl A. “A mechanical pulse duplicator for testing prosthetic mitral and aortic valves.” *Thorax* 1962; 17:280-3.

53. Duran CG, Gunning AJ, McMillan T. “A simple versatile pulse duplicator.” *Thorax* 1964; 19:503-6.

54. Yoganathan AP, Corcoran WH, Harrison EC. “Pressure drops across prosthetic aortic heart valves under steady and pulsatile flow – in vitro measurements.” *J Biomechanics* 1979; 12:153-64.

55. Temple LJ, Serafin R, Calvert NG, Drable JM. “Principles of fluid mechanics applied to some situations in the human circulation and particularly to the testing of valves in a pulse duplicator.” *Thorax* 1964; 19(3):261–7.

56. Chandran KB, Cabell GN, Khalighi B, Chen CJ. “Pulsatile flow past aortic valve bioprostheses in a model human aorta.” *J Biomechanics* 1984; 177(8):609-19.

57. ViVitro Labs Inc. “ViVitro Labs.” Retrieved April 15, 2016, from www.vivitrolabs.com/company

58. Westerhof N, Bosman F, De Vries CJ, Noordergraaf A. “Analog studies of the human systemic arterial tree.” *J Biomech* 1969; 2(2):121-43.

59. Westerhof N, Noordergraaf A. “Arterial viscoelasticity: a generalized model: Effect on input impedance and wave travel in the systematic tree.” *J Biomech* 1970; 3:357–79.

60. Toy SM, Melbin J, Noordergraaf A. “Reduced models of arterial systems.” *IEEE Trans Biomed Eng* 1985; 32(2):174-6.

61. Noordergraaf A, Verdouw D, Boom HB. “The use of an analog computer in a circulation model.” *Prog Cardiovasc Dis* 1963; 5:419–39.

62. HDT-500 pulse duplicator brochure. BDC Laboratories. Wheat Ridge, Colorado, USA, 2016.

63. BDC Laboratories. “Pulsatile pumps.” Retrieved April 29, 2016, from www.bdclabs.com/testing-equipment/pulsatile-pump-systems

64. Okafor IU, Santhanakrishnan A, Raghav VS, Yoganathan AP. “Role of mitral annulus diastolic geometry on intraventricular filling dynamics.” *J Biomech Eng* 2015, 137(12):121007.

65. Vahidkhah K, Cordasco D, Abbasi M, Ge L, Tseng E, Bagchi P, Azadani AN. “Flow-induced damage to blood cells in aortic valve stenosis.” *Ann Biomed Eng* 2016; 44(9):2724-36.

66. Rajeev A, Sivakumaran N, Sujesh S, Muraleedharan CV. “A linear after-load model for a cardio-vascular pulse duplicator.” In *Proceedings of International Conference on Advances in Computing, Communications and Informatics (ICACCI-2012)*. August 3-5, 2012, Chennai, India.

67. Calderan J, Mao W, Sirois E, Sun W. “Development of an in vitro model to characterize the effects of transcatheter aortic valve on coronary artery flow.” *Artif Organs* 2016; .40(6):612-9.

68. Seaman C, McNally A, Biddle S, Jankowski L, Sucosky P. “Generation of simulated calcific lesions in valve leaflets for flow studies.” *J Heart Valve Dis* 2015; 24(1):115-25.

69. Rahmani B, Tzamtzis S, Ghanbari H, Burriesce G, Seifalian A. “Manufacturing and hydrodynamic assessment of a novel aortic valve made of a new nanocomposite polymer.” *J Biomech* 2012; 45(7):1205-11.

70. Burriesci G, Marincola FC, Zervides C. “Design of a novel polymeric heart valve.” *J Med Eng Technol* 2010; 34(1):7-22.

71. Maleki H, Shahriari S, Labrosse M, Rodés-Cabau J, Pibarot P, Kadem L. “Effect of aortic annulus size and prosthesis oversizing on the hemodynamics and leaflet bending stress of transcatheter valves: an in vitro study.” *Can J Cardiol* 2015; 31:1041-6.

72. Bakhtiary F, Dzemali O, Steinsheiffer U, Schimitz C, Glasmacher B, Moritz A, Kleine P. “Opening and closing kinematics of fresh and calcified aortic valve prostheses: An in vitro study.” *J Thorac Cardiovasc Surg* 2007; 134:657-62.

73. Mendelson K, Schoen F. “Heart valve tissue engineering: concepts, approaches, progress, and challenges.” *Ann Biomed Eng* 2006; 34(12):1799-819.

74. Hoerstrup SP, Sodian R, Daebritz S, Wang J, Bacha EA, Martin DP, Moran AM, Guleserian Kj, Sperling JS, Kaushal S, Vacanti JP, Schoen FJ, Mayer JE. “Functional living trileaflet heart valves grown in vitro.” *Circulation* 2000; 102(19):III-44-9.

75. Narita Y, Hata K, Kagami H, Usui A, Ueda M, Ueda Y. “Novel pulse duplicating bioreactor system for tissue-engineered vascular construct.” *Tissue Eng* 2004; 10(7-8):1224-33.

76. Syedain ZH, Meier LA, Reimer J, Tranquillo RT. “Tubular heart valves from decellularized engineered tissue.” *Ann Biomed Eng* 2013; 41(12):2645-54.

77. Hoerstrup S, Zünd G, Sodian R, Schnell A Grüenenfelder J, Turina M. “Tissue engineering of small calibre vascular grafts.” *Eur J Cardiothorac Surg* 2001; 20(1): 164-9.

78. Glower JS, Cheng RC, Giridharan GA, Gillars KJ, Pantalos GM, Litwak KN, Ewert DL, Koenig SC. “In Vitro evaluation of control strategies for an artificial vasculature device.” In *Proceedings of the 26th Annual International Conference of the IEEE (Engineering in Medicine and Biology Society),* 1-5 September, 2004; San Francisco, CA, USA.

79. Yokoyama Y, Kawaguchi O, Shinshi T, Steinseifer U, Takatani S. “A new pulse duplicator with a passive fill ventricle for analysis of cardiac dynamics.” *J Artif Organ* 2010; 13:189-96.

80. Ng KG, Ting CM, Yeo JH, Sim KW, Peh WL, Chua NH, Chua NK, Kwong F. "Progress on the development of the MediWatch ambulatory blood pressure monitor and related devices." *Blood Pressure Monitoring* 2004; 9(3):149-65.

81. Zimpfer D, Schima H, Czerny M, Kasimir MT, Sandner S, Seebacher G, Loser U, Simon P, Grimm M, Wolner E, Ehrlich M. "Experimental stent-graft treatment of ascending aortic dissection." *Ann Torac Surg* 2008; 85:470-3.

82. Schichl K, Affeld K. "A computer controlled versatile pulse duplicator for precision testing of artificial heart valves." *Int J Artif Organs* 1993; 16(10):722-8.

83. Jennings LM, Butterfield M, Walker PG, Watterson KG, Fisher J. "The influence of ventricular input impedance on the hydrodynamic performance of bioprosthetic aortic roots in vitro." *J Heart Valve Dis* 2001; 10(2):269-75.

84. Viscoelastic Impedance Adapter user manual. ViVitro Labs Inc., Victoria, BC, Canada, 2015.

85. Fraser R. "10 ways ViVitro Pulse Duplicator and HiCycle compare to equipment built in-house." Retrieved April 28, 2016, from http://vivitrolabs.com/faq/10-ways-vivitro-pulse-duplicator-and-hicycle-compare-to-equipment-built-in-house/

86. Food and Drug Administration. *Heart valves – Investigational device exemption (IDE) and premarket approval (PMA) applications. Draft guidance for Industry and FDA staff*. Maryland, USA. 2010.

87. Bottio T, Tarzia V, Rizzoli G, Gerosa G. "The changing spectrum of bioprostheses hydrodynamic performance: considerations on in-vitro tests." *Interact Cardiovasc Thorac Surg* 2008; 7(5):750-4.

88. Gerosa G, Tarzia V, Rizzoli G, Bottio T. "Small aortic annulus: The hydrodynamic performances of 5 commercially available tissues valves." *J Thorac Cardiovasc Surg* 2006; 131(5):1058-64.

89. Liu Y, Allaire P, Wu Y, Wood H, Olsen D. "Construction of an artificial heart pump performance test system." *Cardiovasc Eng* 2006; 6:153-60.

90. Van Der Merwe J. "Continued development of a joint-type knee wear simulator." MSc (Mechatronic) thesis, Stellenbosch University, South Africa, 2012.

91. Lee S. "United States Patent: US20140099620 A1 – Modular pulse duplicator system for simulation of cardiovascular hemodynamic functions", April 10, 2014.

92. Lang RM, Bierig M, Devereux RB, Flachskampf FA, Foster E, Pellikka PA, Picard MH, Roman MJ, Seward J, Shanewise JS, Solomon SD, Spencer KT, Sutton MS, Stewart WJ. "Recommendations for chamber quantification." *Eur J Echocardiography* 2006; 7(2):79-108.

93. Cain PA, Ahl R, Hedstrom E, Ugander M, Allansdotter-Johnsson A, Friberg P, Arheden H. “Age and gender specific normal values of left ventricular mass, volume and function for gradient echo magnetic resonance imaging: a cross sectional study.” *BMC Med Imaging* 2009; 9:2.

94. Walker A. “In vitro evaluation of mechanical heart valve performance using a novel test chamber in an automated mock circulatory loop.” MSc (Biomedical Engineering) thesis, Virginia Commonwealth University, USA, 2010.

95. Bazan O, Ortiz JP, Yamashita DY. “Pulse duplicator system for in vitro evaluation of presthetic heart valves – Data acquisition system developed in LabVIEW.” In *Proceedings of 22nd International Congress of Mechanical Engineering (COBEM 2013)*, November 3-7, 2013, Ribeirão Preto, SP, Brazil.

96. MP3 pulse duplicator brochure. Dynatek Labs, Galena, MO, USA.

97. MoviDrive® MDX60B/61B system manual. SEW Eurodrive GmbH & Co KG, Bruchsal, Germany, 2010.

98. Franklin GF, David Powell J, Emami-Naeini A. *Feedback control of dynamic systems.* 6th Edition. Upper Saddle River, New Jersey, USA: Pearson Higher Education, 2010.

99. Vinet A, Nottin S, Lecoq AM, Obert P. “Cardiovascular responses to progressive cycle exercise in healthy children and adults.” *Int J Sports Med* 2002; 23(4):242-6.

100. Laske A, Jenni R, Maloigne M, Vassalli G, Bertel O, Turina M. “Pressure gradients across bileaflet aortic valves by direct measurement and echocardiography.” *Ann Thorac Surg* 1996; 61:48-57.

101. Food and Drug Administration. *Summary of safety and effectiveness data: Epic™ and Epic™ Supra valve.* Premarket approval number P040021/S004. Silver Spring, Maryland, USA, 2007.

102. SuperPump brochure. ViVitro Labs Inc., Victoria, BC, Canada, 2016.

103. CMS50/63/71 Electric cylinders catalog. SEW Eurodrive GmbH & Co KG, Bruchsal, Germany, 2010.

104. D’Avenio G, Grigioni M, Daniele C, Morbiducci U, Hamilton K. “3D velocity field characterization of prosthetic heart valve with two different valve testers by means of stereo-PIV.” *Conf Proc IEEE Eng Med Biol Soc* 2015; 2015:3327-30.

105. SJM Biocor stented valve system product brochure. St Jude Medical Inc., St Paul, Minnesota, USA, 2009.

106. Bottio T, Buratto E, Dal Lin C, Lika A, Rizzoli G, Gerosa G. “Aortic valve hydrodynamics: considerations on the absence of sinuses of Valsalva.” *J Heart Valve Dis* 2012; 21(6):718-23.

107. Salica A, Pisani G, Morbiducci U, Scaffa R, Massai D, Audenino A, Weltert L, Guerrieri Wolf L, De Paulis R. “The combined role of sinuses of Valsalva and flow pulsatility improves energy loss of the aortic valve.” *Eur J Cardiothorac Surg* 2016; 49:1222–7.

108. Pisani G, Scaffa R, Ieropoli O, Dell’Amico EM, Maselli D, Morbiducci U, De Paulis R. “Role of the sinuses of Valsalva on the opening of the aortic valve.” *J Thorac Cardiovasc Surg* 2013; 145:999-1003.

109. Steppan J, Barodka V, Berkowitz DE, Nyhan D. “Vascular stiffness and increased pulse pressure in the aging cardiovascular system.” *Cardiol Res Pract* 2011; 2011:263585.

110. Sugawara M, Uchida K, Kondoh Y, Magosaki N, Niki K, Jones CJH, Sugimachi M, Sunagawa K. “Aortic blood momentum – the more the better for the ejecting heart in vivo?” *Cardiovasc Res* 1997; 33(2):433-46.

111. Boutouyrie P *et al*. “Determinants of pulse wave velocity in healthy people and in the presence of cardiovascular risk factors: ‘establishing normal and reference values’”. *Eur Heart J* 2010; 31(19):2338-50.

Appendix A: Calibration data

A.1 Pressure sensors

The setup for the calibration procedure was identical to that used during normal tests. The pressure port of the transducer under calibration (Wika A-10 1 bar, WIKA Alexander Wiegand SE & Co. KG, Klingenberg, Germany) was connected to the Druck DPI 610 pressure calibrator (GE Measurement & Control Solutions, MA, USA; S/N: 61011739). The output of the transducer, configured for current output mode, was connected to the National Instruments USB-6009 data acquisition card (National Instruments, TX, USA; S/N: 302BF3B) through a 500 Ω precision resistor (Vishay Intertechnology, Inc., PA, USA; P/N: PAPTF56500R00BYEK).

Three calibration runs were performed for each sensor. For each calibration run, the sensor was loaded from 0 bar to 1 bar in steps of 0.2 bar. The current reported by the data acquisition card for each pressure value was noted after the calibrator indicated that the pressure had settled on the target. This normally required adjustment of the pressure source, taking care to not overshoot the target. After reaching 1 bar, the same procedure was followed in reverse, unloading the sensor.

The excellent linearity of all three sensors throughout their range became evident once all calibration data were available. Therefore, a linear function was used to convert from mA to bar, using the average of the calibration points (six values for each pressure step: three load points and three unload points).
The following sections detail the calibration parameters for each sensor.

A.1.1 Ventricular pressure transducer

Table A.1 shows the results of the calibration process for the ventricular pressure transducer while Table A.2 summarises the results of the three runs into the average of each pressure point. The values presented in Table A.2 were used to plot the calibration curve shown in Figure A.1 and to calculate the linear calibration function (included in Figure A.1).

Table A.1: Calibration data for the ventricular pressure transducer.

S/N: 00126108YS		T1	T2	T3
Data point	$P_{applied}$ **(bar)**	$I_{measured}$ **(mA)**	$I_{measured}$ **(mA)**	$I_{measured}$ **(mA)**
1	0	4.070	4.078	4.079
2	0.2	7.258	7.258	7.259
3	0.4	10.455	10.446	10.446
4	0.6	13.654	13.654	13.653
5	0.8	16.832	16.832	16.830
6	1	20.009	20.000	19.998
7	0.8	16.832	16.833	16.832
8	0.6	13.653	13.655	13.655
9	0.4	10.457	10.456	10.458
10	0.2	7.261	7.262	7.268
11	0	4.076	4.080	4.079

Table A.2: Averaged calibration data for each pressure point (ventricular pressure transducer).

$P_{applied}$ **(bar)**	$I_{average}$ **(mA)**
0	4.077
0.2	7.261
0.4	10.453
0.6	13.654
0.8	16.832
1	20.002

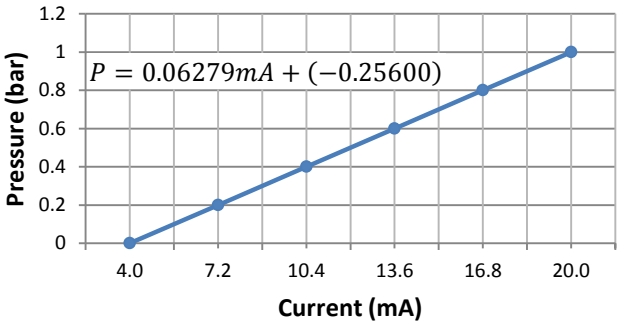

Figure A.1: Calibration curve for the ventricular pressure transducer.

A.1.2 Aortic pressure transducer

Table A.3 shows the results of the calibration process for the ventricular pressure transducer while Table A.4 summarises the results of the three runs into the average of each pressure point. The values presented in Table A.4 were used to plot the calibration

curve shown in Figure A.2 and to calculate the linear calibration function (included in Figure A.2).

Table A.3: Calibration data for the aortic pressure transducer.

S/N: 001260UH1A		T1	T2	T3
Data point	$P_{applied}$ **(bar)**	$I_{measured}$ **(mA)**	$I_{measured}$ **(mA)**	$I_{measured}$ **(mA)**
1	0	4.074	4.075	4.048
2	0.2	7.253	7.254	7.254
3	0.4	10.446	10.446	10.447
4	0.6	13.636	13.637	13.638
5	0.8	16.827	16.823	16.821
6	1	20.013	20.016	20.016
7	0.8	16.827	16.821	16.819
8	0.6	13.647	13.648	13.649
9	0.4	10.447	10.448	10.448
10	0.2	7.264	7.263	7.264
11	0	4.075	4.075	4.075

Table A.4: Averaged calibration data for each pressure point (aortic pressure transducer).

$P_{applied}$ **(bar)**	$I_{average}$ **(mA)**
0	4.070
0.2	7.259
0.4	10.447
0.6	13.643
0.8	16.823
1	20.015

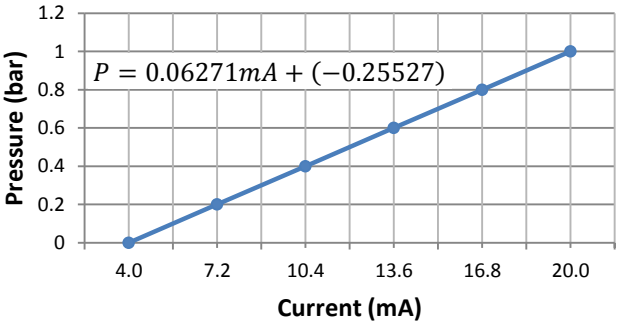

Figure A.2: Calibration curve for the aortic pressure transducer.

A.1.3 Atrial pressure transducer

Table A.5 shows the results of the calibration process for the ventricular pressure transducer whileTable A.6 summarises the results of the three runs into the average of each pressure point. The values presented in Table A.6 were used to plot the calibration curve shown in Figure A.3 and to calculate the linear calibration function (included in Figure A.3).

Table A.5: Calibration data for the atrial pressure transducer.

S/N: 001260UH18		T1	T2	T3
Data point	$P_{applied}$ **(bar)**	$I_{measured}$ **(mA)**	$I_{measured}$ **(mA)**	$I_{measured}$ **(mA)**
1	0	4.084	4.076	4.078
2	0.2	7.258	7.261	7.271
3	0.4	10.448	10.449	10.449
4	0.6	13.651	13.653	13.653
5	0.8	16.824	16.832	16.828
6	1	19.979	19.98	19.991
7	0.8	16.829	16.831	16.838
8	0.6	13.657	13.669	13.664
9	0.4	10.464	10.472	10.472
10	0.2	7.281	7.274	7.283
11	0	4.073	4.084	4.078

Table A.6: Averaged calibration data for each pressure point (atrial pressure transducer).

$P_{applied}$ **(bar)**	$I_{average}$ **(mA)**
0	4.079
0.2	7.271
0.4	10.459
0.6	13.658
0.8	16.830
1	19.983

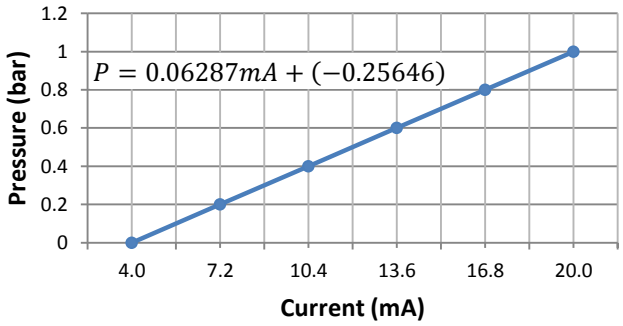

Figure A.3: Calibration curve for the atrial pressure transducer.

A.2 Flowmeter

SIEMENS Industry Sector

Factory Calibration Certificate / Werkskalibrierungszertifikat / Certificat d'étalonnage usine

Topic / Thema / Sujet: SITRANS F Flowmeter / Durchflussmessgerät / Débitmètre

Object / Betreff / Objet:

Siemens order / Siemensauftrag / Commande Siemens	:	0001365470/000020
Flowmeter type / Durchflussmessgerättyp / Type de débitmètre	:	Sitrans FM MAG5100 W
Nominal sensor diameter / Messaufnehmer-Nennweite / Diamètre nominal de capteur	:	DN 15 (1/2")
Product order No. / Produktbestellnummer / N° de référence d'appareil	:	7ME65201VF132AA1
System serial No. / System Seriennummer / N° de série du systeme	:	442302H515
Sensor serial No. / Messaufnehmer Seriennummer / N° de série de capteur	:	087402H435

Technical data / Technische Daten / Données techniques:

Calibration factor / Kalibrierungsfaktor / Facteur d'étalonnage	:	0.157737466
Calibration medium / Kalibriermedium / Moyen de calibration	:	Water / Wasser / Eau
Calibrated full scale flow / Kalibrierter Messbereichsendwert / Fin de plage de mesure étalonnée	:	3 m^3/h / 13.203 US gpm
Calibration rig / Kalibrierstand / Plate-forme d'étalonnage	:	Banc HNU 1

Standards / Normen / Normes: Reference meter method (reference meter calibrated according to ISO 4185-1980) / Referenzmessgerätmethode (Referenzgerät kalibriert laut ISO 4185-1980) / Méthode avec compteur de référence (étalonné suivant ISO 4185-1980)

Results / Ergebnisse / Résultats:

Point # Messpunkt nr Point mesure n°	Flowrate Durchfluss Débit	Fluid temperature Flüssigkeitstemperatur Température du fluide		Reference flow value Referenz Durchflusswert Débit de référence		Flowmeter output / Duchflussmessgerätausgang / Sortie de débitmètre		
						Flowrate Durchflussmenge / Débit		Error Fehler / Erreur
	[%]	[°C]	[°F]	[m^3/h]	[US gpm]	[m^3/h]	[US gpm]	[%]
1	95	21.6	70.9	2.8627	12.6042	2.8645	12.6121	0.06
2	26	21.8	71.2	0.7708	3.3936	0.7700	3.3904	-0.06
3	95	21.6	70.9	2.8624	12.6026	2.8624	12.6026	0.00
4	26	21.8	71.2	0.7697	3.3888	0.7693	3.3872	-0.08

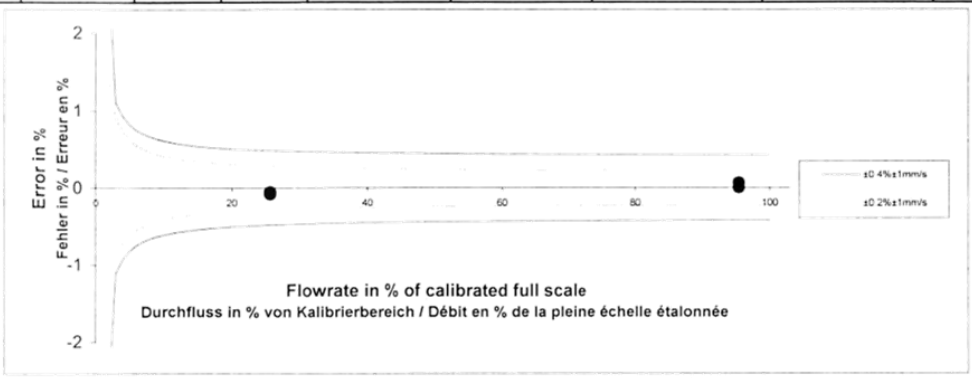

Summary of the results / Zusammenfassung der Ergebnisse: / Sommaire des résultats obtenus : :

- The measured values are within the specified limits / Die gemessenen Werte liegen innerhalb der Toleranzen / Les résultats de mesure se trouvent dans les tolérances définies

Siemens SAS Etablissement de Haguenau	Issued by / Erstellt von / émis par Baritaud	Date / Datum / Date 2015/12/23

A.3 Linear variable differential transformer

The calibration of the linear variable differential transformer (LVDT) (HBM 1-WA/50MM-L, S/N: 173410237, Hottinger-Baldwin-Messtechnik GmbH, Darmstadt, Germany) was performed with the same setup that was used to measure the cam. An HBM Clip AE501 instrumentation amplifier (S/N: 801177327, Hottinger-Baldwin-Messtechnik GmbH, Darmstadt, Germany) was used to excite and amplify the output of the LVDT and a National Instruments USB-6212 data acquisition card (S/N: 18C7531, National Instruments, TX, USA) was used to read the output of the instrumentation amplifier. To maximise the resolution of the measurement, the instrumentation amplifier's variable sensitivity was set up to produce the highest possible output when the LVDT measured the cam's maximum lift. Therefore, the calculated sensitivity is related to the amplified value and does not match the calibration certificate (included in page 99), which was used only to decide which section of the LVDT to calibrate. Since only 20mm were to be calibrated, the section showing the lowest average deviation (from 0 mm to 20 mm) was calibrated using gauge blocks.

Table A.7 contains all the data relevant to the calibration process. The applied displacements correspond to the sizes of the available gauge blocks. To minimise linearity errors, the sensitivity was calculated for each interval and the average used to convert the raw voltage value to a displacement measurement. Figure A.4 shows the acquired calibration data to depict linearity.

Table A.7: Calibration data for the LVDT.

Measure-ment (i)	Applied displacement (mm)	Measured Voltage (V)	$Displ_i$ - $Displ_{i-1}$ (mm)	V_i - V_{i-1} (V)	Calculated sensitivity (V/mm)
1	0	0.58673	- - -	- - -	- - -
2	1	0.83942	1	0.25269	0.25269
3	2	1.08665	1	0.24723	0.24723
4	3	1.33761	1	0.25096	0.25096
5	5	1.83441	2	0.49680	0.24840
6	10	3.08079	5	1.24638	0.24928
7	15	4.32442	5	1.24363	0.24873
8	20	5.55932	5	1.23490	0.24698
				Average	**0.24918**

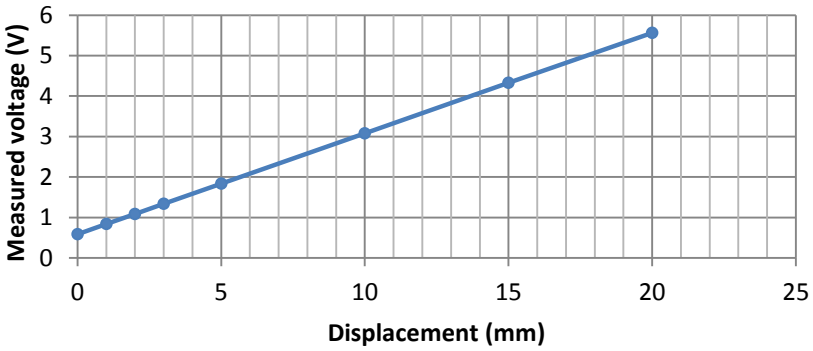

Figure A.4: Raw calibration data used to determine the sensitivity of the LVDT.

Prüfprotokoll

test certificate / protocole d`essai

HBM

Typ: type / type	WA	Auftrag: order no / commission	801193550
Nennmessbereich: range / portée	50 mm	Prüfer: examiner / contrôleur	Thomas
IdentNr: serial no / N°- ident	173410237	Datum: test date / date d`essai	04.09.2013

Prüfergebnisse:
test results / résultats d`essai

Eingangsgröße des Messbereichs [mm] input quantity / échelle d`essai	Abweichung [mm] deviation / écart
0	0.000
5	0.030
10	0.018
15	0.006
20	0.011
25	0.029
30	0.027
35	0.008
40	-0.021
45	-0.016
50	0.000

Aus den Prüfergebnissen berechnete und sonstige messtechnische Eigenschaften:
metrological characteristics calculated from the measuring results and others:
valeurs caractéristiques calculées à partir des résultats d`essai:

Kennwert bei 50 mm sensitivity / sensibilité	80.0 mV/V bei 2.5 V Nennspeisespannung
Max. Linearitätsabweichung max. linearity deviation / erreur de linearité max.	0.06 %

Alle aus den Messergebnissen ermittelten Kenngrößen entsprechen den Spezifikationen gemäß Datenblatt.
All characteristic quantities determined from the measurement results correspond to the specifications per datasheet.
Toutes les grandeurs caractéristiques déterminées à partir des résultats de mesure correspondent aux spécifications selon les caractéristiques techniques.

Allgemeine Zusatzinformationen:
general information / informations complémentaires

Alle weiteren messtechnischen Eigenschaften des Aufnehmers sind durch Typprüfungen und laufende Produktaudits des Qualitätswesens abgesichert.
All other metrological characteristics of the transducer are verified by type testing and regular product audits of the quality department.
Toutes les autres caractéristiques techniques du capteur sont garanties par le Service Qualité, au moyen d`essais et d`audits suivis sur le produit.

Hottinger Baldwin Messtechnik GmbH, Im Tiefen See 45, 64293 Darmstadt, Germany | www.hbm.com
Registered as GmbH (German limited liability corporation) in the commercial register at the local court of Darmstadt, HRB 1147
Company domiciled in Darmstadt | CEO: Andreas Hüllhorst | Chairman of the board: James Charles Webster

Zertifiziert nach ISO 9001 und ISO 14001 / ISO 9001 and ISO 14001 certified / Certification selon ISO 9001 et ISO 14001
Akkreditierungen gemäß ISO 17025 / Accreditations per ISO 17025 / Accréditations selon ISO 17025

Ausgabe 30813 Version c
14.11.2012 Moor
R12: 51.1000 R14:1097.6000 R15:162.0000

115.00-1415PP
KP415

Appendix B: Cam's numerical profile

Table B.1 contains the cam's numerical profile in the form of 500 measurement points. The profile presented was obtained using the process described in Section 3.3.

Table B.1: Numerical description of the cam.

Point	Lift (mm)	Point	Lift (mm)	Point	Lift (mm)	Point	Lift (mm)	Point	Lift (mm)	Point	Lift (mm)
1	0.017	46	1.580	91	7.465	136	12.548	181	15.322	226	15.026
2	0.017	47	1.666	92	7.598	137	12.647	182	15.350	227	14.987
3	0.017	48	1.756	93	7.733	138	12.745	183	15.377	228	14.944
4	0.017	49	1.850	94	7.870	139	12.843	184	15.402	229	14.900
5	0.017	50	1.946	95	8.007	140	12.937	185	15.424	230	14.855
6	0.017	51	2.047	96	8.142	141	13.026	186	15.446	231	14.807
7	0.018	52	2.151	97	8.276	142	13.116	187	15.467	232	14.760
8	0.019	53	2.261	98	8.406	143	13.200	188	15.484	233	14.711
9	0.020	54	2.376	99	8.532	144	13.285	189	15.500	234	14.660
10	0.023	55	2.496	100	8.657	145	13.369	190	15.512	235	14.609
11	0.025	56	2.619	101	8.779	146	13.444	191	15.522	236	14.556
12	0.029	57	2.742	102	8.900	147	13.525	192	15.533	237	14.500
13	0.035	58	2.865	103	9.023	148	13.601	193	15.543	238	14.443
14	0.044	59	2.990	104	9.143	149	13.675	194	15.554	239	14.383
15	0.056	60	3.116	105	9.264	150	13.754	195	15.562	240	14.319
16	0.070	61	3.244	106	9.384	151	13.829	196	15.568	241	14.256
17	0.086	62	3.374	107	9.503	152	13.898	197	15.573	242	14.193
18	0.105	63	3.508	108	9.621	153	13.969	198	15.573	243	14.130
19	0.126	64	3.645	109	9.738	154	14.038	199	15.573	244	14.068
20	0.151	65	3.785	110	9.854	155	14.104	200	15.572	245	14.005
21	0.179	66	3.929	111	9.968	156	14.172	201	15.569	246	13.942
22	0.208	67	4.074	112	10.081	157	14.237	202	15.569	247	13.876
23	0.239	68	4.222	113	10.194	158	14.302	203	15.566	248	13.810
24	0.272	69	4.371	114	10.307	159	14.363	204	15.558	249	13.741
25	0.307	70	4.519	115	10.420	160	14.426	205	15.549	250	13.672
26	0.346	71	4.669	116	10.536	161	14.486	206	15.536	251	13.602
27	0.386	72	4.816	117	10.649	162	14.540	207	15.524	252	13.529
28	0.429	73	4.964	118	10.763	163	14.594	208	15.513	253	13.457
29	0.473	74	5.114	119	10.876	164	14.643	209	15.500	254	13.384
30	0.519	75	5.264	120	10.987	165	14.689	210	15.484	255	13.307
31	0.569	76	5.416	121	11.095	166	14.736	211	15.465	256	13.229
32	0.621	77	5.567	122	11.200	167	14.782	212	15.446	257	13.146
33	0.678	78	5.717	123	11.300	168	14.826	213	15.425	258	13.061
34	0.736	79	5.864	124	11.399	169	14.870	214	15.406	259	12.974
35	0.797	80	6.009	125	11.496	170	14.913	215	15.386	260	12.884
36	0.860	81	6.150	126	11.593	171	14.955	216	15.362	261	12.791
37	0.925	82	6.288	127	11.690	172	14.997	217	15.335	262	12.696
38	0.991	83	6.423	128	11.786	173	15.039	218	15.304	263	12.599
39	1.059	84	6.555	129	11.881	174	15.081	219	15.272	264	12.504
40	1.128	85	6.685	130	11.976	175	15.121	220	15.239	265	12.411
41	1.197	86	6.815	131	12.070	176	15.160	221	15.206	266	12.316
42	1.268	87	6.944	132	12.164	177	15.195	222	15.172	267	12.224
43	1.342	88	7.073	133	12.259	178	15.229	223	15.137	268	12.130
44	1.418	89	7.203	134	12.354	179	15.260	224	15.101	269	12.033
45	1.498	90	7.333	135	12.450	180	15.291	225	15.065	270	11.937

Table B.1: Numerical description of the cam. (Continued)

Point	Lift (mm)	Point	Lift (mm)	Point	Lift (mm)	Point	Lift (mm)	Point	Lift (mm)	Point	Lift (mm)
271	11.841	316	7.464	361	3.138	406	0.565	451	0.024	496	0.020
272	11.746	317	7.364	362	3.055	407	0.532	452	0.006	497	0.019
273	11.654	318	7.263	363	2.971	408	0.500	453	0.006	498	0.019
274	11.560	319	7.163	364	2.888	409	0.469	454	0.006	499	0.018
275	11.465	320	7.063	365	2.806	410	0.440	455	0.005	500	0.017
276	11.369	321	6.962	366	2.727	411	0.411	456	0.006		
277	11.272	322	6.860	367	2.651	412	0.384	457	0.006		
278	11.176	323	6.757	368	2.576	413	0.359	458	0.006		
279	11.079	324	6.654	369	2.504	414	0.336	459	0.006		
280	10.981	325	6.552	370	2.432	415	0.313	460	0.006		
281	10.884	326	6.451	371	2.364	416	0.292	461	0.006		
282	10.787	327	6.352	372	2.298	417	0.271	462	0.006		
283	10.692	328	6.254	373	2.234	418	0.252	463	0.007		
284	10.598	329	6.158	374	2.171	419	0.236	464	0.006		
285	10.504	330	6.063	375	2.107	420	0.222	465	0.006		
286	10.411	331	5.969	376	2.044	421	0.210	466	0.006		
287	10.317	332	5.875	377	1.982	422	0.199	467	0.007		
288	10.225	333	5.781	378	1.920	423	0.188	468	0.008		
289	10.134	334	5.684	379	1.861	424	0.179	469	0.008		
290	10.043	335	5.587	380	1.802	425	0.168	470	0.008		
291	9.954	336	5.489	381	1.742	426	0.157	471	0.008		
292	9.864	337	5.392	382	1.683	427	0.143	472	0.008		
293	9.774	338	5.294	383	1.624	428	0.128	473	0.009		
294	9.683	339	5.196	384	1.564	429	0.112	474	0.010		
295	9.592	340	5.097	385	1.505	430	0.097	475	0.010		
296	9.502	341	4.997	386	1.447	431	0.083	476	0.010		
297	9.407	342	4.897	387	1.391	432	0.071	477	0.010		
298	9.311	343	4.795	388	1.337	433	0.060	478	0.010		
299	9.212	344	4.694	389	1.284	434	0.049	479	0.010		
300	9.109	345	4.593	390	1.233	435	0.039	480	0.010		
301	9.007	346	4.493	391	1.183	436	0.030	481	0.011		
302	8.903	347	4.396	392	1.134	437	0.024	482	0.011		
303	8.798	348	4.300	393	1.086	438	0.018	483	0.012		
304	8.692	349	4.206	394	1.039	439	0.013	484	0.013		
305	8.584	350	4.113	395	0.994	440	0.009	485	0.013		
306	8.478	351	4.021	396	0.950	441	0.005	486	0.014		
307	8.374	352	3.928	397	0.907	442	0.003	487	0.013		
308	8.271	353	3.836	398	0.865	443	0.001	488	0.013		
309	8.170	354	3.745	399	0.824	444	0.001	489	0.012		
310	8.067	355	3.655	400	0.784	445	0.000	490	0.012		
311	7.964	356	3.567	401	0.746	446	0.000	491	0.013		
312	7.863	357	3.479	402	0.709	447	0.000	492	0.015		
313	7.761	358	3.392	403	0.672	448	0.001	493	0.017		
314	7.662	359	3.306	404	0.636	449	0.002	494	0.019		
315	7.563	360	3.221	405	0.600	450	0.010	495	0.019		

A polynomial was fitted to the above numerical data using a least squares method (the original dataset has five digits of precision). A 6^{th} order polynomial yields a coefficient of determination $R^2 = 0.99978$ indicating a very good fit.

After having found the correct order for the polynomial, the fitting routine was run again on the same dataset after it was normalised. This is useful because the profile produced by this polynomial can be scaled easily. Further, although the polynomial is based on 500 data points, the tool shown in Section 4.2 makes it easy to generate a dataset of any length. Equation B.1 is the polynomial for the normalised data and Figure B.1 shows the experimental data and the fitted curve superposed for comparison. Although the polynomial fitting the original dataset is not presented, Table B.2 contains the parameters indicating the goodness of fit for both.

$$y = 0.0077564 - (0.002912 \times x) + (0.0001562 \times x^2) - (8.5816918 \times 10^{-7} \times x^3) + (1.4658378 \times 10^{-9} \times x^4) - (3.1147732 \times 10^{-13} \times x^5) - (7.8220802 \times 10^{-16} \times x^6) \quad \text{(B.1)}$$

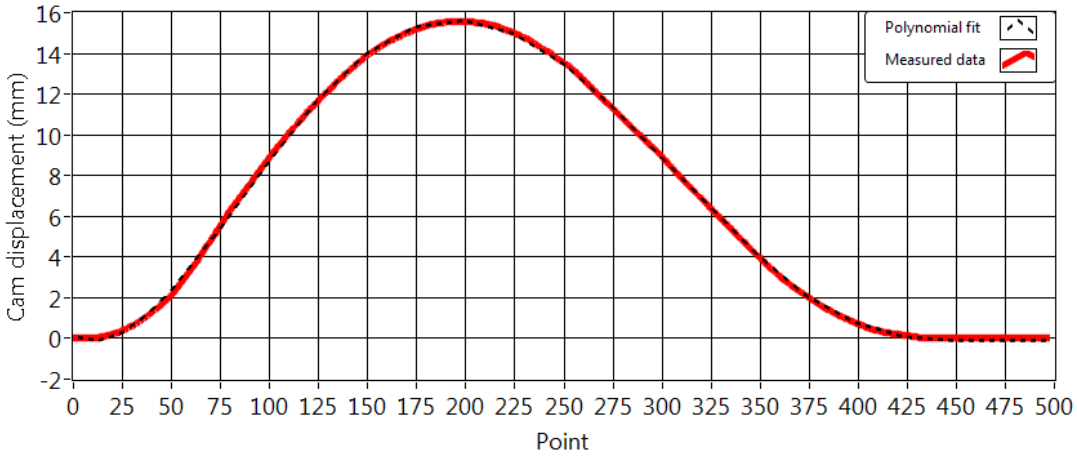

Figure B.1: Graphical comparison of measured and fitted data.

Table B.2: Measures of fit for the respective polynomials. (RMSE: root mean square error; SSE: sum of square errors; R^2: coefficient of determination.)

Parameter	Original dataset	Normalised dataset
RMSE	0.08728	0.0056
SSE	3.7862	0.01561
R^2	0.99978	0.99978

Appendix C: ISO test data

The tables in this appendix contain the full set of data for the 10 heartbeats that were analysed for each test for each valve. The statistical summary at the end of each table was included in Section 4.5. Figure C.1 to Figure C.4 represent a single heartbeat, related to the comparative tests performed on the 23mm St Jude Epic Supra PHV, and complement Table C.16 to Table C.19, respectively. The figures were included to allow the reader to observe the progression of the pressure and flow curves as the stroke volume increases and to allow the graphical visualisation of features which cannot be accounted for numerically but that contribute to the results that were reported.

The following nomenclature and abbreviations apply to the tables, listed in the order of the column headers:

- Table C.1 to Table C.8 and Table C.15:

  EOA: Effective orifice area
  ΔP: Pressure drop across the open valve
  MAP: Mean arterial pressure
  Q_{mean}: mean flow rate
  Systole: Systolic fraction
  T_{sys}: Systolic time

- Table C.9 to Table C.14:

  V_{reg_total}: Total regurgitant volume
  $V_{closing}$: Closing volume
  $V_{leakage}$: Leakage volume
  Q_{mean}: Mean flow rate
  $-\Delta P_{mean}$: Mean back pressure across the closed valve
  MAP Mean arterial pressure

- Table C.16 to Table C.19:

  PSPD: Peak systolic pressure difference
  MSPD: Mean systolic pressure difference
  MSAP: mean systolic arterial pressure
  MSVP mean systolic ventricular pressure
  SWL: Stroke work loss
  Systole Systolic fraction
  T_{sys}: Systolic time

SJM Epic 21 mm Valve 1

Table C.1: ISO Test 1 results for SJM Epic 21 mm Valve 1.

Beat	EOA (cm^2)	ΔP (mmHg)	MAP (mmHg)	Q_{mean} (L/min)	Systole (%)	T_{sys} (ms)
1	0.85	17.46	99.17	4.63	36.4	312
2	0.86	17.18	98.50	4.65	36.4	312
3	0.86	17.39	98.96	4.73	36.4	312
4	0.85	18.00	98.97	4.67	35.8	307
5	0.86	17.34	98.67	4.67	36.2	310
6	0.86	17.17	98.81	4.66	36.6	314
7	0.87	17.40	98.81	4.72	35.8	307
8	0.86	17.16	98.22	4.65	36.4	312
9	0.86	18.20	99.13	4.76	35.4	304
10	0.86	17.47	99.38	4.72	35.9	308
Mean	**0.86**	**17.48**	**98.86**	**4.69**	**36.1**	**309.8**
SD	**± 0.01**	**± 0.33**	**± 0.32**	**± 0.04**	**± 0.4**	**± 3.0**
Max	**0.87**	**18.20**	**99.38**	**4.76**	**36.6**	**314**
Min	**0.85**	**17.16**	**98.22**	**4.63**	**35.4**	**304**

Table C.2: ISO Test 2 results for SJM Epic 21 mm Valve1.

Beat	EOA (cm^2)	ΔP (mmHg)	MAP (mmHg)	Q_{mean} (L/min)	Systole (%)	T_{sys} (ms)
1	0.55	7.49	99.69	1.87	34.3	294
2	0.57	7.12	99.47	1.92	35.4	303
3	0.56	7.30	99.97	1.92	35.6	305
4	0.57	7.10	100.15	1.94	35.2	302
5	0.57	7.18	100.23	1.91	35.5	304
6	0.56	7.57	100.16	1.95	34.7	297
7	0.56	7.46	100.55	1.92	34.3	294
8	0.56	7.40	100.72	1.93	34.8	298
9	0.55	7.56	100.65	1.87	34.4	295
10	0.56	7.43	100.69	1.93	34.3	294
Mean	**0.56**	**7.36**	**100.23**	**1.92**	**34.8**	**298.6**
SD	**± 0.01**	**± 0.17**	**± 0.41**	**± 0.03**	**± 0.5**	**± 4.2**
Max	**0.57**	**7.57**	**100.72**	**1.95**	**35.6**	**305**
Min	**0.55**	**7.10**	**99.47**	**1.87**	**34.3**	**294**

SJM Epic 21 mm Valve 2

Table C.3: ISO Test 1 results for SJM Epic 21 mm Valve 2.

Beat	EOA (cm^2)	ΔP (mmHg)	MAP (mmHg)	Q_{mean} (L/min)	Systole (%)	T_{sys} (ms)
1	0.81	20.34	100.74	4.76	35.4	303
2	0.81	19.93	100.97	4.69	35.5	304
3	0.81	20.25	100.43	4.69	35.1	301
4	0.82	19.56	100.46	4.69	35.2	302
5	0.82	20.11	101.40	4.73	35.0	300
6	0.80	20.11	100.41	4.65	35.4	303
7	0.82	19.91	100.54	4.69	35.2	302
8	0.80	20.10	100.18	4.65	35.1	301
9	0.81	20.19	100.38	4.69	35.1	301
10	0.82	19.90	100.39	4.70	35.1	301
Mean	**0.81**	**20.04**	**100.59**	**4.69**	**35.2**	**301.8**
SD	**± 0.01**	**± 0.21**	**± 0.34**	**± 0.03**	**± 0.2**	**± 1.2**
Max	**0.82**	**20.34**	**101.40**	**4.76**	**35.5**	**304**
Min	**0.80**	**19.56**	**100.18**	**4.65**	**35.0**	**300**

Table C.4: ISO Test 2 results for SJM Epic 21 mm Valve 2.

Beat	EOA (cm^2)	ΔP (mmHg)	MAP (mmHg)	Q_{mean} (L/min)	Systole (%)	T_{sys} (ms)
1	0.50	5.53	100.02	1.48	35.0	300
2	0.48	5.65	99.96	1.37	34.7	297
3	0.51	5.53	100.24	1.49	34.5	296
4	0.49	5.62	100.57	1.40	34.3	294
5	0.51	5.32	100.74	1.46	35.1	301
6	0.49	5.35	100.28	1.39	35.6	305
7	0.50	5.42	100.13	1.45	34.9	299
8	0.49	5.57	100.10	1.41	34.7	297
9	0.50	5.44	99.99	1.44	35.0	300
10	0.49	5.48	100.12	1.43	35.0	300
Mean	**0.50**	**5.49**	**100.22**	**1.43**	**34.9**	**298.9**
SD	**± 0.01**	**± 0.10**	**± 0.24**	**± 0.04**	**± 0.3**	**± 2.9**
Max	**0.51**	**5.65**	**100.74**	**1.49**	**35.6**	**305**
Min	**0.48**	**5.32**	**99.96**	**1.37**	**34.3**	**294**

SJM Epic 21 mm Valve 1

Table C.5: ISO Test 3 results for SJM Epic 21 mm Valve1.

Beat	EOA (cm^2)	ΔP (mmHg)	MAP (mmHg)	Q_{mean} (L/min)	Systole (%)	T_{sys} (ms)
1	0.71	11.02	98.33	3.06	35.4	303
2	0.70	11.09	98.30	3.00	34.9	299
3	0.71	11.05	98.60	3.09	35.7	306
4	0.70	11.03	99.07	3.07	36.1	309
5	0.70	11.19	99.45	3.07	35.2	302
6	0.70	11.28	99.62	3.03	35.0	300
7	0.71	10.93	99.48	3.07	35.4	303
8	0.70	10.98	99.33	3.00	35.5	304
9	0.70	11.25	99.41	3.08	35.4	303
10	0.69	11.21	99.21	3.02	35.7	306
Mean	**0.70**	**11.10**	**99.08**	**3.05**	**35.4**	**303.5**
SD	**± 0.01**	**± 0.12**	**± 0.47**	**± 0.03**	**± 0.3**	**± 2.8**
Max	**0.71**	**11.28**	**99.62**	**3.09**	**36.1**	**309**
Min	**0.69**	**10.93**	**98.30**	**3.00**	**34.9**	**299**

Table C.6: ISO Test 4 results for SJM Epic 21 mm Valve1.

Beat	EOA (cm^2)	ΔP (mmHg)	MAP (mmHg)	Q_{mean} (L/min)	Systole (%)	T_{sys} (ms)
1	0.91	30.88	100.69	7.00	35.5	304
2	0.94	28.84	101.08	6.93	36.6	314
3	0.94	28.76	100.76	6.98	36.8	315
4	0.94	29.38	101.11	6.95	35.9	308
5	0.94	28.83	101.08	7.02	36.4	312
6	0.94	28.90	101.38	6.95	36.5	313
7	0.92	30.42	101.52	7.09	35.6	305
8	0.91	30.48	101.41	6.91	35.8	307
9	0.93	28.72	101.11	6.99	37.0	317
10	0.93	30.03	101.18	6.95	35.7	306
Mean	**0.93**	**29.52**	**101.13**	**6.98**	**36.2**	**310.1**
SD	**± 0.01**	**± 0.80**	**± 0.25**	**± 0.05**	**± 0.5**	**± 4.4**
Max	**0.94**	**30.88**	**101.52**	**7.09**	**37.0**	**317**
Min	**0.91**	**28.72**	**100.69**	**6.91**	**35.5**	**304**

SJM Epic 21 mm Valve 2

Table C.7: ISO Test 3 results for SJM Epic 21 mm Valve 2.

Beat	EOA (cm^2)	ΔP (mmHg)	MAP (mmHg)	Q_{mean} (L/min)	Systole (%)	T_{sys} (ms)
1	0.71	11.24	98.66	3.11	35.4	303
2	0.71	11.29	98.80	3.13	35.2	302
3	0.71	11.13	98.40	3.08	35.1	301
4	0.71	11.30	98.53	3.10	35.2	302
5	0.71	11.28	98.99	3.09	35.1	301
6	0.71	11.28	98.61	3.11	35.7	306
7	0.71	11.03	98.03	3.08	36.2	310
8	0.70	11.17	97.86	3.10	35.5	304
9	0.71	11.42	98.42	3.10	35.4	303
10	0.70	11.16	98.32	3.11	36.2	310
Mean	**0.71**	**11.23**	**98.46**	**3.10**	**35.5**	**304.2**
SD	**± 0.00**	**± 0.10**	**± 0.32**	**± 0.01**	**± 0.4**	**± 3.2**
Max	**0.71**	**11.42**	**98.99**	**3.13**	**36.2**	**310**
Min	**0.70**	**11.03**	**97.86**	**3.08**	**35.1**	**301**

Table C.8: ISO Test 4 results for SJM Epic 21 mm Valve 2.

Beat	EOA (cm^2)	ΔP (mmHg)	MAP (mmHg)	Q_{mean} (L/min)	Systole (%)	T_{sys} (ms)
1	0.90	31.56	96.37	6.93	35.8	307
2	0.91	30.94	96.36	6.95	35.9	308
3	0.90	31.69	96.39	6.92	35.5	304
4	0.92	30.63	96.61	7.02	35.8	307
5	0.90	31.87	96.71	6.90	35.0	300
6	0.91	30.95	96.61	6.95	35.5	304
7	0.90	31.45	96.01	6.86	35.6	305
8	0.91	31.34	96.46	7.05	36.1	309
9	0.90	31.43	96.48	7.05	35.8	307
10	0.92	30.71	96.81	7.05	36.3	311
Mean	**0.91**	**31.26**	**96.48**	**6.97**	**35.7**	**306.2**
SD	**± 0.01**	**± 0.40**	**± 0.21**	**± 0.07**	**± 0.3**	**± 2.9**
Max	**0.92**	**31.87**	**96.81**	**7.05**	**36.3**	**311**
Min	**0.90**	**30.63**	**96.01**	**6.86**	**35.0**	**300**

SJME 21 mm Valve 1

Table C.9: ISO Test 5 results for SJM Epic 21 mm Valve1.

Beat	V_{reg_total} (mL)	$V_{closing}$ (mL)	$V_{leakage}$ (mL)	Q_{mean} (L/min)	$-\Delta P_{mean}$ (mmHg)	MAP (mmHg)
1	26.88	13.79	13.09	4.43	79.97	94.11
2	24.37	12.99	11.38	4.36	79.34	93.80
3	26.68	12.40	14.28	4.44	79.57	93.71
4	25.65	13.17	12.47	4.42	79.89	93.82
5	24.54	12.39	12.16	4.38	80.04	92.99
6	26.31	13.15	13.16	4.40	78.49	92.44
7	25.76	13.48	12.28	4.34	78.40	92.50
8	26.27	13.69	12.58	4.38	78.66	92.43
9	26.41	14.00	12.41	4.40	78.66	92.58
10	26.21	13.68	12.53	4.40	79.06	92.75
Mean	**25.91**	**13.27**	**12.63**	**4.39**	**79.21**	**93.11**
SD	**± 0.81**	**± 0.53**	**± 0.72**	**± 0.03**	**± 0.61**	**± 0.64**
Max	**26.88**	**14.00**	**14.28**	**4.44**	**80.04**	**94.11**
Min	**24.37**	**12.39**	**11.38**	**4.34**	**78.40**	**92.43**

Table C.10: ISO Test 6 results for SJM Epic 21 mm Valve1.

Beat	V_{reg_total} (mL)	$V_{closing}$ (mL)	$V_{leakage}$ (mL)	Q_{mean} (L/min)	$-\Delta P_{mean}$ (mmHg)	MAP (mmHg)
1	22.15	9.31	12.84	3.89	119.81	142.08
2	23.82	9.49	14.33	3.97	119.84	141.94
3	21.64	9.17	12.48	3.85	120.18	141.75
4	23.99	9.49	14.50	3.99	119.92	141.92
5	22.02	9.38	12.63	3.86	119.60	142.34
6	23.93	9.53	14.40	3.97	119.68	141.89
7	21.78	9.29	12.50	3.84	118.84	141.84
8	23.85	10.27	13.58	3.98	119.09	142.16
9	21.71	9.92	11.79	3.87	119.47	142.50
10	23.79	10.21	13.57	3.98	119.48	142.61
Mean	**22.87**	**9.61**	**13.26**	**3.92**	**119.59**	**142.10**
SD	**± 1.02**	**± 0.37**	**± 0.90**	**± 0.06**	**± 0.38**	**± 0.28**
Max	**23.99**	**10.27**	**14.50**	**3.99**	**120.18**	**142.61**
Min	**21.64**	**9.17**	**11.79**	**3.84**	**118.84**	**141.75**

SJM Epic 21 mm Valve 2

Table C.11: ISO Test 5 results for SJM Epic 21 mm Valve 2.

Beat	V_{reg_total} (mL)	$V_{closing}$ (mL)	$V_{leakage}$ (mL)	Q_{mean} (L/min)	$-\Delta P_{mean}$ (mmHg)	MAP (mmHg)
1	24.25	12.89	11.36	4.38	79.46	93.38
2	25.80	12.95	12.85	4.43	79.16	93.39
3	24.10	13.00	11.10	4.38	80.51	93.68
4	25.57	12.17	13.40	4.43	80.05	93.94
5	23.92	12.43	11.49	4.35	80.81	93.75
6	26.07	12.93	13.13	4.43	80.72	93.92
7	24.50	13.29	11.21	4.37	79.99	93.96
8	26.18	11.96	14.22	4.44	80.01	93.85
9	24.63	12.29	12.34	4.37	80.34	94.04
10	26.07	12.26	13.81	4.42	80.39	94.19
Mean	**25.11**	**12.62**	**12.49**	**4.40**	**80.15**	**93.81**
SD	**± 0.86**	**± 0.42**	**± 1.09**	**± 0.03**	**± 0.50**	**± 0.25**
Max	**26.18**	**13.29**	**14.22**	**4.44**	**80.81**	**94.19**
Min	**23.92**	**11.96**	**11.10**	**4.35**	**79.16**	**93.38**

Table C.12: ISO Test 6 results for SJM Epic 21 mm Valve 2.

Beat	V_{reg_total} (mL)	$V_{closing}$ (mL)	$V_{leakage}$ (mL)	Q_{mean} (L/min)	$-\Delta P_{mean}$ (mmHg)	MAP (mmHg)
1	22.39	10.26	12.13	4.07	118.43	130.52
2	24.60	9.02	15.58	4.19	117.80	130.84
3	21.55	8.68	15.58	4.00	117.92	130.45
4	22.33	9.86	12.48	4.00	118.86	130.70
5	24.29	10.08	14.21	4.16	119.01	131.97
6	24.80	10.18	14.62	4.14	118.22	132.06
7	23.98	10.17	13.81	4.08	117.88	132.20
8	22.65	9.94	12.71	4.03	118.30	132.22
9	25.21	10.21	15.01	4.19	118.17	132.14
10	24.67	10.20	14.47	4.12	118.79	132.16
Mean	**23.65**	**9.86**	**14.06**	**4.10**	**118.34**	**131.53**
SD	**± 1.22**	**± 0.52**	**± 1.19**	**± 0.07**	**± 0.41**	**± 0.74**
Max	**25.21**	**10.26**	**15.58**	**4.19**	**119.01**	**132.22**
Min	**21.55**	**8.68**	**12.13**	**4.00**	**117.80**	**130.45**

SJM Epic 21 mm Valve 1

Table C.13: ISO Test 7 results for SJM Epic 21 mm Valve1.

Beat	V_{reg_total} (mL)	$V_{closing}$ (mL)	$V_{leakage}$ (mL)	Q_{mean} (L/min)	$-\Delta P_{mean}$ (mmHg)	MAP (mmHg)
1	16.08	5.84	10.24	3.00	154.37	194.38
2	16.37	5.94	10.43	3.04	153.56	193.83
3	16.66	5.86	10.80	3.07	154.52	193.94
4	15.39	6.08	9.30	2.92	153.67	193.87
5	17.95	6.29	11.65	3.21	153.88	194.03
6	14.95	5.63	9.32	2.86	152.68	194.15
7	17.61	5.97	11.63	3.21	154.92	195.25
8	15.45	5.67	9.79	2.92	154.78	195.52
9	16.90	5.91	10.99	3.12	155.25	195.64
10	16.64	5.72	10.24	3.06	154.82	194.90
Mean	**16.37**	**5.91**	**10.44**	**3.04**	**154.18**	**194.51**
SD	**± 0.96**	**± 0.19**	**± 0.80**	**± 0.12**	**± 0.76**	**± 0.70**
Max	**17.95**	**6.29**	**11.65**	**3.21**	**155.25**	**195.64**
Min	**14.95**	**5.63**	**9.30**	**2.86**	**152.68**	**193.83**

SJM Epic 21 mm Valve 2

Table C.14: ISO Test 7 results for SJM Epic 21 mm Valve 2.

Beat	V_{reg_total} (mL)	$V_{closing}$ (mL)	$V_{leakage}$ (mL)	Q_{mean} (L/min)	$-\Delta P_{mean}$ (mmHg)	MAP (mmHg)
1	11.30	5.12	6.18	2.10	153.85	191.47
2	14.03	5.67	8.36	2.47	156.94	192.89
3	13.02	5.13	7.88	2.32	157.14	194.53
4	12.79	5.22	7.57	2.35	156.75	194.87
5	13.47	5.17	8.30	2.43	157.38	194.90
6	11.57	4.99	6.57	2.20	157.39	194.58
7	13.76	4.88	8.87	2.49	157.96	193.93
8	12.62	4.73	7.89	2.33	156.89	193.89
9	12.24	4.76	7.48	2.27	156.91	194.30
10	14.14	4.92	9.22	2.53	155.60	194.02
Mean	**12.89**	**5.06**	**7.83**	**2.35**	**156.68**	**193.94**
SD	**± 0.93**	**± 0.26**	**± 0.90**	**± 0.13**	**± 1.10**	**± 0.99**
Max	**14.14**	**5.67**	**9.22**	**2.53**	**157.96**	**194.90**
Min	**11.30**	**4.73**	**6.18**	**2.10**	**153.85**	**191.47**

SJM Regent 25 mm

Table C.15: ISO Test 1 results for SJM Regent 25 mm.

Beat	EOA (cm^2)	ΔP (mmHg)	MAP (mmHg)	Q_{mean} (L/min)	Systole (%)	T_{sys} (ms)
1	1.86	3.65	97.47	3.98	36.1	309
2	1.84	3.49	97.93	3.98	37.2	319
3	1.85	3.50	98.35	4.00	36.8	315
4	1.84	3.54	98.52	3.98	36.6	314
5	1.85	3.52	98.57	4.00	36.6	314
6	1.81	3.63	98.42	3.97	37.7	323
7	1.83	3.56	98.39	4.00	37.5	321
8	1.78	3.71	98.27	3.96	37.7	323
9	1.78	3.65	97.64	3.84	38.0	326
10	1.88	3.43	97.27	3.96	36.5	313
Mean	**1.83**	**3.57**	**98.08**	**3.97**	**37.1**	**317.7**
SD	**± 0.03**	**± 0.08**	**± 0.45**	**± 0.05**	**± 0.6**	**± 5.2**
Max	**1.88**	**3.71**	**98.57**	**4.00**	**38.0**	**326**
Min	**1.78**	**3.43**	**97.27**	**3.84**	**36.1**	**309**

SJM Epic 23 mm

Table C.16: Results for SJM Epic 23 mm Test 1.

Beat	PSPD (mmHg)	MSPD (mmHg)	MSAP (mmHg)	MSVP (mmHg)	SWL (%)	Systole (%)	T_{sys} (ms)
1	11.99	6.01	92.17	98.26	6.19	32.4	278
2	10.65	5.60	91.81	97.49	5.83	33.1	284
3	10.60	5.90	92.39	98.33	6.04	32.8	281
4	11.10	5.88	92.78	98.69	6.00	33.1	284
5	10.82	5.84	92.33	98.21	5.98	33.0	283
6	11.05	5.81	92.96	98.70	5.81	32.9	282
7	10.34	5.83	92.65	98.56	6.00	33.0	283
8	10.98	5.98	92.32	98.27	6.05	33.0	283
9	13.56	6.19	92.09	98.29	6.30	32.9	282
10	10.58	6.04	92.32	98.36	6.14	33.1	284
Mean	**11.17**	**5.91**	**92.38**	**98.32**	**6.03**	**33.0**	**282.4**
SD	**± 0.90**	**± 0.15**	**± 0.32**	**± 0.32**	**± 0.14**	**± 0.2**	**± 1.7**
Max	**13.56**	**6.19**	**92.96**	**98.70**	**6.30**	**33.1**	**284**
Min	**10.34**	**5.60**	**91.81**	**97.49**	**5.81**	**32.4**	**278**

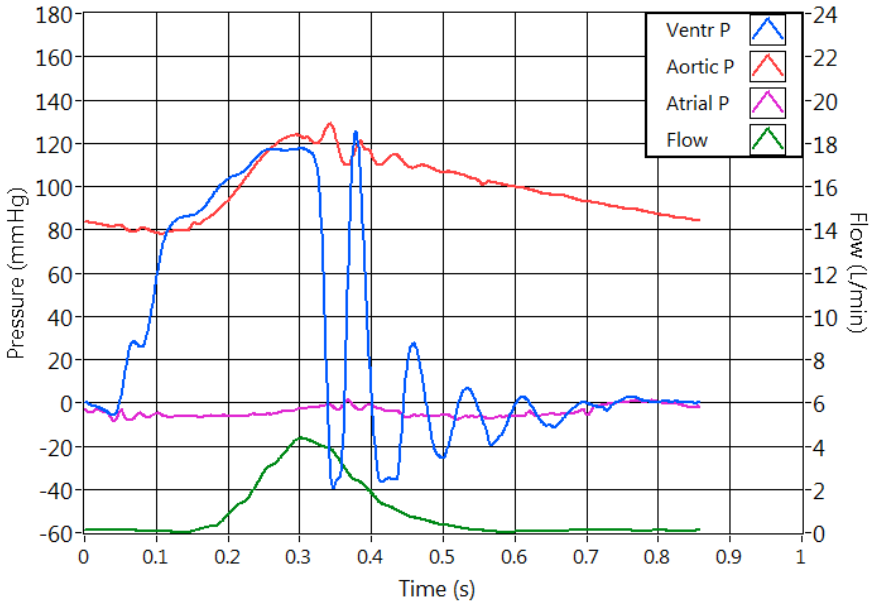

Figure C.1: Graphical results for SJM Epic 23 mm Test 1.

Table C.17: Results for SJM Epic 23 mm Test 2.

Beat	PSPD (mmHg)	MSPD (mmHg)	MSAP (mmHg)	MSVP (mmHg)	SWL (%)	Systole (%)	T_{sys} (ms)
1	25.39	12.56	95.04	107.60	11.67	34.5	296
2	25.81	12.70	95.23	107.92	11.76	34.4	295
3	24.89	12.32	95.33	107.72	11.50	34.7	297
4	25.39	12.67	95.37	107.97	11.67	34.7	297
5	24.60	12.66	94.79	107.44	11.77	35.1	301
6	25.23	12.65	94.63	107.36	11.86	34.7	297
7	23.53	12.05	94.94	106.99	11.26	34.4	295
8	24.44	12.28	94.74	107.02	11.47	34.7	297
9	25.37	12.69	94.21	106.89	11.87	34.7	297
10	24.55	12.21	94.80	107.00	11.41	34.5	296
Mean	**24.92**	**12.48**	**94.91**	**107.39**	**11.62**	**34.6**	**296.8**
SD	**± 0.63**	**± 0.23**	**± 0.34**	**± 0.38**	**± 0.19**	**± 0.2**	**± 1.6**
Max	**25.81**	**12.70**	**95.37**	**107.97**	**11.87**	**35.1**	**301**
Min	**23.53**	**12.05**	**94.21**	**106.89**	**11.26**	**34.4**	**295**

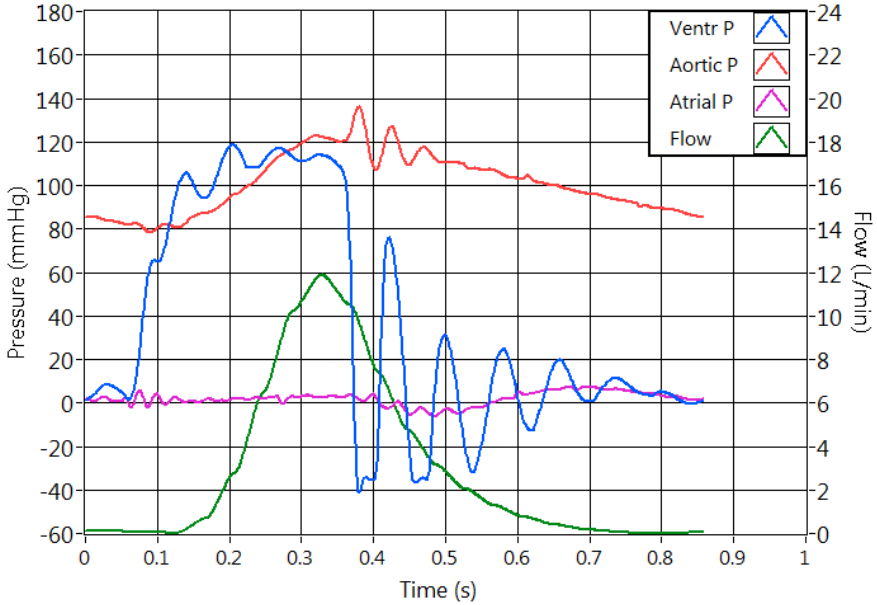

Figure C.2: Graphical results for SJM Epic 23 mm Test 2.

Table C.18: Results for SJM Epic 23 mm Test 3.

Beat	PSPD (mmHg)	MSPD (mmHg)	MSAP (mmHg)	MSVP (mmHg)	SWL (%)	Systole (%)	T_{sys} (ms)
1	23.81	14.51	93.82	108.33	13.39	35.9	308
2	24.58	14.35	93.98	108.33	13.25	35.9	308
3	24.37	14.44	93.90	108.42	13.40	35.5	304
4	24.18	14.50	93.34	107.83	13.44	35.7	306
5	24.38	14.70	92.85	107.46	13.59	35.7	306
6	24.13	14.32	93.54	107.86	13.27	35.8	307
7	24.07	14.10	93.86	107.96	13.06	35.8	307
8	25.62	14.92	93.25	108.17	13.79	35.9	308
9	24.19	14.48	93.40	107.88	13.42	35.8	307
10	24.58	14.55	93.75	108.29	13.43	36.1	309
Mean	**24.39**	**14.49**	**93.57**	**108.05**	**13.41**	**35.8**	**307.0**
SD	**± 0.47**	**± 0.21**	**± 0.34**	**± 0.29**	**± 0.19**	**± 0.2**	**± 1.3**
Max	**25.62**	**14.92**	**93.98**	**108.42**	**13.79**	**36.1**	**309**
Min	**23.81**	**14.10**	**92.85**	**107.46**	**13.06**	**35.5**	**304**

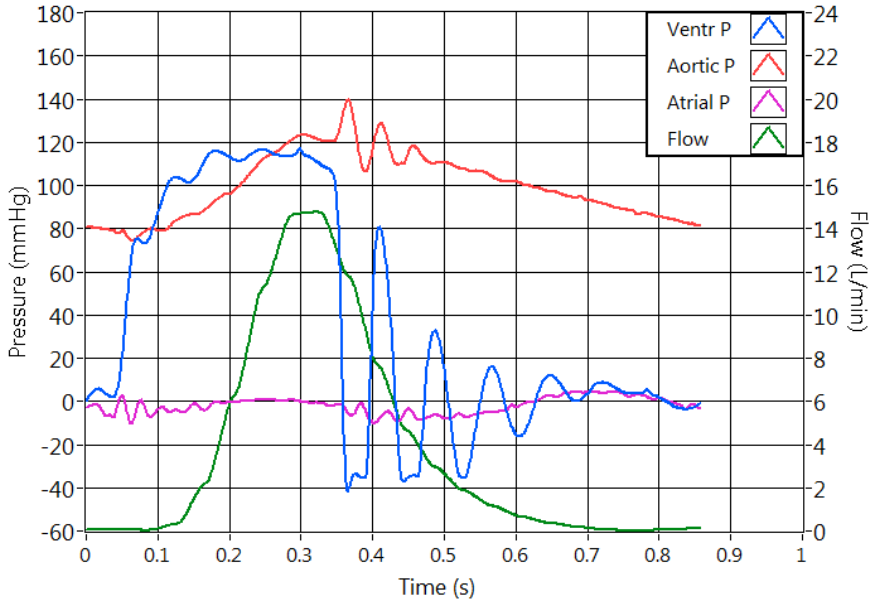

Figure C.3: Graphical results for SJM Epic 23 mm Test 3.

Table C.19: Results for SJM Epic 23 mm Test 4.

Beat	PSPD (mmHg)	MSPD (mmHg)	MSAP (mmHg)	MSVP (mmHg)	SWL (%)	Systole (%)	T_{sys} (ms)
1	45.63	19.47	93.40	112.83	17.22	37.1	318
2	44.32	19.07	93.69	112.74	16.90	37.1	318
3	44.00	19.22	93.74	112.96	17.02	37.6	322
4	44.34	19.06	94.11	113.15	16.83	37.3	320
5	44.95	19.49	94.14	113.63	17.15	36.3	311
6	44.39	19.14	94.57	113.71	16.84	37.6	322
7	44.19	18.68	94.67	113.35	16.48	37.6	322
8	46.50	19.54	94.19	113.73	17.18	37.3	320
9	49.48	19.54	94.02	113.47	17.14	37.1	318
10	44.30	18.81	93.63	112.42	16.72	37.9	325
Mean	**45.16**	**19.17**	**94.02**	**113.20**	**16.95**	**37.3**	**319.6**
SD	**± 1.68**	**± 0.29**	**± 0.39**	**± 0.43**	**± 0.23**	**± 0.4**	**± 3.6**
Max	**49.48**	**19.54**	**94.67**	**113.73**	**17.22**	**37.9**	**325**
Min	**44.00**	**18.68**	**93.40**	**112.42**	**16.48**	**36.3**	**310**

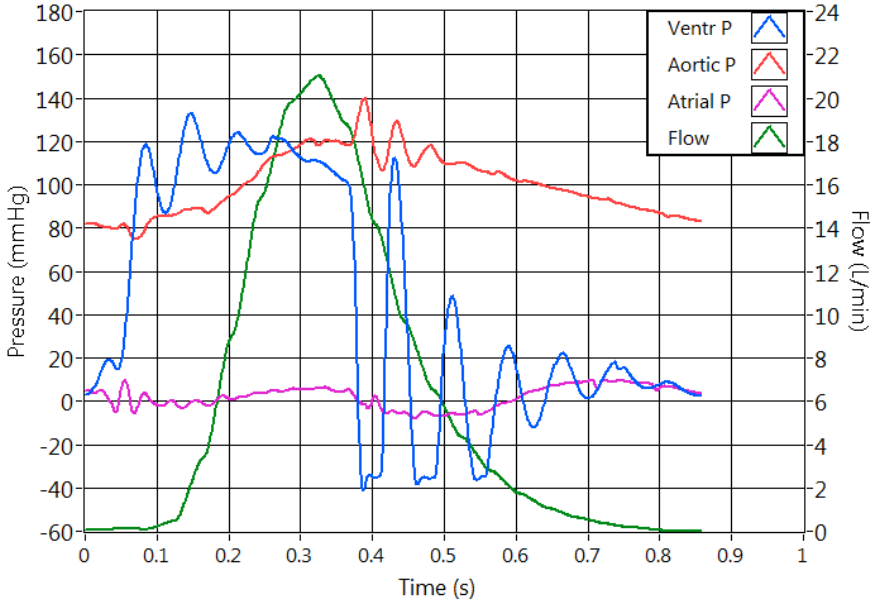

Figure C.4: Graphical results for SJM Epic 23 mm Test 4.

Appendix D: Cost details

National Instruments, SEW and Siemens components were imported by their respective South African representatives and are therefore more susceptive to price fluctuations. All other components and materials were procured from local suppliers.

The expenses taken into account relate to the hardware and manufacturing costs required to have the CPD in its final specification, as described in Section 3.2.3. However, this does not include assembly or development time which accounts for programming, calibration, tuning and testing. The amounts shown in Table D.1 are in 2015 South African Rand (ZAR). These amounts are retail prices and do not include the Value Added Tax (VAT) of 14%.

Table D.1: Costs for the CPD in its final specification. (VAT: value added tax).

	Cost/unit	Qty	Line total	Subtotal
INSTRUMENTATION AND CONTROL				
SEW MoviDrive	R 15 427	1	R 15 427	
Encoder card for SEW MoviDrive	R 2 127	1	R 2 127	
SEW Electric cylinder	R 25 807	1	R 25 807	
Pressure sensor	R 2 010	3	R 6 030	
Flowmeter + Signal converter	R 33 900	1	R 33 900	
Submersible heater	R 650	1	R 650	
Temperature controller	R 800	1	R 800	
Pt100 temperature sensor	R 180	1	R 180	
24V Power supply (20W)	R 320	1	R 320	
NI myRIO 1900	R 11 990	1	R 11 990	
NI USB-6009	R 6 420	1	R 6 420	
NI LabVIEW (Full Development System)	R 10 000	1	R 10 000	
				R 113 651
MATERIAL				
Compliance chamber	R 2 000	1	R 2 000	
Resistor	R 450	1	R 450	
Left ventricular outflow tract	R 600	1	R 600	
Reservoir	R 600	1	R 600	
Pump	R 1 800	1	R 1 800	
E-cylinder support & rod connection	R 300	1	R 300	
Ventricular chamber	R 500	1	R 500	
Ventricular compliance chamber	R 650	1	R 650	
Frame	R 1 500	1	R 1 500	
Miscellaneous hardware	R 1800	1	R 1 800	
				R 10 200
MANUFACTURING LABOUR	**Cost/hour**			
Compliance chamber	R 350	18	R 6 300	
Resistor	R 350	12	R 4 200	
Left ventricular outflow tract	R 350	14	R 4 900	
Reservoir	R 350	6	R 2 100	
Pump	R 350	24	R 8 400	
E-cylinder support & rod connection	R 350	6	R 2 100	
Ventricular chamber	R 350	10	R 3 500	
Ventricular compliance chamber	R 350	8	R 2 800	
Frame	R 350	8	R 2 800	
				R 37 100
TOTAL exVAT				**R 160 951.00**
VAT @ 14%				**R 22 533.14**
GRAND TOTAL				**R 183 484.14**

Appendix E: Graphical user interfaces

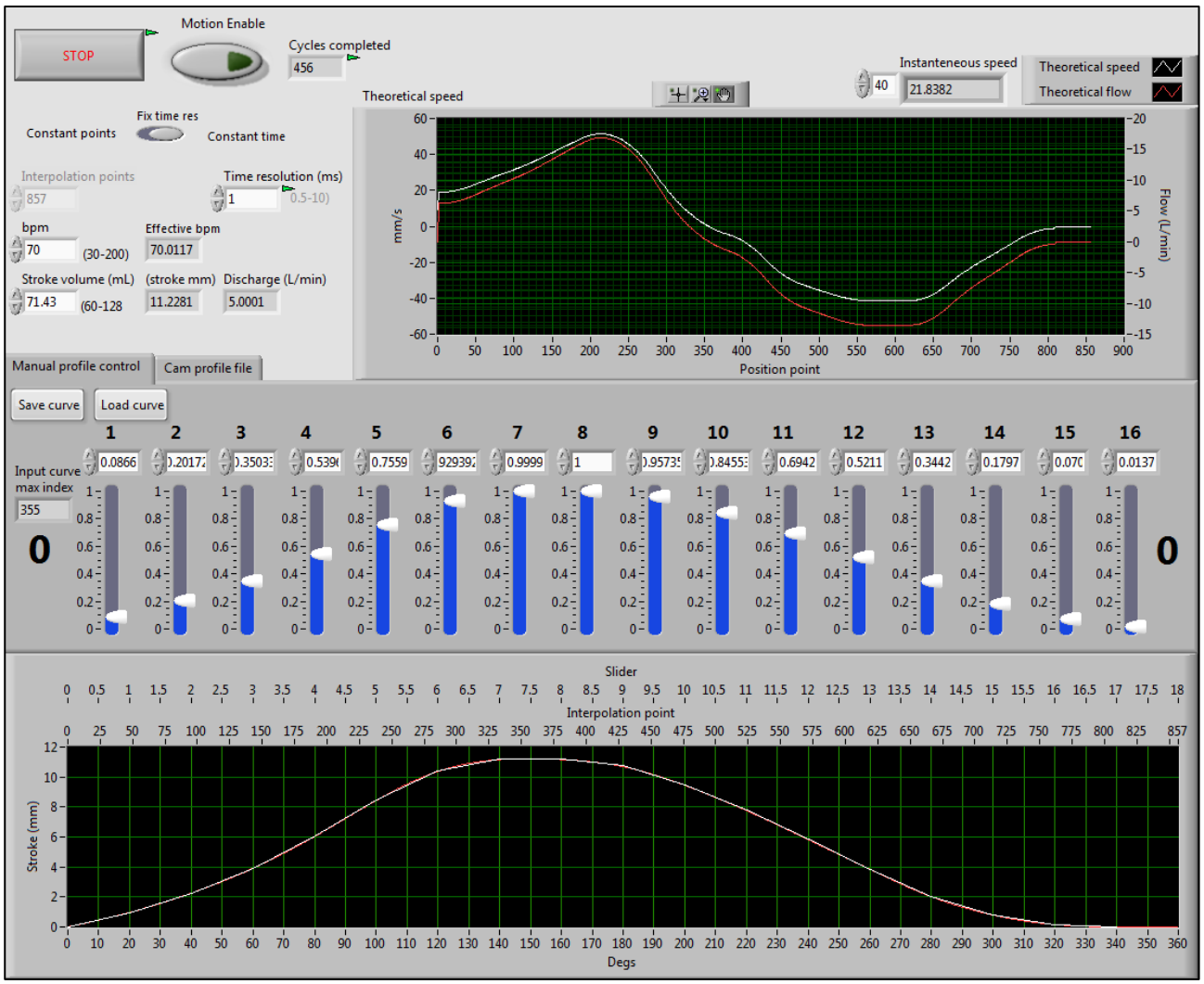

Figure E.1: Main window (motion definition and control).

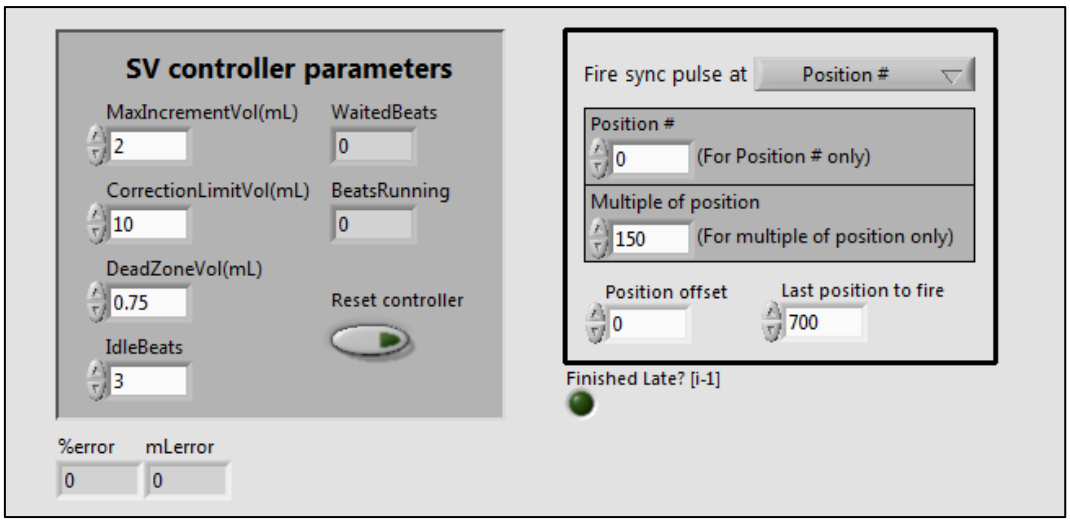

Figure E.2: RIOorquestrator front panel (stroke volume controller and parameters for external synchronisation pulse).

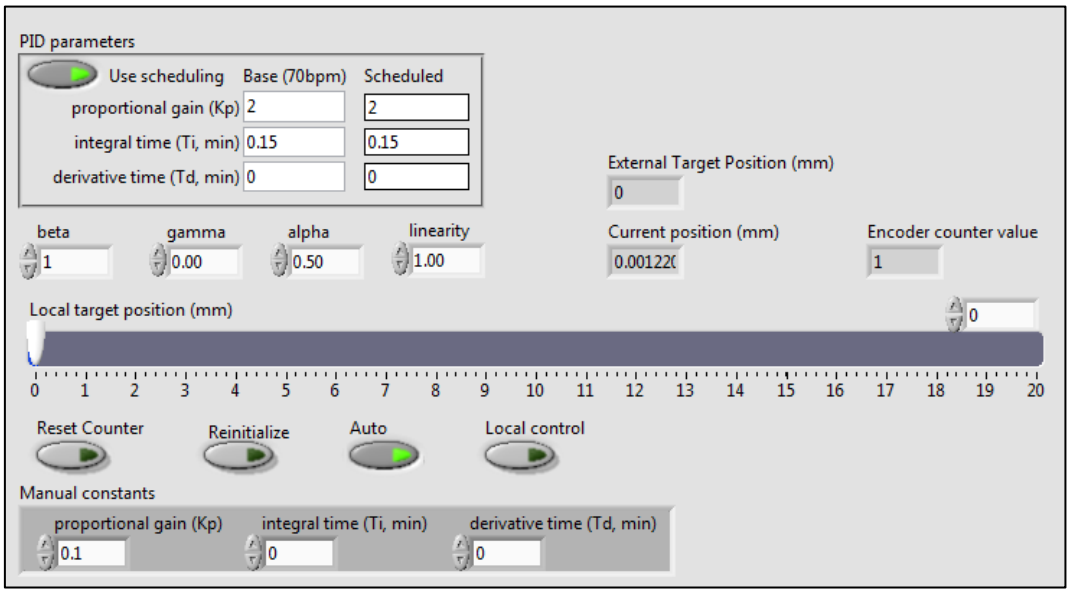

Figure E.3: PIDloop front panel (PID controller and manual positioning parameters).

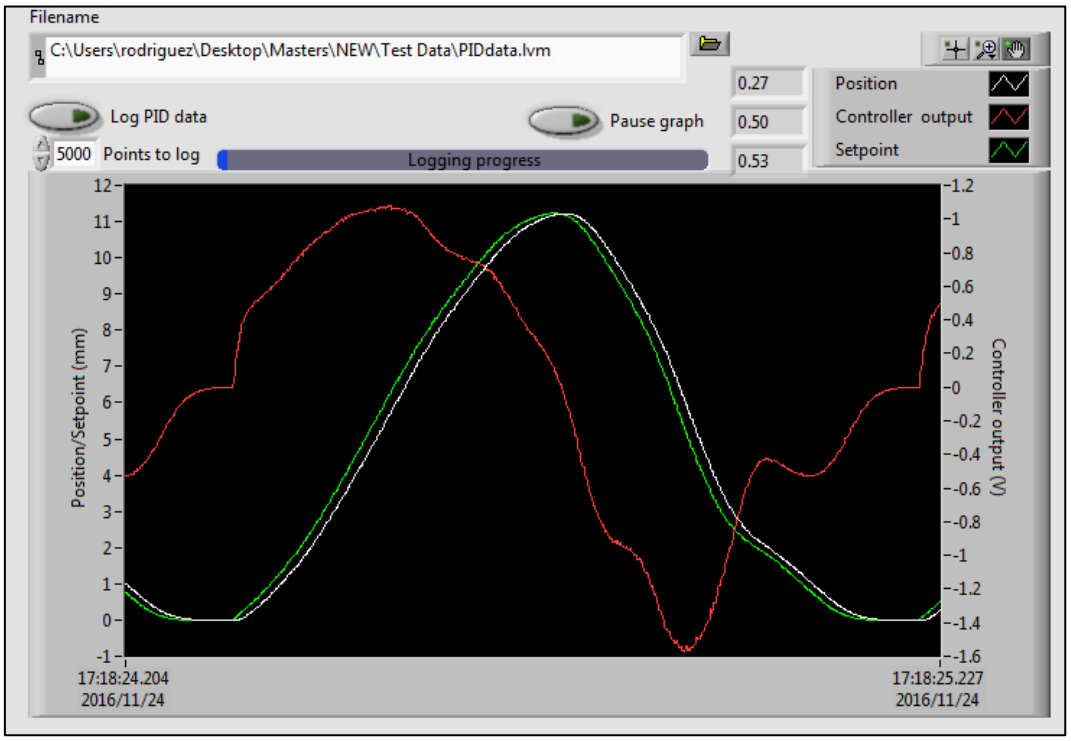

Figure E.4: PIDmonitor front panel (electric cylinder performance monitoring and logging).

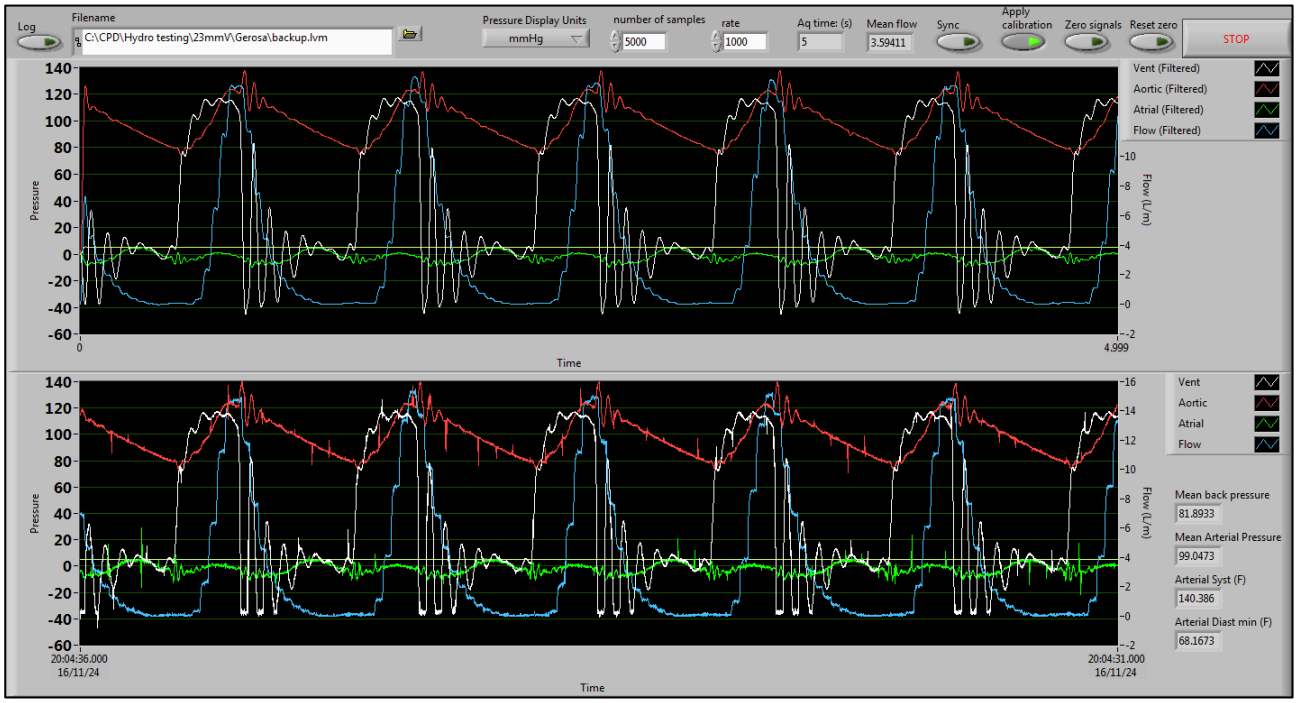

Figure E.5: Data acquisition window (data display, analysis and calibration as well as acquisition control).